PROCEEDINGS

of the

Fourteenth
International Tissue Elasticity Conference™

Bardolino, Lake Garda, Verona, Italy
September 21 – 24, 2015

PROCEEDINGS

of the

Fourteenth International Tissue Elasticity Conference™

Bardolino, Lake Garda, Verona Italy

September 21-24, 2015

Table of Contents

QUESTIONS OR COMMENTS ARE WELCOME AT ANY TIME AT <secretariat@elasticityconference.org>

Some abstracts may have been edited by the reviewers for clarity of presentation.

Foreword

Dear Conference Delegate:

On behalf of the general organizing team welcome to the 14th annual International Tissue Elasticity Conference™ (ITEC™), and to the town of Bardolino in the beautiful area of Lake Garda, near Verona, Italy. We are delighted to be here for our first ITEC™ in Italy. The venue should provide a peaceful and comfortable retreat, with excellent conference facilities and a relaxing atmosphere within which we can present and discuss our science, as well as renew and create friendships. You may wish to take the time to explore. Bardolino has a highly recommended olive oil museum, within walking distance of the conference hotel. There are also many vineyards in the area, and a wine museum nearby. About a week after our conference is over the spectacular Bardolino Wine Festival begins, marking the maturation and distribution of the new Bardolino wine. The Bardolino area is also excellent for excursions, either on Lake Garda or for walking in the Dolomites. Nearby Verona is rich in culture and history. (Not long before our conference begins, the Arena di Verona Festival 2015 will have finished. This is a summer festival of opera shows, held every year since 1936 in Verona's ancient Roman amphitheatre). Alternatively, you may wish simply to explore the town of Bardolino's pretty streets, shopping and lakeside promenade. You will find medieval city walls, beautiful churches from the 9th century and the ruins of a 14th century castle.

This year we are delighted to run ITEC™ in sequence with the fifth Sono-Elastography Meeting, a largely clinical elastography forum which is held annually in Italy. ITEC™ began before commercial elastography systems were on the market, and is proud to have played a part in fostering the innovation that led to such such systems, the first generation of which is now widely available from a broad range of manufacturers. In this "Elastography Week" our common aim is to provide a unique and unified forum that will bring together researchers in physics, engineering and clinical applications from around the world to ultimately contribute to new technical developments in elasticity imaging and to broadening its clinical application and utility. We very much hope that the basic scientists and the clinicians will enjoy this opportunity to communicate and learn from each other. To assist this interaction we have arranged Thursday 24th September to be an overlap day, of clinical applications and manufacturers sessions, with a joint reception in the evening that replaces our usual good-bye pizza party. I would like to thank Fabrizio Calliada, Mario Canepari, Giovanna Ferraioli and Carlo Filice, the scienfitic committee of the Sono-Elastogrpahy Meeting, for their kind co-operation in bringing about this juxtaposition of meetings.

I am greatly looking forward to the performance of Duophonic, who will provide our musical entertainment at the Conference Dinner on the evening of Tuesday 22nd September 2015. The duo, Roberta Zampieri (vocalist) and Massimo Lambertini (pianist) was born from the belief that any kind of music, be it rock, soul, jazz, pop or classical, can be adapted to just two sound sources, "Duophonic", voice and piano. The repertoire you will hear will be an elegant and refined reinterpretation of famous Italian and international successes from pop, rock, light, and dance, replicated in a unique acoustic atmosphere, ranging from classical to modern music. Adaptations will be from artists such as Coldplay, Adele, Michael Jackson, Paolo Conte, Sakamoto, Nina Simone and many more.

I am sad to say that Jonathan and Karen Ophir will again not be able to join us. Jonathan and Karen are two of the Founding Organizers of ITEC, and they were the principle driving force behind the ITEC series of conferences from 2002-2012. They have kindly sent their good wishes for the conference, as printed on the following page. We wish them both well and hope that we can involve them in the conference at some point, via Skype.

This year we return to the format of starting the conference with two tutorial speakers, one basic science and one clinical. I am delighted that Rémi Souchon has agreed to open ITEC 2014 with a lecture that aims to provide an understanding of the physics involved in elastography. Rémi has been at the forefront of elastography research for at least 20 years and his introductory physics tutorial is particularly appropriate for our sequential meetings this year. To complement this, our clinical tutorial will be presented by An Tang, who will educate us on liver disease and liver imaging, and will highlight unmet clinical needs in this area. It is a substantial task to prepare an ITEC tutorial, and I am grateful to both Rémi and An for agreeing to pass on their knowledge and experience in this way.

Many volunteers and colleagues have helped to bring about this conference, especially our conference secretary, Cheryl Taylor. Please join me in thanking Cheryl for, once again, working tirelessly to make the conference a timely success. It is a pleasure also to acknowledge contributions from the administration of the Institute of Cancer Research, especially Liam Blake and Alan Hill for assistance in financial and legal matters, and Neil Walford for assistance with audio-visual equipment. Finally, we are extremely grateful to all those who have participated as helpers, sponsors, reviewers, session chairs, award judges and contributors, without whom the conference could not happen.

When Jonathan Ophir and Kevin Parker first conceived this conference series they expressed the purpose as "to advance the field of measurement and imaging of the elastic attributes of soft tissues through tutorials and scientific presentations of the state of the art in the field, within a unique and unified forum that would bring together researchers from several countries and ultimately contribute to the rapid development and clinical introduction of this new medical imaging technology". Our presence here suggests that we all strongly agree that we continue to value such a conference. However, ITEC must evolve if it is to continue to serve the needs of researchers and practitioners in the field of tissue elasticity measurement and imaging. Please complete the feedback forms in this Proceedings Book or, if you prefer, speak directly to me or Cheryl to discuss your suggestions. Feedback is of immense value to us in planning future ITECs.

May your research be inspired by the presentations and discussions during the 14th ITEC, and may you make new friends, establish productive collaborations and renew old acquaintances.

Next year will be the 15th annual ITEC and we will be planning something appropriately special.

Jeffrey Bamber
General Conference Organizer
Bardolino, Lake Garda, Italy, September 21-24, 2015

Message from the Founding Organizers

Austin, Texas, September 3rd, 2015

Dear friends and colleagues:

We are writing you this note in lieu of greeting you in person at ITEC '15 in Bardolino, Italy.

Another year has gone by, and we are in reasonably good health. After surgery and chemo since last year, Jonathan's doctors are optimistic. Jonathan retired from service at University of Texas as of August 31, 2015 and will continue as a Professor Emeritus thereafter. Karen continues to do well on biologics and keeps busy around the house.

We know Jeff and Cheryl are doing their best to keep the meeting exciting and inspiring.

We will miss seeing our friends and colleagues as well as meeting the new delegates every year. We hope that you will have a stimulating academic experience and much wonderful camaraderie.

All the best,

Jonathan and Karen Ophir
Founding Organizers

CONFERENCE–AT–A–GLANCE

Fourteenth International Tissue Elasticity Conference™
Hotel Caesius Therme & Spa Resort – Lake Garda, Italy September 21–24, 2015

Monday, September 21

9:00A – 12:00P	**Set Up:**	Oral Presenters load presentations (CD or USB Stick)	Meeting Room Gardenia
		Poster Presenters set up presentations	Meeting Room Iris
		Exhibitors set up exhibits	Meeting Room Iris
9:00A – 5:30P		Registration Desk Open	Foyer
2:00P- 5:30P	**Session EEX:**	Equipment Exhibit	Meeting Room Iris
12:00P- 2:00P	**Session TUT:**	**Tutorials**	Meeting Room Gardenia
2:00P – 2:30P		*Coffee Available*	Foyer
2:30P- 4:30P	**Session SAS:**	**Oral Presentations of Finalists for Student Awards Session**	Meeting Room Gardenia
4:30P – 5:00P		*Recess/Exhibitor viewing*	Meeting Room Iris
5:00P- 5:30P	**Session POS**	**Poster Session – Live Oral Summaries**	Meeting Room Gardenia
7:00P – 9:00P		*Opening Dinner Reception*	Benacus Restaurant

Tuesday, September 22 **8:45A – 10:00P**

9:00A – 5:00P		Registration Desk Open	Foyer
9:00A – 5:00P	**Session EEX:**	Equipment Exhibit	Meeting Room Iris
8:45A – 9:00A		Opening Remarks	Meeting Room Gardenia
9:00A – 10:30A	**Session MIP–1:**	**Methods for Imaging Elastic Tissue Properties – I**	Meeting Room Gardenia
10:30A – 11:00A		*Coffee Break*	Foyer
11:00A – 11:30A	**Session SIP:**	**Signal and Image Processing – I**	Meeting Room Gardenia
11:30A – 12:30P	**Session BTM:**	**Biomechanical Tissue Modeling**	Meeting Room Gardenia
1:00P – 2:30P		*Group Lunch*	Benacus Restaurant
2:30P – 4:15P	**Session CAA -1:**	**Clinical and Animal Applications**	Meeting Room Gardenia
4:15P – 4:45P		*Coffee Break*	Foyer
4.45P – 5:15P	**Session CVE:**	**Cardiovascular Elasticity**	Meeting Room Gardenia
7:00P – 10:00P		*Conference Dinner*	Augustus Restaurant

Wednesday, September 23 **9:00A – 5:30P**

9:00A – 5:00P		Registration Desk Open	Foyer
9:00A – 5:00P	**Session EEX:**	Equipment Exhibit	Meeting Room Iris
9:00A – 10:07A	**Session MPT:**	**Mechanical Properties of Tissues**	Meeting Room Gardenia
10:10A – 10:45A		*Coffee Break*	Foyer
10:45A – 11:07A	**Session CMM:**	**Complementary & Multi-Modality Elasticity Techniques**	Meeting Room Gardenia
11:07A – 11:37A	**Session MMT:**	**Mechanical Measurements Techniques for Tissues**	Meeting Room Gardenia
11:37A – 12:07P	**Session FIP:**	**Forward and Inverse Problems**	Meeting Room Gardenia
12:07P – 12:44P	**Session INS–1:**	**Instrumentation including Phantoms**	Meeting Room Gardenia
1:00P – 2:30P		*Group Lunch*	Benacus Restaurant
2:30P – 4:07P	**Session MIP–2:**	**Methods for Imaging Elastic Tissue Properties – II**	Meeting Room Gardenia
4:15P – 4:45P		*Coffee Break*	Foyer
4:45P – 5:15P	**Session MIP–3:**	**Methods for Imaging Elastic Tissue Properties – III**	Meeting Room Gardenia

5.15P – 5:30P		**Group Photo**	TBA
5:30P		*Free Evening –No Conference Activities*	

Thursday, September 24		**9:00A – 9:30P**	
9:00A – 5:00P		Registration Desk Open	Foyer
9:00A – 5:00P	**Session EEX:**	Equipment Exhibit	Meeting Room Iris
9:00A – 10:35A	**Session CAA -2:**	**Clinical and Animal Applications – II**	Meeting Room Gardenia
10:35A – 11:00A		*Coffee Break*	Foyer
11:00A – 12:30P	**Session CAA -3:**	**Clinical and Animal Applications – III**	Meeting Room Gardenia
12:30P – 1:00P	**Session INS -2:**	**Instrumentation including Phantoms – II**	Meeting Room Gardenia
1:00P – 2:30P		*Group Lunch*	Benacus Restaurant
2:30P – 3:20P	**Session CAA -4:**	**Clinical and Animal Applications – IV**	Meeting Room Gardenia
3:20P – 3:40P	**Session INS -3:**	**Instrumentation including Phantoms – III**	Meeting Room Gardenia
3:40P – 4:30P	**Session CAA -5:**	**Clinical and Animal Applications – V**	Meeting Room Gardenia
4:30P – 4:50P		*Coffee Break*	Foyer
4:50P – 5:30P	**Session CAA -6:**	**Clinical and Animal Applications – VI**	Meeting Room Gardenia
7:30P – 9:30P		*Closing Cocktail Party (Proceedings Book Signing)*	Benacus Restaurant

PROGRAM

Fourteenth International Tissue Elasticity Conference™

Lake Garda, Verona, Italy

September 21-24, 2015

Monday, September 21 12:00P – 9:00P

9:00A – 12:00P Presentation Set Up

All Oral Presenters load presentations onto Conference computers — Meeting Room Gardenia
Poster Presenters set up presentation — Meeting Room Iris
Exhibitors set up exhibits — Meeting Room Iris

9:00A – 5:30P Registration Desk Open — Foyer

2:00P – 5:30P Session EEX: Equipment Exhibit — Meeting Room Iris

Monday 12:00P – 2:00P
Session TUT: Tutorials:
Chair: JC Bamber, UK *Co–Chair: F Calliada, Italy* Meeting Room Gardenia

Page No.

12:00P – 12:45P

066 UNDERSTANDING ELASTOGRAPHY – PHYSICS FOR MDs. 24
Rémi Souchon[1], Stefan Catheline[1], Olivier Rouvière[1,2]*
[1] INSERM, Lyon, FRANCE; [2]Hospices Civils de Lyon, FRANCE.

12:45P – 1:00P Discussion

1:00P – 1:45P

019 UNMET NEEDS IN LIVER IMAGING: A CLINICAL PERSPECTIVE. 25
A Tang[1,2], G Cloutier[1,3].*
[1]University of Montréal Hospital Research Center, Montréal, Quebec, CANADA; [2]University of Montréal Hospital Center, Montréal, Quebec, CANADA; [3]Laboratory of Biorheology and Medical Ultrasonics, Montréal, Quebec, CANADA.

1:45P – 2:00P Discussion

2:00P – 2:30P COFFEE AVAILABLE — Meeting Room Iris

Monday 2:30P – 4:30P
Session SAS: Oral Presentations of Finalists for Student Awards Session
Chair: E Harris, UK *Co–Chair: S Sumi, Japan* Meeting Room Gardenia

Page No.

2:30P – 2:45P

005 TOMOGRAPHIC MAGNETIC RESONANCE ELASTOGRAPHY BY MULTIFREQUENCY WAVE NUMBER INVERSION. 26
Heiko Tzschätzsch[1]*, Jing Guo[1], Florian Dittmann[1], Jürgen Braun[2], Ingolf Sack[1]
[1]Charité - Universitätsmedizin Berlin, Departments of Radiology, Charitéplatz 1, Berlin, GERMANY; [2]Medical Informatics, Hindenburgdamm 30, Berlin, GERMANY..

(Session SAS continued on next page)

* *indicates Presenter*

(Session SAS continued from previous page)

2:45P – 3:00P

007 IMPROVING BRAIN TUMOR SURGERY USING INTRA-OPERATIVE SHEAR WAVE ELASTOGRAPHY AND ULTRASENSITIVE DOPPLER. 27

M Imbault[1]*, D Chauvet[2], L Capelle[2], C Demené[1], M Mossad[1], C Karachi[2], A-L Boch[2], J-L Gennisson[1],M Tanter[1].
[1]Institut Langevin, ESPCI, CNRS, INSERM, Paris, FRANCE.2. Pitié Salpêtrière Hospital, Paris, FRANCE.

3:00P – 3:15P

009 STORAGE AND LOSS MODULI IMAGING IN SOFT SOLIDS USING SUPERSONIC SHEAR IMAGING TECHNIQUE. 28

E Budelli[1,2], J Brum[3] , M Bernal[1] , T Deffieux[1] , M Tanter[1], C Negreira[3] , J-L Gennisson[1].*
[1]Institut Langevin, ESPCI, CNRS, INSERM, Paris, FRANCE.; [2] Facultad de Ingeniería-Universidad de la República, Montevideo, URUGUAY; [3] Facultad de Ciencias-Universidad de la República, Montevideo URUGUAY.

3:15P – 3:30P

010 *IN VIVO* TRANSTHORACIC CARDIAC SHEAR WAVE ELASTOGRAPHY USING ULTRAFAST HARMONIC COHERENT COMPOUND IMAGING. 29

M Correia[1], J Provost[1], S Chatelin[1], O Villemain[1], M Tänter[1], M Pernot[1].*
[1]Institut Langevin, ESPCI, PSL, CNRS INSERM, Paris, FRANCE.

3:30P – 3:45P

013 ACCURACY OF ARTERIAL SHEAR WAVE ELASTOGRAPHY BY PHASE VELOCITY ANALYSIS – VALIDATION WITH MECHANICAL TESTING IN PHANTOMS. 30

E Maksuti[1,2], D Larsson[1], E Widman[1,2], MW Urban[3], M Larsson[1,2], A Bjällmark[1,2].*
[1]KTH Royal Institute of Technology, Stockholm, SWEDEN; [2]Karolinska Institutet, Solna, SWEDEN; [3]Mayo Clinic College of Medicine, Rochester, MN, USA

3:45P – 4:00P

022 A RESOLUTION STUDY IN PASSIVE ELASTOGRAPHY. 31

A Zorgani[1],R Souchon[1],S Catheline[1]*
[1]U1032, INSERM, Lyon, FRANCE.

4:00P – 4:15P

059 QUANTITATIVE POROELASTIC PROPERTY IMAGING COMBINING SHEAR WAVE AND STRAIN ELASTOGRAPHY. 32

M Theodorou[1], J Fromageau[1,2,] N deSouza[1,23] , JC Bamber[1,2]*
[1]Institute of Cancer Research, Sutton, UNITED KINGDOM; [2]Royal Marsden NHS Foundation Trust, Sutton, UNITED KINGDOM.

4:15P – 4:30P

011 INTERVENTIONAL MAGNETIC RESONANCE ELASTOGRAPHY FOR THE MONITORING OF MR-GUIDED PERCUTANEOUS THERMAL ABLATIONS. 33

N Corbin[1], E Breton[1], M de Mathelin[1], J Vappou[1].*
[1]ICube, Université de Strasbourg, CNRS, IHU Strasbourg, Strasbourg, FRANCE.

4:30P – 5:00P

RECESS/EXHIBITOR VIEWING Meeting Room Iris

* *indicates Presenter*

Monday 5:00P – 5:20P
Session POS: Poster Session – Live Oral Summaries
Chair: AK Thittai, India *Co–Chair: H Rivaz, Canada* Meeting Room Iris

Page No.

5:00P – 5:02P

002 A NOVEL TACTILE SENSOR FOR ELASTOGRAPHY OF SUPERFICIAL ORGANS. 34
J Fu[1], F Li[1]*
[1]Perking University, Beijing, CHINA.

5:02P – 5:04P

027 SOME INCLUSIONS IN A HARDER SURROUNDING SHOW UP AS THE SO CALLED 'BLACK HOLE PHENOMENON' WITHOUT MEASURED ELASTICITY ON SHEAR WAVE ELASTOGRAPHY (SWE). 35
B.Jin[1], A Evans[1], X Zhou[1], S Cochran[1], K Skerl[1].*
[1]University of Dundee, Scotland. UNITED KINGDOM.

5:04P – 5:06P

031 SHEAR WAVE ELASTOGRAPHY STIFFNESS CORRELATES WITH FIBRO-GLANDULAR COMPOSITION OF BREAST TISSUE. 36
K Skerl[1], S Vinnicombe[1,2], K Thomson[2], A Evans[1].*
[1]University of Dundee, Scotland, UNITED KINGDOM; [2]Ninewells Hospital & Medical School, Dundee, Scotland, UNITED KINGDOM.

5:06P – 5:08P

036 IN VITRO QUANTIFICATION AND REPRODUCIBILITY OF ELASTICITY MEASUREMENTS USING FIVE DIFFERENT ELASTOGRAPHY PLATFORMS. 37
A Mulabecirovic[1], M Vesterhus,[1,2] O H Gilja, [1,2] R Flesland Havre,[1.]*
[1]Haukeland University Hospital, Bergen, NORWAY; [2]University of Bergen, Bergen, NORWAY.

5:08P – 5:10P

039 HIGH SPEED BEAMFORMING USING FAST FOURIER'S TRANSFORM AND MIGRATION FOR ARBITRARY SIMULTANEOUS PLURAL TRANSMISSIONS AND USING VIRTUAL SOURCE BEHIND TRANSDUCER. 38
C Sumi[1].*
[1]Sophia University, Tokyo, JAPAN.

5:10P – 5:12P

040 ACCURACY COMPARSION OF AXIAL AND LATERAL STRAIN MEASUREMENTS ACHIEVED USING PLURAL STEERED BEAMS AND PLANE WAVES AND SUPER RESOLUTION IMAGING. 39
C Sumi[1].*
[1]Sophia University, Tokyo, JAPAN.

5:12P – 5:14P

055 USING A CONTROLLED ACCELERATION OF THE HEAD TO ACCESS VISOELATIC PROPERTIES OF BRAIN TISSUE. 40
J Bindl[1], A L Kofahi[1], S Theilenberg[1], S Napiletzki[1], J Finsterbusch[2], C Urbach[1], K Maier[1].*
[1]University of Bonn, Bonn, GERMANY; [2]University Medical Center Hamburg-Eppendorf, Hamburg, GERMANY.

5:14P – 5:16P

057 AUTOMATIC SELECTION OF REPRESENTATIVE FRAMES FROM AXIAL-SHEAR STRAIN ELASTOGRAM CINE-LOOP. 41
B Rao[1], S Vikram[1], A K Thittai[1].*
[1]Indian Institute of Technology, Madras, INDIA.

(Session POS continues on next page)

* *indicates Presenter*

(Session POS continued from previous page)

5:16P – 5:18P

047 THE SIMULATION STUDY TO EVALUATE THE EFFECT OF LIVER VISCOSITY ON SHEAR WAVE PROPAGATION BY THE TRANSIENT ELASTOGRAPHY. 42

JH Shao[1], F Zhai[1], JW Luo[1], HC Xing[2], JX Zhao[2], J Cheng[2], Q He[1], L. Tong[1].*
[1]Tsinghua University, Beijing, CHINA; [2]Beijing Ditan Hospital, Beijing, CHINA

5:18P – 5:20P

048 DISCUSSION ABOUT THE EFFECT OF LIVER ELASTICITY IN ASSESSMENT OF LIVER FIBROSIS IN PATIENTS WITH CHRONIC HEPATITIS B AND THE INFLUENCE OF FACTORS ON IT. 43

JH Shao[1], HC Xing[2],JW Luo[1], F Zhai[1], JX Zhao[2], J Cheng[2], Q He[1], L. Tong[1]*.*
[1]Tsinghua University, Beijing, CHINA; [2]Beijing Ditan Hospital, Beijing, CHINA.

5:20P – 6:00P Discussion

Monday 7:00P – 9:00P
Opening Dinner Reception Benacus Restaurant

Tuesday, September 22 9:00A – 10:00P

9:00A – 5:00P
Registration Desk Open Foyer
9:00A – 5:00P Session EEX: Equipment Exhibit Meeting Room Iris
9:00A – 5:00P Session POS: Posters Meeting Room Iris

Tuesday 8:45A – 9:00A
OPENING REMARKS Meeting Room Gardenia
JC Bamber, UK.

Tuesday 9:00A – 10:30A
Session MIP–1: Methods for Imaging Elastic Tissue Properties – I
Chair: T Hall, USA *Co–Chair: S Catheline, France* Meeting Room Gardenia

Page No.

9:00A – 9:15A

051 REAL-TIME STEERING FOR INDUCING AND MONITORING HIFU ABLATION USING HARMONIC MOTION IMAGING. 44

Yang Han[1], Thomas Payen[1], Shutao Wang[1], Elisa Konofagou[1,2].*
[1]Department of Biomedical Engineering, Columbia University, New York, NY, USA; [2]Department of Radiology, Columbia University, New York, NY, USA..

9:15A – 9:30A

004 CONTACTLESS REMOTE INDUCTION OF SHEAR WAVES IN SOFT TISSUES USING A TRANSCRANIAL MAGNETIC STIMULATION DEVICE 45

P Grasland-Mongrain[1], E Miller-Jolicoeur[1], A Tang[2,3], S Catheline[4,5], G Cloutier[1,2,6]*
[1]University of Montreal, Québec, CANADA; [2], University of Montreal, Québec, CANADA; [3]University of Montreal Hospital Research Center, Québec, CANADA; [4]INSERM, Lyon, France; [5]Université de Lyon, France; [6]Institute of Biomedical Engineering, Québec, CANADA.

9:30A – 9:45A

018 ASSESSMENT OF CORNEAL BIOMECHANICAL PROPERTIES BASED ON MODIFIED RAYLEIGH-LAMB FREQUENCY EQUATION. 46

SR Aglyamov[1], Z Han[2], J Li[2], M Singh[2], S Wang[2,3], S Vantipalli[4], C Wu[1], C Liu[1], M D Twa[4], KV Larin[1,3].*
[1]University of Texas at Austin, Austin, Texas, USA; [2]University of Houston, Houston, Texas, USA; [3]Baylor College of Medicine, Texas, USA; [4]University of Alabama, AL, USA.

(Session MIP continues on next page)

* *indicates Presenter*

(Session MIP continued from previous page)

9:45A – 10:00A

020 DETECTION OF STEATOHEPATITIS IN A RAT MODEL: LOW VERSUS HIGH FREQUENCY ULTRASOUND ELASTOGRAPHY FOR ASSESSMENT OF LIVER SHEAR STIFFNESS. 47

S Kazemirad[1,2], E Zhang[1,2], B Chayer[1,2], F Destrempes[1,2], B Nguyen[3], M Bilodeau[4], P Bodson-Clermont[2], G Cloutier[1,2], A Tang[2].*

[1]Laboratory of Biorheology and Medical Ultrasonics, Quebec, CANADA; [2]University of Montreal Hospital Research Center, Montreal, Quebec, CANADA; [3]Department of Pathology, University of Montreal Hospital Center, Montreal, Quebec, CANADA; [4]Liver Unit, University of Montreal Hospital Center , Montreal, Quebec, CANADA.

10:00A – 10:15A

023 SHEAR WAVE ULTRASOUND VISCOELASTOGRAPHY FOR MODEL-INDEPENDENT QUANTIFICATION OF COMPLEX MODULUS. 48

S Kazemirad[1,2], A Ouared[1,2], A Tang[2], G Cloutier[1,2].*

[1]Laboratory of Biorheology and Medical Ultrasonics, Montreal, Quebec, CANADA; [2]University of Montreal Hospital Research Center, Montreal, Quebec, CANADA.

10:15A – 10:30A

001 AN ELASTOGRAPHY METHOD BASED ON THE SCANNING CONTACT RESONANCE OF A PIEZOELECTRIC CANTILEVER. 49

Ji Fu[1], Faxin Li[1].*

[1]Peking University, Beijing, CHINA.

10:30A – 11:00A

COFFEE BREAK Meeting Room Iris

Tuesday 11:00A – 11:30A
Session SIP: SIGNAL AND IMAGE PROCESSING

Chair: AK Thittai, India *Co–Chair: M Fatemi, USA* Meeting Room Gardenia

Page No.

11:00A – 11:15A

016 A PILOT COMPARISON BETWEEN ELASTIC REGISTRATION AND RADIO-FREQUENCY-BASED BLOCK MATCHING IN TRANSVERSELY ISOTROPIC MEDIA. 50

H Li[1]; W-N Lee[1].*

[1]The University of Hong Kong, Hong Kong, CHINA.

11:15A – 11:30A

050 INCORPORATING SECOND-ORDER DERIVATIVES INTO REAL-TIME REGULARIZED ULTRASOUND ELASTOGRAPHY. 51

*H Rivaz[1]**

[1]Concordia University, Montreal, CANADA.

Tuesday 11:30A – 12:30P
Session BTM: BIOMECHANICAL TISSUE MODELING

Chair: M Fatemi, USA *Co–Chair: J Vappou, France* Meeting Room Gardenia

Page No.

11:30A – 11:45A

044 VOXEL-WISE FRACTIONAL-SPRINGPOT SOFT TISSUE VISCOELASTIC PARAMETER MAPPING WITH MULTIFREQUENCY MAGNETIC RESONANCE ELASTOGRAPHY. 52

E. Barnhill[1], P. Kennedy[1], I. Sack[2], J. Braun[2], N. Roberts[1].*

[1]University of Edinburgh, Edinburgh, UK; [2] Charité Universitätsmedizin Berlin, Berlin, GERMANY.

(Session BTM continues on next page)

* *indicates Presenter*

(Session BTM continued from previous page)

11:45A – 12:00P

060 3D FRACTIONAL VISCOELASTICITY TO MODEL ARTERIAL BEHAVIOUR. 53
O Barrera[1], G Alotta[1,2].*
[1]University of Oxford, Oxford, UK; [2]University of Palermo, Sicily, ITALY.

12:00P – 12:15P

061 CHARACTERIZATION OF ARTEFACTS IN SHEAR WAVE ELASTOGRAPHY FOR IMPROVED BREAST CANCER ASSESSMENT. 54
R De Luca[1,2,3], J Fromageau[1], F Marinozzi[3], JC Bamber[1].*
[1]Institute of Cancer Research and Royal Marsden Hospital, Sutton, England, UNITED KINGDOM; [2]Italian Foundation for Cancer Research, Milan, ITALY; [3]Sapienza University of Rome, Mechanical and Aerospace Engineering, Rome, ITALY.

12:15P – 12:30P

063 **LONGITUDINAL SHEAR WAVE AND TRANSVERSE COMPRESSIONAL WAVE IN ELASTIC SOLIDS.** 55
S. Catheline*[1], R.Souchon[1], J-Y. Chapelon[1], N. Benech[2].
[1]LabTau, INSERM, University of Lyon, Lyon, FRANCE [2]Laboratorio de Acústica Ultrasonora, Instituto de Física, Facultad de Ciencias, Montevideo, URUGUAY.

1:00P – 2:30P

GROUP LUNCH Benacus Restaurant

Tuesday 2:30P – 4:15P
Session CAA–1: Clinical and Animal Applications – I

Chair: D Cosgrove, UK *Co–Chair: H Feltovich, USA* Meeting Room Gardenia

Page No.

2:30P – 2:45P

014 ON THE RESPONSE OF LIVER STIFFNESS TO BLOOD PERFUSION REVEALED BY TIME HARMONIC ELASTOGRAPHY IN HEALTHY VOLUNTEERS AND PATIENTS WITH HEPATIC HYPERTENSION. 56
S Ipek-Ugay[1], H Tzschätzsch[1], C Althoff[1], T Fischer[1], C Hudert[2], J Guo[1], J Braun[3], I Sack[1].*
[1]Departments of Radiology, [2]Pediatric Endocrinology, and [3]Medical Informatics, Charité - Universitätsmedizin Berlin, Berlin, GERMANY.

2:45P – 3:00P

045 VALIDATION OF SHEAR-WAVE ELASTOGRAPHY CUTOFF VALUES FOR LIVER FIBROSIS STAGING. 57
JR Grajo[1], M Dhyani[1], AK Bhan[1], AE Samir[1].*
[1]Massachusetts General Hospital, Boston, MA, USA.

3:00P – 3:15P

025 ASSESSMENT OF AXILLARY LYMPH NODES WITH SHEAR WAVE ELASTOGRAPHY: PRELIMINARY *IN VIVO* HUMAN STUDY. 58
M. Denis[1], A. Gregory[1], M. Bayat[1], D.D. Meixner[1], R.T. Fazzio[1], M. Fatemi[1], A. Alizad[1].*
[1]Mayo Clinic College of Medicine, Rochester, MN, USA.

3:15P – 3:30P

026 MALIGNANT BREAST TISSUE CHANGES CREATE ANISOTROPY ON SHEAR WAVE ELASTOGRAHY. 59
K. Skerl[1], S. Vinnicombe[1], K. Thomson[1], D. McLean[1], E. Gianotti[1,2], A. Evans[1].*
[1]University of Dundee, Dundee, Scotland, UNITED KINGDOM; [2]"Mario Serio", University of Florence, Firenze, ITALY.

(Session CAA continues on next page)

* *indicates Presenter*

(Session CAA continued from previous page)

3:30P – 3:45P

029 *IN VIVO* SHEAR WAVE ELASTOGRAPHY OF THE RHESUS MACAQUE CERVIX: PRELIMINARY RESULTS AND CHALLENGES. 60

IM Rosado-Mendez[1], LC Carlson[1], QW Guerrero[1], B Huang[1], ML Palmeri[2], H Feltovich[1,3], TJ Hall[1]*
[1]University of Wisconsin-Madison, Madison, WI, USA; [2]Duke University, Durham, NC, USA; [3]Intermountain Healthcare, Provo, UT, USA.

3:45P – 4:00P

042 ULTRASOUND STRAIN MAPPING FOR MEASURING ACHILLES TENDON COMPRESSION IN PATIENTS WITH INSERTIONAL ACHILLES TENDINOPATHY. 61

RL Chimenti[1], AS Flemister[2], J Ketz[2], M Bucklin[1], MR Buckley[1], MS Richards[2].*
[1]University of Rochester, Rochester, NY, USA; [2]University of Rochester Medical Center, Rochester, NY, USA.

4:00P – 4:15P

062 HIGH RESOLUTION PROSTATE MR ELASTOGRAPHY USING EXTRACORPORAL ACTUATION. 62

A. Hoang Dinh[1], R. Souchon[1], S Lounis[3], JM Ménager[3], S Catheline[1], JY Chapelon,[1] O.Rouvière [1,2].*
[1] INSERM U1032, LabTAU, University of Lyon, Lyon, FRANCE; [2] Hospice civil of Lyon, Lyon Est Hospital, Lyon, FRANCE; [3]IRM Lyon-Villeurbanne, Villeurbanne, FRANCE.

4:15P – 4:45P

COFFEE BREAK Meeting Room Iris

Tuesday 4:45P – 5:15P
Session CVE: Cardiovascular Elasticity

Chair: G Cloutier, Canada *Co–Chair: T Payen, USA* Meeting Room Gardenia

Page No.

4:45P – 5:00P

032 VISUALIZING PRINCIPAL STRAINS OF THE COMMON CAROTID ARTERY USING PLANE WAVE IMAGING. 63

R Nayak[1], SJ Huntzicker[1], G Schifitto[2], MM Doyley[1].*
[1]University of Rochester, Rochester, New York, USA; [2]University of Rochester Medical Center, Rochester, New York, USA.

5:00P – 5:15P

043 ULTRASOUND ELASTOGRAPHY FOR ASSESSING ABDOMINAL AORTIC ANEURYSMAL RUPTURE RISK. 64

L Yang[1], CC Johnson[2], N Couper[1], B Zarras[1], D Mix[3], MS Richards[3].*
[1]University of Rochester, Rochester, NY, USA; [2]Rochester Institute of Technology, Rochester, NY, USA; [3]University of Rochester Medical Center, Rochester, NY, USA.

Tuesday 7:00P – 10:00P
Conference Dinner

Augustus Restaurant
Proceedings Book Signing

* *indicates Presenter*

Wednesday, September 23 9:00A – 5:30P

9:00A – 5:00P
Registration Desk Open — Foyer
9:00A – 5:00P Session EEX: Equipment Exhibit — Meeting Room Iris
9:00A – 5:00P Session POS: Posters — Meeting Room Iris

Wednesday 9:00A – 10:07A
Session MPT: Mechanical Properties of Tissues–I
Chair: R Souchon, France *Co–Chair: JL Gennisson, France* Meeting Room Gardenia

Page No.

9:00A – 9:15A

008 4D ULTRAFAST SHEAR WAVE IMAGING. 65
JL Gennisson[1*], J Provost[1], T Deffieux[1], C Papadacci[1], M Imbault[1], M Pernot[1], M Tanter[1].
[1]Institut Langevin, ESPCI, PSL, CNRS, INSERM, Paris, FRANCE.

9:15A – 9:22A

017 ESTIMATION OF POROELASTIC PARAMETERS OF LYMPHEDEMATOUS TISSUE. 66
M. Kaczmarek[1], J. Nowak[1], W. L. Olszewski[2], M. Zaleska[2].*
[1]Kazimierz Wielki University, Bydgoszcz, POLAND; [2]Medical Research Center, Polish Academy of Sciences, Warsaw, POLAND.

9:22A – 9:37A

021 PARA-SPINAL MUSCLES STIFFNESS DISTRIBUTION ON NORMAL SUBJECTS IN STANDING POSISITON. 67
C. L. K Cheng[1], YP Zheng[1].*
[1]The Hong Kong Polytechnic University, Hong Kong, CHINA.

9:37A – 9:52A

030 INFLUENCE OF APPLIED PRESSURE ON 2D SHEAR WAVE ELASTOGRAPHY (SWE) IN A PHANTOM STUDY. 68
K. Skerl[1], B. Eichhorn[2], R. Poltorjanoks[1], B. Jin[1], S. Cochran[1], A. Evans[1].*
[1]University of Dundee, Dundee, Scotland, UK; [2]Schuler-Konstruktionen GmbH, Nuremberg, GERMANY.

9:52A – 10:07A

052 *IN VIVO* QUANTIFICATION OF THE NONLINEAR SHEAR MODULUS IN BREAST LESIONS: FEASABILITY STUDY. 69
M. Bernal[1], F. Chamming's[2], M. Couade[3], J. Bercoff[3], Mickaël Tanter[1], JL Gennisson[1*]
[1]Institut Langevin, ESPCI ParisTech, PSL, CNRS UMR 7587, INSERM, Paris, FRANCE; [2]Radiology Department, Hôpital Européen Georges Pompidou, Paris, France ;[3]Supersonic Imagine, Aix en Provence, FRANCE.

10:10A – 10:45A
COFFEE BREAK — Meeting Room Iris

* *indicates Presenter*

Wednesday 10:45A – 11:07A
Session CMM: Complementary and Multi-Modality Elasticity Techniques
Chair: S Catheline, France *Co–Chair: O Barrera, UK* Meeting Room Gardenia

Page No.

10:45A – 10:52A

034 COMPARING MR AND ULTRSOUND SHEAR WAVE ELASTICITY MEASUREMENTS IN HETEROGENEOUS MEDIA. 70
J.L. Yue[1 2] , M. Tardieu[1], F. Julea[1], L. Leenhardt[3], X. Maître[1], C. Pellot-Barakat[2].*
[1]Univ Paris-Sud, Imagerie par Résonance Magnétique Médicale et Multi-Modalités, CNRS, Orsay, FRANCE; [2]Imagerie Moléculaire *in vivo*, Inserm/CEA/Univ Paris-Sud-CNRS, CEA/I2BM/SHFJ, Orsay, FRANCE; [3]Médecine Nucléaire, APHP, Pitié-Salpétrière, Paris, FRANCE.

Page No.

10:52A – 11:07A

041 THERMAL PROPERTY RECONSTRUCTION VIA REDUCING ULTRASONIC TEMPERATURE MEASUREMENT NOISE USING POLYNOMIAL FITTING METHOD. 71
C Sumi[1].*
[1]Sophia University, Tokyo, JAPAN.

Wednesday 11:07A – 11:37A
Session MMT: Mechanical Measurements Technique for Tissues
Chair: R Souchon, France *Co–Chair: SR Aglyamov, USA* Meeting Room Gardenia

Page No.

11:07A – 11:22A

006 2D TIME HARMONIC ULTRASOUND ELASTOGRAPHY AT LOW FRAME RATES. 72
H Tzschätzsch[1], J Braun[1], I Sack[1].*
[1]Charité - Universitätsmedizin Berlin, Berlin, GERMANY; [2]Medical Informatics, Berlin, GERMANY.

11:22A – 11:37A

065 ACOUSTIC PARTICLE PALPATION: A NOVEL STRESS SOURCE FOR ELASTICITY IMAGING. 73
H Koruk[1,2], A El Ghamrawy[1], AN Pouliopoulos[1], JJ Choi[1].*
[1]Imperial College London, UNITED KINGDOM; [2]MEF University, Istanbul, TURKEY.

Wednesday 11:37A – 12:07P
Session FIP: Forward and Inverse Problems
Chair: O Barrera, UK *Co–Chair: R Souchon, France* Meeting Room Gardenia

Page No.

11:37A – 11:52A

015 AN AUTOMATIC DIFFERENTIATION OF THE 1D VISCOELASTIC GREEN'S FUNCTIONS FOR MAGNETIC RESONANCE ELASTOGRAPHY RECONSTRUCTION IN ANISOTROPIC TISSUE. 74
S Chatelin[1,2], N Corbin[1], I Charpentier[1], J Vappou[1].*
[1]ICube, University of Strasbourg, CNRS, Strasbourg, FRANCE; [2]IHU Institute of Image. Surgery, Strasbourg, FRANCE.

11:52A – 12:07P

053 NUMERICAL SIMULATION OF WAVE PROPAGATION IN SOFT SOLID FOR ULTRASOUND ELASTOGRAPHY. 75
W.Ye [1;3], A.Combescure[1], A.Bel-Brunon[1], S. Catheline[2], M. Rochette[3].*
[1]INSA-Lyon, LaMCoS, FRANCE ; [2] INSERM LabTAU, FRANCE ; [3]ANSYS, FRANCE.

* *indicates Presenter*

Wednesday 12:07P – 12:44P
Session INS–1: Instrumentation including Phantoms – I

Chair: I Sack, Germany *Co–Chair: J Fromageau, UK* Meeting Room Gardenia

Page No.

12:07P – 12:22P

024 SIMULATION AND EVALUATION OF ANISOTROPY ON 2D SHEAR WAVE ELASTOGRAPHY (SWE) IN A PHANTOM STUDY. 76

B. Jin[1], A. Evans[1], X. Zhou[1], S. Cochran[1], K. Skerl[1].*

[1]University of Dundee, Dundee, Scotland, UNITED KINGDOM.

12:22P – 12:37P

037 PRELIMINARY ANALYSIS OF RSNA-QIBA ULTRASOUND SHEAR WAVE SPEED PHASE II PHANTOM STUDY RESULTS. 77

TJ Hall[1], M Palmeri[2], S Chen[3], T Lynch[4], P Carson[5], BS Garra[6,7], A Milkowski[8], K Nightingale[2], N Rouze[2], P Song[3], M Urban[3], K Wear[6], H Xie[9], R Barr[10], V Shamdasani[11], M Macdonald[12], Y Miyajima[13].*

[1]University of Wisconsin, Madison, USA; [2]Duke University, Durham, USA; [3]Mayo Clinics, Rochester, USA; [4]CIRS, Norfolk, USA; [5]University of Michigan, MI, USA; [6]United States Food and Drug Administration, MD, USA; [7]Veterans Administration Hospital, Washington, DC, USA; [8]Siemens Medical Solutions USA, Inc., Ultrasound Division, Mountainview, CA, USA; [9]Philips Research North America, Briarcliff Manor, NY, USA; [10]Radiology Consultants, Youngstown, PA, Inc., USA; [11]Philips Healthcare-Ultrasound, Bothell, WA, USA; [12]GE Healthcare, USA, [13]Toshiba Medical Research Institute USA, Inc., Tustin, CA, USA.

12:37P – 12:44P

046 A MANUFACTURER INDEPENDENT ULTRASOUND ELASTOGRAPHY ADD-ON MODULE. 78

M Salah[1], M Tarek[1], A Sayed[2,3], AM Mahmoud[1]*.*

[1]Cairo University, Giza, EGYPT; [2]Dar Al Fouad Hospital, Giza, EGYPT; [3]Helwan University, Helwan, Cairo, EGYPT.

1:00P – 2:30P

GROUP LUNCH Benacus Restaurant

Wednesday 2:30P – 4:07P
Session MIP–2: Methods for Imaging Elastic Tissue Properties – II

Chair: M Richards, USA *Co–Chair: R De Luca, Italy* Meeting Room Gardenia

Page No.

2:30P – 2:45P

038 HARMONIC MOTION IMAGING FOR ELASTICITY MAPPING OF ABDOMINAL ORGANS *IN VIVO.* 79

T Payen[1], C Palermo[2], S Sastra[2], H Chen[1], Y Han[1], K Olive[2], E E Konofagou[1,3].*

[1]Biomedical Engineering, Columbia University, New York, NY, USA; [2]Herbert Irving Comprehensive Cancer Center, Columbia University, New York, NY, USA; [3]Department of Radiology, Columbia University, New York, NY, USA.

2:45P – 3:00P

049 EFFECTS OF COHERENT COMPOUNDING ON PULSE WAVE IMAGING (PWI) IN PHANTOMS AND *IN VIVO.* 80

IZ Apostolakis[1], RX Li1, MDJ McGarry[1], EA Bunting[1], EE Konofagou[1].*

[1]Columbia University, New York, NY, USA.

3:00P – 3:15P

056 IMPROVING ROTATION ELASTOGRAM QUALITY USING SYNTHETIC APERTURE TECHNIQUE. 81

Lokesh B[1], Bhaskara Rao Chintada[1], A K Thittai[1].*

[1]Indian Institute of technology, Madras, INDIA.

(Session MIP-2 continued on next page)

* *indicates Presenter*

(Session MIP-2 continued from previous page)

3:15P – 3:30P

054 MEASUREMENT OF MOTION IN BRAIN TISSUE AFTER EXCITATION BY A DROP EXPERIMENT. 82

S. Theilenberg[1], J. Bindl[1], A.-L. Kofahl[1], S. Napiletzki[1], B. Schemmann[1], B. Schu-Schätter[1], J. Finsterbusch[2], C. Urbach[1], K. Maier.[1]*

[1]University of Bonn, Bonn, GERMANY; [2]University of Medical Center Hamburg-Eppendorf, Hamburg, GERMANY.

3:30P – 3:45P

058 COMPARABILITY STUDY OF FALL-INDUCED PHASE CONTRAST IMAGES OF PHANTOMS AND THE HUMAN BRAIN. 83

S. Theilenberg[1], J. Bindl[1], A.-L. Kofahl[1], S. Napiletzki[1], B. Schemmann[1], B. Schu-Schätter[1], J. Finsterbusch[2], C. Urbach[1], K. Maier.[1]*

[1]University of Bonn, Bonn, GERMANY; [2]University Medical Center Hamburg-Eppendorf, Hamburg, GERMANY.

3:45P – 3:52P

033 HAND-HELD SOUND-SPEED IMAGING FOR THE RECONSTRUCTION OF BULK MODULUS AND POISSON RATIO IN A COMMERCIAL TISSUE-MIMICKING PHANTOM.. 84

SJ Sanabria[1], CF Otesteanu[1], O Goksel[1]*

[1]Computer Vision Laboratory, Dept. of Inf Tech and Elec Eng, ETH Zurich, SWITZERLAND.

3:52P – 4:07P

064 INVESTIGATING THE RELEVANCE OF STIFFNESS IMAGES OF AN ULTRASOUND TOMOGRAPHY SCANNER. 85

J Fromageau[1], A Messa[1], A D'Aquino[1], M Ledger[1], A Swerdlow[1], N Duric[2,3],M Schmidt[1], E O'Flynn[1] JC Bamber[1].*

[1]Institute of Cancer Research and Royal Marsden NHS Foundation Trust, Downs Road, Sutton, England, UNITED KINGDOM; [2]Karmanos Cancer Institute, Wayne State University, Detroit, Michigan, USA; [3]Delphinus Medical Technologies, Plymouth, Michigan, USA.

4:10P – 4:45P

COFFEE BREAK Meeting Room Iris

Wednesday 4:45P – 5:15P

Session MIP–3: Methods for Imaging Elastic Tissue Properties – III

Chair: JL Gennisson, France *Co–Chair: TJ Hall, USA* Meeting Room Gardenia

Page No.

4:45P – 4:52P

003 EXTENDED SHEAR WAVEFRONT GENERATION USING CUBIC WAVEFRONT MODULATING METHOD. 86

C-Y Huang[1], W-H Cheng[1], C-W Chang[1].*

[1]Industrial Technology Research Institute, Hsinchu, TAIWAN.

4:52P – 5:07P

035 TOTAL-VARIATION REGULARIZATION OF HAND-HELD LIMITED-ANGLE SOUND-SPEED TOMOGRAPHY BASED ON COHERENT REFLECTOR FOR BREAST CANCER DETECTION. 87

SJ Sanabria[1], O Goksel[1].*

[1]Computer Vision Laboratory, ETH Zurich, SWITZERLAND.

5:07P – 5:14P

012 INTRAOPERATIVE STRAIN ELASTOSONOGRAPHY IN BRAIN TUMOR SURGERY. 88

F. Prada [1], L. Mattei[1], A. Moiraghi[2], A. Rampini[2], M. Del Bene[2], F. DiMeco[1].*

[1] Fondazione I.R.C.C.S Istituto Neurologico Carlo Besta, Milan, MI, ITALY; [2] Università Degli Studi Di Milano, Milan, ITALY.

* *indicates Presenter*

5:15P – 5:30P
GROUP PHOTO

After 5:30P No Conference Activities.

9:00A – 5:00P
Registration Desk Open — Foyer
9:00A – 4:30P Session EEX: Equipment Exhibit — Meeting Room Iris
9:00A – 5:00P Session POS: Posters — Meeting Room Iris

Thursday 9:00A – 10:35A
Session CAA–2: Clinical and Animal Applications – II: Liver

Chair: C Filice, Italy *Co–Chair: C Fugazzola, Italy* Meeting Room Gardenia

Page No.

9:00A – 9:20A
075 CLINICAL POINT OF VIEW. 89
C Filice[1].*
[1]University of Pavia, Pavia, ITALY.

9:20A – 9:50A
074 DIFFUSE LIVER DISEASE. 90
G Ferraioli[1].*
[1]University of Pavia, Pavia, ITALY.

9:50A – 10:05A
078 LIVER STEATOSIS 91
*R Lissandrin[1]**
[1]University of Pavia, Pavia, ITALY.

10:05A – 10:25A
077 FOCAL LIVER MASSES: DIFFERENTIATION OF BENIGN FROM MALIGNANT WITH SONOELASTOGRAPHY 92
*S R Wilson[1]*Hojun Yu[2].*
[1]University of Calgary, Foothills Medical Centre, Calgary, CANADA; [2]Queen Elizabeth II Hospital, Grande Prairie AB CANADA.

10:25A – 10:35A Discussion

10:35A – 11:00A COFFEE BREAK — Meeting Room Iris

Thursday 11:00A – 12:30P
Session CAA–3: Clinical and Animal Applications – III: Breast and Thyroid

Chair: V Cantisani, Italy Meeting Room Gardenia

Page No.

11:00A – 11:20A
068 BREAST ELASTOGRAPHY: AN OVERVIEW. 93
RG Barr[1,2].*
[1]Northeastern Ohio Medical University, Rootstown, Ohio, USA; [2]Southwoods Imaging, Youngstown, Ohio, USA.

(Session CAA-3 continues on next page)

* *indicates Presenter*

(Session CAA-3 continued from previous page)

11:20A – 11:40A

070 BREAST CANCER SONOELASTOGRAPHY: CONSIDERATIONS COMING FROM DAILY PRACTICE OF A RADIOLOGIST. 94

*AP Masciotra[1]**

[1]Casa di Cura Villa Maria, Campobasso, ITALY.

11:40A – 12:00P

069 THYROID.ELASTOGRAPHY: AN OVERVIEW. 95

*RG Barr[1,2]**.

[1]Northeastern Ohio Medical University, Rootstown, Ohio, USA; [2]Southwoods Imaging, Youngstown, Ohio, USA.

12:00P – 12:20P

072 SHEAR WAVE AND StRAIN ELASTOGRAPHY IN SUPERFICIAL ORGANS. 96

*V Cantisani[1]**.

[1]Department of Radiological, Oncologic, Pathology Sciences, Policlinico Umberto I, Univ. Sapienza, Rome, VialeReginaElena324, 00197, Rome, ITALY.

12:20P – 12:30P Discussion

Thursday 12:30P – 1:00P
Session INS–2: Manufactures – II

Chair: V Cantisani, Italy Meeting Room Gardenia

12:30P – 12:40P

ESAOTE

12:40P – 12:50P

HITACHI-ALOKA

12:50P – 1:00P Discussion

1:00P – 2:30P

GROUP LUNCH Benacus Restaurant

Thursday 2:30P – 3:20P
Session CAA–4: Clinical and Animal Applications – IV: GI Tract and Pancreas

Chair: P Cabassa, Italy *Co–Chair: G Ferraioli, Italy* Meeting Room Gardenia

Page No.

2:30P – 2:50P

073 US-ELASTOGRAPHY IN THE ASSESSMENT OF PATHOLOGICAL BOWEL WALLS: TECHNICALFEASIBILITY, INTEROBSERVER VARIABILITY AND DISEASE ACTIVITY CORRELATION. 97

Laura Romanini[1], Alessandro Colleoni[2].*

[1]University of Pavia, Pavia, ITALY; [2]University of Brescia, Brescia, ITALY.

2:50P – 3:10P

067 ELASTOGRAPHY OF THE PANCREAS. 98

*L Romanini[1]**.

[1]Pavia, ITALY.

3:10P – 3:20P Discussion

Thursday 3:20P – 3:40P
Session INS–3: Manufactures – III
Chair: P Cabassa, Italy *Co–Chair: G Ferraioli, Italy* Meeting Room Gardenia

3:20P – 3:30P
PHILIPS

3:30P – 3:40P Discussion

Thursday 3:40P – 4:35P
Session CAA–5: Clinical and Animal Applications – V: Prostate & Musculoskeletal
Chair: F Calliada, Italy *Co–Chair: D Cosgrove, UK.* Meeting Room Gardenia

Page No.

3:40P – 4:00P
071 COMPARISON OF STRAIN AND REAL-TIME SHEAR WAVE ULTRASOUND ELASTOGRAPHY IN THE DETECTION AND CHARACTERIZATION OF PROSTATE CANCER. 99
A Goddi[1]*, G Magistretti[1], A Sacchi[1], A Roggia[2], R Novario[3].
[1]SME-Diagnostica per Immagini Medical Center, Vares, ITALY; [2] CAMPUS Medical Center, Varese, ITALY; [3]University Hospital of Varese, Varese, ITALY.

4:00P – 4:20P
076 MUSCULOSKELETAL ELASTOSONOGRAPHY 100
P Minafra[1,], C. Bortolotto[2].*
[1]Euromedic International, Modena, [2]Institute of Radiology, Policlinico S. Matteo - Pavia University, ITALY.

4:20P – 4:30P Discussion

4:30P – 4:50P COFFEE BREAK Meeting Room Iris

Thursday 4:50P – 5:30P
Session CAA–6: Clinical and Animal Applications – VI: General
Chair: F Calliada, Italy *Co–Chair: D Cosgrove, UK.* Meeting Room Gardenia

079 NEW ELASTO TECHNOLOGIES: THE CLINICAL NEED
*RG Barr[1,2]**
[1]Northeastern Ohio Medical University, Rootstown, Ohio, USA; [2]Southwoods Imaging, Youngstown, Ohio, USA.

5:20P – 5:30P
079 CONCLUSIONS
*DO Cosgrove[1]**
[1]Imperial College, Hammersmith, London, UNITED KINGDOM.

Thursday 7:30P – 9:30P
Joint Conference Reception *Proceedings Book Signing* Benacus Restaurant

* *indicates Presenter*

Hitachi Medical Systems. *Zue, SWITZERLAND.*	*Verasonics, Inc.* *Redmond, Washington, USA.*
HITACHI Inspire the Next ALOKA illuminate the change	Verasonics®

* *indicates Presenter*

AUTHOR INDEX

AUTHOR INDEX

Session TUT: Tutorials:

Monday, September 21 12:00P– 2:00P

066 **UNDERSTANDING ELASTOGRAPHY – PHYSICS FOR MDs**

Rémi Souchon[1], Stefan Catheline[1], Olivier Rouvière[1,2]*

[1]INSERM, Lyon, FRANCE; [2]Hospices Civils de Lyon, FRANCE

Up until recently, elastography [1,2] was available in research laboratories only. But in the very last years, elasticity imaging has reached the market, and it is becoming available to the non-specialist. Making good use of modern imaging modalities (CT, Doppler, MRI, PET) requires some education about the underlying physics. The same observation holds true for elastography.

This tutorial aims at providing physicians with an understanding of the physics involved in elastography, and with an overview of existing techniques.

It will take you through:
- a short historical overview,
- a brief introduction to mechanics
(strain, stress, compression waves, shear waves, Young's modulus, shear modulus)

Then we will focus of commercially available techniques:
- ultrasound strain imaging
- shear wave imaging
- magnetic resonance elastography (MRE)

We will also address some of the issues the user needs to be aware of when using elasticity imaging, or when reading / analyzing literature related to the field:
- Mechanical models
- Frequency and viscosity
- Precompression and nonlinearity
- Scale, wavelength, and resolution
- Guided waves

We will finally conclude with novel techniques that may be present in your scanner in the near future.

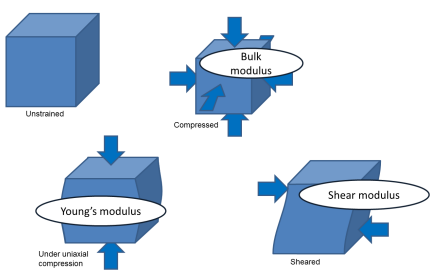

References: [1] Bamber J et al. EFSUMB Guidelines and Recommendations of the Clinical Use of Ultrasound Elastography. Part 1: Basic Principles and Terminology. Ultraschall in Med 2013; 34:169-184. [2] Shiina T et al. WFUMB Guidelines and Recommendations for Clinical Use of Elastography: Part 1: Basic Principles and Terminology. Ultrasound in Med & Biol 2015, 41(5): 1126-1147.

019 **UNMET NEEDS IN LIVER IMAGING: A CLINICAL PERSPECTIVE.**

An Tang[1,2], Guy Cloutier[1,3].*

[1]University of Montreal Hospital Research Center, Montreal, Quebec, CANADA; [2]University of Montreal Hospital Center, Montreal, Quebec, CANADA; [3]Laboratory of Biorheology and Medical Ultrasonics, Montreal, Quebec, CANADA.

Background: Over the past two decades, ultrasound-based and MR-based elastography techniques have evolved from investigational prototypes to clinical tools used for patient care. The main clinical indication of elastography in the abdomen is detection and staging of liver fibrosis [1]. Depending on the clinical setting and indication, different modalities may be preferred according to their respective strengths and limitations [2]. Technical innovations in liver elastography should target unsolved clinical problems not addressed by current imaging techniques.

Aims: (1) To provide an educational primer on liver imaging from a clinical perspective. (2) To provide an overview of diffuse and focal liver disease. (3) To highlight unmet clinical needs in liver imaging and barriers to adoption.

Methods: In this educational lecture, we will discuss the investigation of patients with diffuse and focal liver disease from the perspective of a radiologist specialized in liver imaging. This talk will succinctly review the clinical workflow, provide a classification of diffuse and focal liver disease, confounders of diagnostic performance, technical confounders, and cost-effectiveness.

Results: We will: (1) discuss the clinical settings in which patients are imaged for liver disease (incidental finding, screening, surveillance, diagnosis, staging, assessment of transplant eligibility, treatment planning and monitoring of treatment response) and the implications on the type of imaging technique favored; (2) provide a classification of diffuse liver disease by highlighting the key histological features (fibrosis, inflammation, fat, iron or biliary anomalies) that characterize each disease; (3) provide a classification of focal liver disease, including common benign and malignant tumors; (4) briefly discuss factors that influence estimates of diagnostic accuracy (spectrum bias, misclassification penalty, disease heterogeneity); (5) highlight technical factors that confound liver elastography measurements (breathing, central venous pressure, hepatic venous congestion, fasting vs. postprandial state); (6) discuss the need for cost-effectiveness in medicine by emphasizing the requirements for screening techniques (low-cost, wide availability, high sensitivity) vs. those for diagnostic techniques (high specificity, reproducibility).

Conclusions: The clinical setting in which liver disease is investigated influences the choice of imaging modality. Existing imaging techniques permit broad classification of diffuse and focal liver disease. Key clinical challenges include differentiation of inflammation from fibrosis, characterization of hepatocellular adenomas subtypes, and differentiation of cholangiocarcinoma from hepatocellular carcinoma. Further, reduction of stiffness variability due to technical factors would facilitate adoption of mechanical biomarkers for monitoring of liver disease. Beyond technical performance and diagnostic accuracy, the choice of elastography techniques also depends on logistical considerations and cost-effectiveness.

Acknowledgements: Dr An Tang receives funding for research activities on ultrasound elastography and MR elastography from the Canadian Institutes of Health Research - Institute of Nutrition, Metabolism, and Diabetes (CIHR-INMD #273738 and #301520); a New Researcher Startup Grant from the Centre de Recherche du Centre Hospitalier de l'Université de Montréal (CRCHUM); and a Junior 1 Career Award from the Fonds de recherche du Québec en Santé and Association des Radiologistes du Québec (FRQS-ARQ #26993).

References: [1] Cosgrove D, Piscaglia F, Bamber J, et al. EFSUMB guidelines and recommendations on the clinical use of ultrasound elastography. Part 2: Clinical applications. *Ultraschall Med*. 2013;34(3):238-53.
[2] Tang A, Cloutier G, Szeverenyi NM, Sirlin CB. Ultrasound Elastography and MR Elastography for Assessing Liver Fibrosis: Part 2, Diagnostic Performance, Confounders, and Future Directions. *AJR Am J Roentgenol*. 2015:1-8.
[3] Zhang E, Wartelle-Bladou C, Lepanto L, Lachaine J, Cloutier G, Tang A. Cost-utility analysis of nonalcoholic steatohepatitis screening. *European Radiology*. 2015:1-13.

* *indicates Presenter*

005 **TOMOGRAPHIC MAGNETIC RESONANCE ELASTOGRAPHY BY MULTIFREQUENCY WAVE NUMBER INVERSION.**

Heiko Tzschätzsch[1], Jing Guo[1], Florian Dittmann[1], Jürgen Braun[2], Ingolf Sack[1].*
[1]Charité - Universitätsmedizin Berlin, Departments of Radiology, Charitéplatz 1, Berlin, GERMANY; [2]Medical Informatics, Hindenburgdamm 30, Berlin, GERMANY.

Background: In MR elastography (MRE) stiffness maps are generated by local frequency estimation [1], direct algebraic Helmholtz inversion (AHI) [1], finite element methods [2] or multi-frequency direct inversion [3]. Latter method, multifrequency dual elastic visco (MDEV) inversion, has been used for calculating high resolution elastograms with pixel-wise resolved anatomical details of elasticity and viscosity [4]. Despite large improvements in the resolution capacity of MRE by MDEV inversion, multifrequency based elastograms still suffers from noise with respect to the consistency and reproducibility of values [5].

Aim: To overcome current limitations of MRE with respect to detail resolution and consistency of elastograms by noise-robust MDEV inversion.

Methods: The new algorithm retrieves wave numbers k of multifrequency shear wave fields by first-order derivative operators, henceforth referred to as k-MDEV. In a first step, k-MDEV requires in-plane Gauss-smoothing of raw (complex-valued) MRI images prior to phase unwrapping and temporal Fourier-transformation. In a second step, twelve radial spatio-temporal filters including a linear high-pass in 2D k-space are used for extracting the harmonic plane shear waves. The wave numbers recovery by eq. (1) yields for voxel position x,y,z with varying frequency ω_i wave field components j and wave direction n:

$$k'_j(x,y,z,\omega_i,n) = \left\| \nabla \left(\frac{u_j(x,y,z,\omega_i,n)}{|u_j(x,y,z,\omega_i,n)|} \right) \right\| \qquad (1),$$

$$\frac{1}{c(x,y,z)} = \frac{\sum_{i,j,n} \frac{k'_j(x,y,z,\omega_i,n)}{\omega_i} w}{\sum_{i,j,n} w} \qquad (2)$$

Since the quality of k'_j-maps depends on the degree by which the shear waves penetrated into the tissue, eq. (2) accounts for wave amplitudes $|u|$ by a mean amplitude weight with exponent 4: $w = |u_j(x,y,z,\omega_i,n)|^4$.

Results: Figure 1 shows wave speed- (c)-maps produced by classical single-frequency MRE (60 Hz), MDEV-inversion based multifrequency MRE and the proposed k-MDEV inversion based MRE in a transversal slice through the abdomen of a healthy volunteer. Especially in deeper areas where shear waves are more damped, the new method produces consistent c-values enabling us to analyze multiple types of tissue from the same scan. Within the shown image we identified the liver (left lobe, right lobe, caudal lobe), the spleen, the kidney (renal cortex, hillus), the intervertebral disk, spinal cord, stomach, muscle, and subcutaneous fat. The obtained wave speed values are close to the values published in the literature of multifrequency MRE of the liver [4], the kidney [6] and the intervertebral disk [7].

Conclusions: The resolution of anatomical details by k-MDEV based MRE resembles that of a tomographic modality like MRI, however, providing a quantitative and biophysical based image contrast.

References: [1] Manduca A et al.: Med Image Anal, 7(4): pp. 465-473, 2003. [2] Van Houten E et al.: Magn Reson Med, 42: pp. 779-786, 1999. [3] Papazoglou S et al.: Phys Med Biol, 53: pp. 3147-3158, 2008. [4] Hirsch S et al., Magn Reson Med, 71: pp. 267-277 2013. [5] Guo J et al.: PlosOne 8(8):e71807. [6] Streitberger J et al.: J Biomech, 47(3): pp. 639-44, 2014. [7] Streitberger J et al.: Magn Reson Med, doi: 10.1002/mrm.25505, 2014.

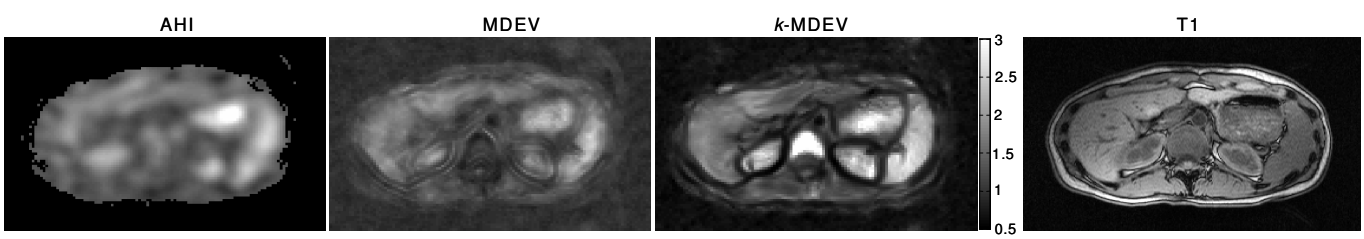

Figure 1. Shear wave speed-maps obtained by algebraic Helmholz inversion (AHI), MDEV-inversion, and k-MDEV-inversion compared to an anatomical high-resolution T1-weighted MRI scan of same slice position.

007 **IMPROVING BRAIN TUMOR SURGERY USING INTRA-OPERATIVE SHEAR WAVE ELASTOGRAPHY AND ULTRASENSITIVE DOPPLER.**

Marion Imbault[1]*, Dorian Chauvet[2], Laurent Capelle[2], Charlie Demené[1], Mathieu Mossad[1], Carine Karachi[2], Anne-Laure Boch[2], Jean-Luc Gennisson[1], Mickaël Tanter[1].

[1]Institut Langevin, ESPCI ParisTech, CNRS UMR 7587, Paris, FRANCE ; [2] Pitié Salpêtrière Hospital, Neurosurgery Department, Paris, FRANCE.

Background: Improving quality of brain tumor resection is a major concern for neurosurgeons. Shear Wave Elastography (SWE) and ultrasensitive Doppler could be decisive in this issue. By giving access to tissue stiffness, SWE is an emerging technology that enables surgical procedure guidance [1]. A clinical study was undertaken, including normal brain and tumors, collecting data using intraoperative SWE and ultrasensitive Doppler.

Aims: The aim of this study is to improve shear wave imaging for brain tissue investigation by correlating in vivo stiffness data and histology. At the same time micro blood flow was studied in vivo during surgery by using a new ultrasensitive Doppler mode.

Methods: Shear waves were generated by using ultrasonic acoustic radiation force, and imaged in real-time with a linear array driven by an ultrafast ultrasound scanner (Aixplorer, Supersonic Imagine) up to 20000 frames/s. The study was then performed intra-operatively on 63 adult patients presenting with brain tumors. While stiffness measurements were systematically compared to histology, micro blood flow close to the tumor was also studied by using ultrasensitive Doppler mode.

Results: Histology allows classification of the different types of brain tumor into four main groups: meningiomas (N=16), low-grade gliomas (N=14), high-grade gliomas (N=18) and metastases (N=15). SWE was able to characterize each group of tumor by a mean elasticity value, respectively: 33.1 ± 5.9 kPa (3.3 ± 0.6 m/s), 23.7 ± 4.9 kPa (2.8 ± 0.6 m/s), 11.4 ± 3.6 kPa (1.9 ± 0.6 m/s) and 16.7 ± 2.5 kPa (2.4 ± 0.4 m/s) (cf. Fig. 1.). Statistical analysis using ROC curve analysis shows that SWE could help for diagnosis during tumor resection by distinguishing benign tumors (meningiomas, low grade-gliomas) from malignant tumors (high-grade gliomas, metastasis) (AUROC: 0.77, $p<0.0001$). Regarding the use of ultrasensitive Doppler during surgery, it enhanced blood volume visualization and thus reduced hemorrhage by improving small vessel localization.

Conclusions: The combination of these two techniques, by giving access to both mechanical properties and blood flow, can improve quality of brain tumor resection and consequently patients' quality of life.

Acknowledgements: The research leading to these results has received funding from the European Research Council under the European Union's Seventh Framework Programme (FP7/2007-2013) / ERC grant agreement n° 339244-FUSIMAGINE. This work was also partly supported by the Agence Nationale de la Recherche under the program "Future Investments" with the reference Laboratory of Excellence ANR-10-LABX-24 LABEX WIFI within the French Program "Investments for the Future" under reference ANR-10-IDEX-0001-02 PSL and the program "Investissements d'avenir" ANR-10-IAIHU-06..

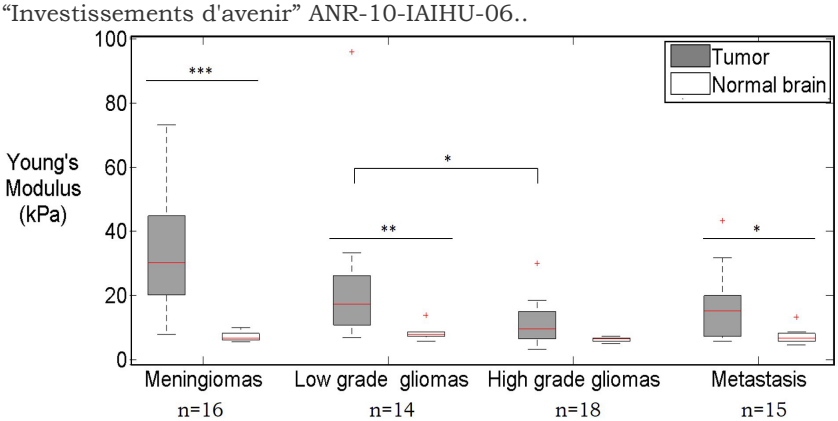

Fig. 1. Young's Modulus in kPa of both tumor and normal brain for the four analyzed types of tumors, meningiomas, low-grade gliomas, high-grade gliomas and metastasis. For each category the n represent the number of patients. * $p<0.05$, ** $p<0.01$, *** $p<0.001$ stand for each type of tumor for the p value between normal brain and tumor. The star (*) between low-grade and high grade gliomas stand for the p-value between this two tumorous tissue.

Reference:

[1] Chan et al.: 2014. A novel technique of detecting MRI-negative lesion in focal symptomatic epilepsy: Intraoperative ShearWave Elastography. Epilepsia n/a–n/a. doi:10.1111/epi.12562

* *indicates Presenter*

009 **STORAGE AND LOSS MODULI IMAGING IN SOFT SOLIDS USING SUPERSONIC SHEAR IMAGING TECHNIQUE.**

Eliana Budelli[1,2], Javier Brum[3] , Miguel Bernal[1] , Thomas Deffieux[1] , Mickael Tanter[1], Carlos Negreira[3], Jean-Luc Gennisson.[1]*

[1] Institut Langevin, ESPCI ParisTech, PSL Research University, CNRS UMR 7587, INSERM, Paris, FRANCE; [2] Instituto de Ingeniería Química, Facultad de Ingeniería, Universidad de la República, Montevideo, URUGUAY; [3] Laboratorio de Acústica Ultrasonora, Instituto de Física, Facultad de Ciencias, Universidad de la República, Montevideo, URUGUAY

Background: Non-invasive evaluation of rheological behavior of soft tissues may provide an important diagnosis tool. In order to fully characterize the rheological behavior through storage (G') and loss (G") moduli, it is necessary to estimate both shear wave velocity (V) and attenuation (α). This is not possible using the available commercial ultrasound systems, since they only provide shear elasticity estimation by shear wave speed assessment. Moreover, as the generated shear waves in the commercial mode are not plane, a diffraction correction is needed in order to estimate α. With this end, Deffieux et al [1] and Nenadic et al [2] proposed to use of a cylindrical wave approximation to correct for diffraction effects.

Aims: The aim of this work is twofold: first to study numerically and experimentally the validity of the cylindrical wave approximation. Second, to use it to image V and α, and consequently G' and G", in an isotropic viscoelastic medium.

Methods: A Green's function algorithm (anisotropic and viscoelastic) [3] was carried out to establish numerically the validity of the cylindrical approximation. Then, experimental validation was conducted in an agar-gelatin phantom generating shear waves in two different ways: 1/By using a vibrating plate at different frequencies (100-600 Hz) as plane shear wave source (Transient elastography technique TE). 2/By using the radiation force of ultrasound as cylindrical shear wave source (Supersonic Shear Imaging (SSI) technique). In both cases, the shear wave propagation was acquired with an ultrafast ultrasound scanner (Aixplorer, Supersonic Imagine(SI), France) driving an 8MHz probe (SL 15-4, SI, France). V_{TE},V_{SSI} and α_{TE} at each frequency were recovered from the phase and amplitude decay versus distance respectively and were used as reference values. α_{SSI} was calculated applying the diffraction correction when suitable. Finally, experiments were carried out using the SSI technique in a two layered phantom with the same stiffness but different attenuation. One layer was made by adding 10% glycerol to the agar-gelatin mixture in order to increase G''.

Results: Numerical results proved the cylindrical wave approximation to be valid in the center of the pushing line and at distance x equivalent to k*x >1, being k the shear wave number. Under these conditions, we found experimentally, for example at 300Hz, a corrected $\langle\alpha_{SSI}\rangle$ = 44±6 Np/m in good agreement with α_{TE} = 46±2 Np/m. Finally, for the two layered phantom (Fig.1) images of G' and G" were calculated from V_{SSI} and the corrected α_{SSI} images at 300 Hz by using the expressions in [4]. A difference of 50% in the mean values of G'' was observed between the left (no glycerol) and right (10% glycerol) side of the image.

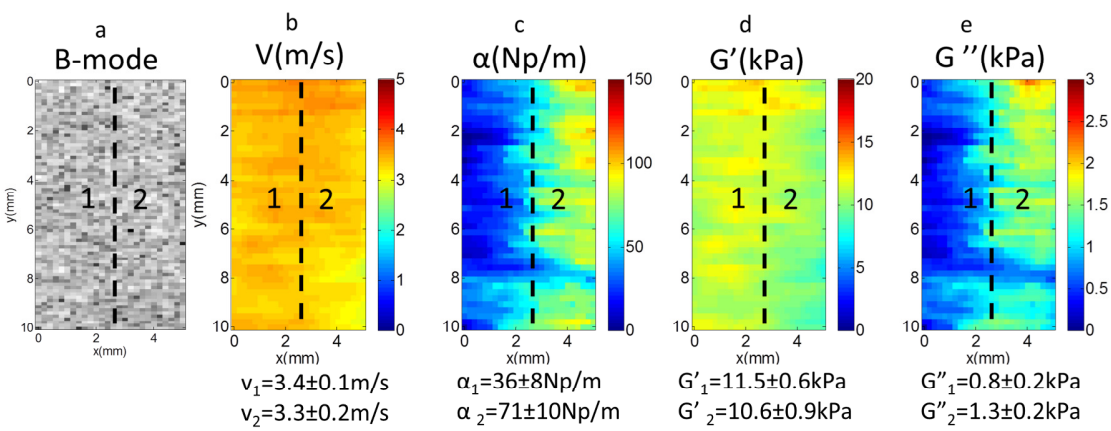

Fig 1. (a)B-mode, (b) velocity, (c) attenuation, (d) G' and (e) G'' images for the two layered phantom. The dashed line indicates the boundary between the two layers Left layer 0% glycerol- Right layer 10% glycerol

Conclusions: We demonstrated numerically and experimentally that the cylindrical correction is valid under certain conditions. Under these conditions G' and G" images were successfully calculated for a heterogeneous viscoelastic medium. From G' and G'', elasticity and viscosity images may be deduced using any chosen rheological model.

Acknowledgements: Project ECOS-Sud U14S04, CAMPUS-Fance, Programa Grupos I+D CSIC- UdelaR

References: [1] Deffieux et al. : IEEE TMI 2009, [2] Nenadic et al., IEEE IUS 2014, [3] Chatelin PMB 2015 et al., [4] Gennisson et al., UMB 2006.

010 ***IN VIVO* TRANSTHORACIC CARDIAC SHEAR WAVE ELASTOGRAPHY USING ULTRAFAST HARMONIC COHERENT COMPOUND IMAGING**

Mafalda Correia[1], Jean Provost[1], Simon Chatelin[1], Olivier Villemain[1], Mickael Tänter[1], Mathieu Pernot[1].*

[1]Institut Langevin, ESPCI, PSL, CNRS, INSERM, 1 rue Jussieu, Paris, FRANCE.

Background: Shear Wave Elastography Imaging (SWEI) is a non-invasive ultrasound technique for quantitative elasticity mapping. However, transthoracic shear wave elastography of the myocardium remains a challenge due to imaging artifacts, as clutter noise, phase aberration or ultrasound reverberations. Recently, different techniques have been proposed to improve cardiac shear wave propagation detection: Pulse-Inversion (PI) Harmonic Shear Wave Elastography [1], and Ultrafast Coherent Diverging-wave Compound Imaging [2], by limiting reverberation and clutter noise artifacts and by increasing the field-of-view and signal-to-noise ratio (SNR) respectively.

Aims: In this study, we present Ultrafast Harmonic Coherent Compounding Imaging, a technique that couples PI Harmonic Imaging, using a sliding-window approach, to Ultrafast Coherent Compound Imaging using diverging-waves transmission. Our technique allows to increase shear wave propagation detection, at high frame rate and high field-of-view, outperforming both Ultrafast Coherent Diverging-wave Compound Imaging and PI Imaging alone.

Methods: An Aixplorer system (Supersonic Imagine, France) was used to perform Ultrafast Harmonic Coherent Compound SWEI acquisitions. *In vivo* transthoracic cardiac experiments were performed in healthy volunteers (N=6) through a parasternal short axis view, using a 2.75-MHz linear phased-array probe (Vermon S.A., France). Shear waves were generated during end-diastole on the left-ventricular wall by acoustic radiation force ($MI_{0.3}$ = 1.8, $Ispta_{0.3}$ < 154 mW/cm^2). One to three harmonic diverging-waves were spatially coherently compounded at Frame-Rate Imaging > 1480 frames/s. Shear wave speeds (cs) were estimated through linear least-squares fit of temporal 1-D cross-correlation applied on spatiotemporal tissue velocity images.

Results: Figure 1 presents the spatiotemporal axial tissue displacements images averaged within 3-mm depth at the myocardial wall center for one of the six volunteers. In most cases, Pulse-Inversion Harmonic SWEI alone, without diverging-wave coherent-compounding, not detected discernable shear wave propagation. For all volunteers, Ultrafast Harmonic Coherent Compound showed higher consistence for shear wave motion tracking, higher SNR, and a more accurate shear wave speed estimation.

Conclusions: This approach combines spatial-compounding and pulse-inversion harmonic imaging advantages, such as high frame rate acquisitions and imaging artifacts reduction, essential to improve *in vivo* human transthoracic myocardial SWEI for quantitative stiffness mapping.

Acknowledgements:

This work was supported from European Research Council grant under the European Union's Seventh Framework Program (FP/2007-2013)/ ERC Grant Agreement n° 311025.

References:

[1] P. Song, et al.: IEEE Trans Med Imaging, 2013.

[2] C. Papadacci, et al.: IEEE Trans Ultrason Ferroelectr Freq Control, 2014.

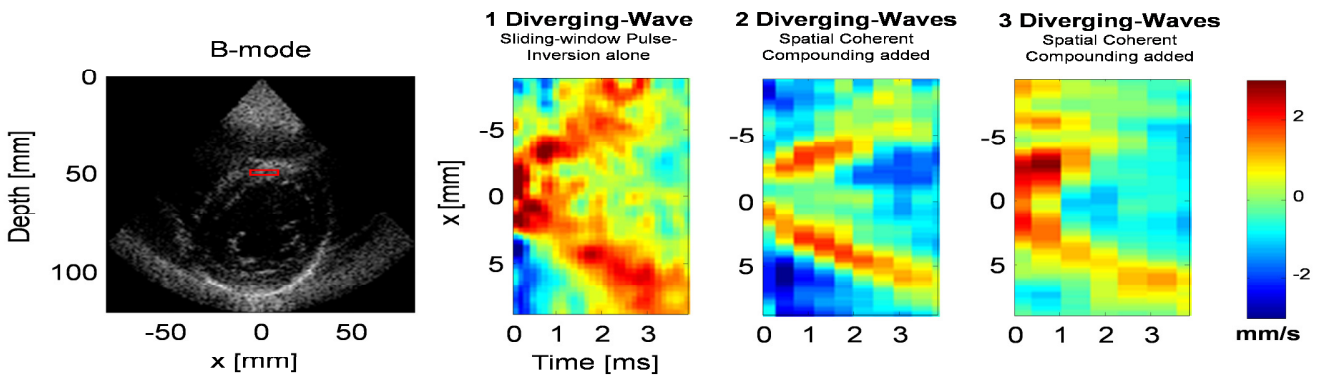

Figure 1

* *indicates Presenter*

013 **ACCURACY OF ARTERIAL SHEAR WAVE ELASTOGRAPHY BY PHASE VELOCITY ANALYSIS – VALIDATION WITH MECHANICAL TESTING IN PHANTOMS.**

E Maksuti[1,2], D Larsson[1], E Widman[1,2], MW Urban[3], M Larsson[1,2], A Bjällmark[1,2].*
[1]KTH Royal Institute of Technology, Stockholm, SWEDEN; [2]Karolinska Institutet, Solna, SWEDEN; [3]Mayo Clinic College of Medicine, Rochester, MN, USA

Background: Arterial stiffness is an independent risk factor shown to correlate with a wide range of cardiovascular diseases. Shear Wave Elastography (SWE) by phase velocity analysis, i.e. taking geometrical dispersion into account, has been suggested to quantitatively measure local arterial shear modulus [1,2]. However, an accuracy assessment of the technique by comparison with a reference method has not been previously performed.

Aims: The aim of this study was to assess the accuracy of SWE by phase velocity analysis in pressurized arterial phantoms and compare the results with mechanical testing.

Methods: Nine carotid artery phantoms (length = 10 cm, inner diameter = 0.6 cm, wall thickness = 0.3 cm) with different stiffness were constructed (10% poly(vinyl alcohol), 3% graphite) by exposing the solution to three, four or five freeze-thaw cycles (12h-12h, three phantoms for each condition), where a higher number of cycles corresponds to a stiffer material. The phantoms were inserted into a specifically designed enclosure, surrounded by water, connected to a water column generating four different static intraluminal pressures (60, 80, 100 and 120 mmHg) and pre-stretched (Figure 1a). The radiation force generation and the ultrafast imaging were performed with an Aixplorer system (Supersonic Imagine, France) with a customized research package. The in-phase and quadrature data were processed to track the shear wave propagation using a two-dimensional autocorrelation algorithm and Fourier analysis was used to derive the dispersion curve, i.e. phase velocity as a function of frequency. The phase velocity data were fitted to an antisymmetric zero-order Lamb wave model (for frequencies greater than 500 Hz) from which the shear modulus was estimated. For comparison, the arterial phantoms were mounted on the mechanical testing device Instron 5567 (Instron, Norwood, MA, USA) by means of customized end fixtures, pre-stretched and pressurized, in order to mimic the same loading conditions as for the SWE measurements.

Results: SWE measurements based on phase velocity analysis showed good agreement with mechanical testing (Figure 1b), with relative error between the two techniques equal to 8.8 ± 6.0 % in the evaluated stiffness range (40-100 kPa). The relative error did not significantly vary between measurements when grouped for different values of intraluminal pressure, freeze-thaw cycles or region of interest placement between the anterior and posterior phantom wall.

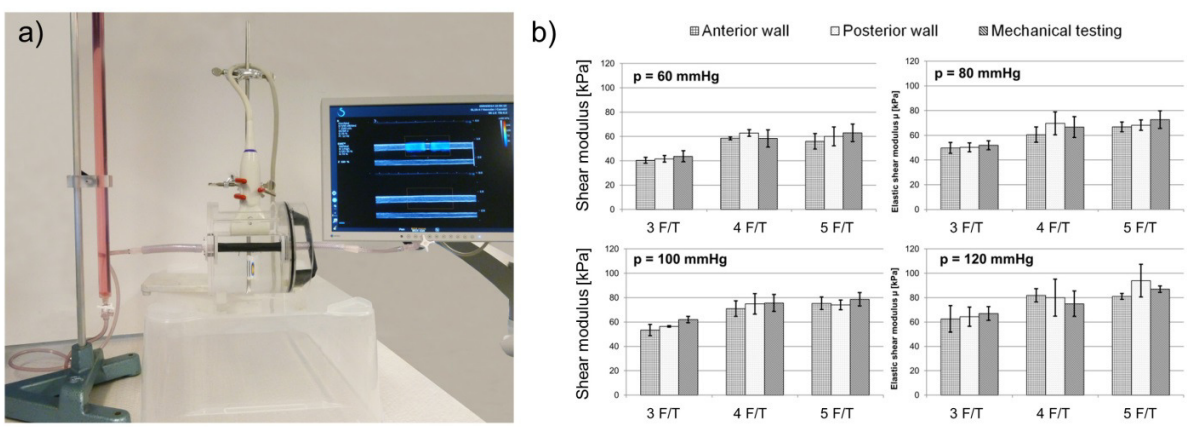

Figure 1 - (a) Shear wave elastography (SWE) acquisition setup. (b) Comparison of shear moduli for the anterior and posterior wall of the arterial phantoms for different freeze/thaw (F/T) cycles at different values of intraluminal pressure measured with SWE and mechanical testing.

Conclusions: Results from this study showed that SWE by phase velocity analysis can accurately measure stiffness in arterial phantoms when validated against mechanical testing.

Acknowledgements: The study was supported by VINNOVA VINNMER Marie Curie International qualification grant 2011-01365 and the Swedish Research Council grant 2012-2795.

References: [1] Couade M, et al.: Quantitative assessment of arterial wall biomechanical properties using shear wave imaging. Ultrasound Med Biol 2010; 36:1662–76. [2] Bernal M, et al. Material property estimation for tubes and arteries using ultrasound radiation force and analysis of propagating modes. J Acoust Soc Am 2011; 129:1344–54.

022 **A RESOLUTION STUDY IN PASSIVE ELASTOGRAPHY**.

A Zorgani[1],R Souchon[1],S Catheline[1].*

[1]LabTAU U1032, INSERM, Lyon, FRANCE.

Background: Early cancer diagnosis is an important issue in oncology and medical imaging. The ability of the imaging systems to detect small cancer nodules depends on their spatial resolution. Shear wave elasticity imaging techniques known as elastography, have already shown their ability to locally retrieve the tissue elasticity and therefore suspicious nodules. The resolution of shear wave elastography is investigated in this presentation. Shear waves are generally generated by external sources (radiation force or mechanical shakers). In Passive Elastography, no source is used. It is based on the correlation of the physiological noise-like shear wave field induced by muscles activity, heart beating, and blood pulsatility.

Aims: This work aims to evaluate the spatial resolution of passive elastography and to compare it to the resolution of ultrasound on B-Mode imaging.

Methods: The experiments were conducted on a homemade gelatin phantom. Inclusions with different elasticities imbedded in the phantom were obtained by changing the concentration of gelatin. A random shear wave field is generated in the sample with multiple magnetic shakers. In a first step, using standard speckle tracking algorithm, the displacement field is measured inside the sample at a high frame rate (1000 frames/second) using 5, 10 and 20 MHz? ultrasound probes connected to an ultrafast Verasonics® Vantage ultrasound scanner. Then with algorithms based on spatiotemporal noise correlation, local shear wave speed maps are retrieved.

Results: Shear wave speed maps are presented (fig 1.c and d) and compared to the B-Mode images (fig 1.a and b). The contrast in the elasticity maps enables to clearly distinguish both small inclusions with a diameter of 4.5 mm and spaced with 2.5 mm from the background (fig 1.d), and a triangle edge of 2.5 mm (fig 1.c). Other results using different frequencies of ultrasound probes - which changes the spatial resolution of the imaging system were tested and will be presented. They all indicate that a resolution much smaller than the shear wavelength of ≈1.5cm is observed.

Conclusions: This study shows that, with an unchanged shear wave field, resolution increases with the ultrasound frequency. It demonstrates that elastography is not limited by the shear wavelength but by the resolution of the imaging system.

References:

. [1] S. Catheline, et al.: (2013). Tomography from diffuse waves: passive shear wave imaging using low frame rate scanners, Appl. Phys. Lett. 103, 014101.

. [2] R. Righetti et al.: (2002). Axial resolution in elastography. Ultrasound in Medicine & Biology, 101-113.

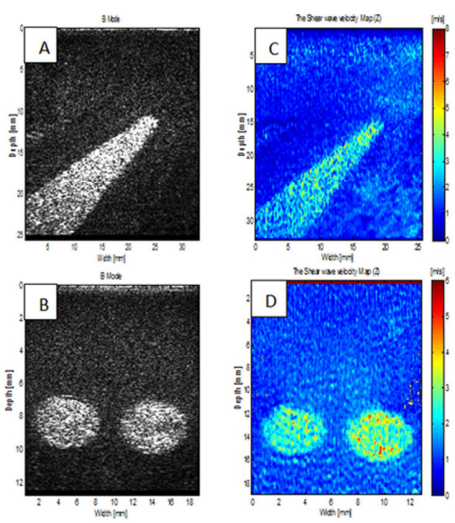

Fig 1. (A) and (B) Sonograms showing inclusions. (C) and (D) Shear wave speed maps. The contrast of the shear wave speed shows clearly the inclusions.

* *indicates Presenter*

059 **QUANTITATIVE POROELASTIC PROPERTY IMAGING COMBINING SHEAR WAVE AND STRAIN ELASTOGRAPHY.**

M Theodorou[1,] J Fromageau[1,2,] N deSouza[1,2,] , JC Bamber[1.]*

[1]Cancer Research UK Cancer Imaging Centre, Sutton, London, UNITED KINGDOM; [2]Royal Marsden NHS Foundation Trust, Sutton, London, UNITED KINGDOM

Background: Soft tissue contains mobile fluid that creates a time-dependent and spatially-varying internal strain field under sustained compression [1], which may be imaged dynamically by repeated scanning with ultrasound (US). The resulting technique, known as poroelastography [2], allows the measurement of the product of the tissue's aggregate modulus and permeability, H_Ak, and its Poisson's ratio, ν [1].

Aims: The aim of this study was to evaluate the potential of simultaneous dynamic imaging with shear wave elastography and strain elastography to separate the components of H_Ak, and therefore to recover k, independently of ν and Young's modulus, E.

Methods: Poroelastic phantom experiments were performed using an Aixplorer® US scanner (SuperSonic Imagine) and a linear array US transducer (SL15-4) with central frequency 7.5 MHz. Cylindrical samples made of agarose gel (type I-B and VI, Sigma-Aldrich), with concentrations ranging from 1.5% (w/v) to 7% (w/v), were subjected to a sustained axial compression (Instron 3342®) under computer control. The fluid-rich gels were scanned with the US beam aligned along their radial direction. Initial global axial strains of either 3% or 7% were applied over a time interval of 1 s. A frame rate of 1 transmit-focused radiofrequency (RF) echo image per second was used to capture the early and rapidly changing part of the relaxation. The frame rate was then decreased to 1 image every 20 s, for a total data acquisition time of 60 min. Two-dimensional cross-correlation RF echo-tracking was performed between the last pre-compression frame and all subsequent frames, followed by linear least-squares strain estimation, providing strain relative to the instant before compression. Images of ν and the product H_Ak were produced by fitting the time-dependent strain data to a poroelastic model. The supersonic shear imaging (SSI) [3] mode of the scanner was used to monitor the E of each sample by acquiring elasticity maps interleaved between the echo images.

Results: By combining the mean pixel values of the H_Ak, ν and E maps, the permeability of agarose was extracted with an estimated uncertainty of ± 5.8%. The E of the sample was observed to decrease during the 1 hour of relaxation from an initial value of 111.5 to a final value of 107 ± 24 KPa and from 119.4 to 107.1 ± 14 KPa, for 3% and 7% applied strain respectively. These changes could be due to the nonlinear response of agarose, pore size variation and/or the absence of perfect slip boundary conditions. Nevertheless, they are negligible relative to a 72.3% change in radial strain that was observed over the same time period and was associated with the poroelastic response.

Conclusions: With further development, this quantitative technique could enable a more complete characterization of the poroelastic behavior of soft tissue for tumour diagnosis, treatment stratification and monitoring response.

References:

[1] GP Berry et al.: Ultra Med Biol., 32, 2006b.
[2] E Konofagou et al.: Ultra Med Biol., 27, 2001.
[3] M Tanter et al.: Ultra Med Biol., 34, 2008.

011 **INTERVENTIONAL MAGNETIC RESONANCE ELASTOGRAPHY FOR THE MONITORING OF MR-GUIDED PERCUTANEOUS THERMAL ABLATIONS**

Nadège Corbin[1], Elodie Breton[1], Michel de Mathelin[1], Jonathan Vappou[1].*
[1]ICube, Université de Strasbourg, CNRS, IHU Strasbourg, Strasbourg, FRANCE..

Background: Monitoring of percutaneous thermal ablations is essential in order to ensure complete destruction of the tumor and to avoid damage to healthy surrounding tissue. MR-thermometry is currently the gold standard for the monitoring of MR-guided ablations in real-time. However, temperature does not provide a direct information about tissue structural integrity while thermal ablations have been shown to result in an increase of shear modulus [1]. Measuring mechanical properties in real-time could therefore improve the monitoring of thermal ablations.

Aims: We propose a dedicated interventional MRE (iMRE) method aiming at providing elasticity maps in real-time for better monitoring of MR-guided percutaneous thermal ablations.

Methods: Experiments were carried out on a 1.5T interventional MRI system. A complete system was developed specifically for interventional MRI. A piezoelectric actuator is mounted on the needle used for a specific percutaneous procedure in order to generate a shear wave directly within the region of interest. The displacement induced by the needle MRE driver is encoded by an interactive spoiled gradient echo sequence (based on Beat-IRT, Siemens, Germany) with motion encoding. Slice position and orientation can be changed without interrupting the acquisition. Fractional encoding [2] allows reducing the repetition time to one mechanical excitation period. Preliminary experiments [3] have shown that the use of 3 phase difference images with different delays between excitation and encoding provides similar elastogram quality while decreasing significantly the acquisition time compared to the conventional 4 phase-offsets protocol. In order to increase the refresh rate, a sliding window method is implemented: the first elastogram is reconstructed with the first 3 phase difference images, the following elastograms are reconstructed with each new phase difference image and the 2 previous ones. A Local Frequency estimation[4]-based algorithm is applied in real-time on the resulting data.

Results: Feasibility and stability of iMRE were demonstrated in vivo in swine at 100 Hz with a variation of 5% over 30 elastograms acquired during one breath hold of 80 s (Fig.1). Ability to monitor elasticity changes was assessed in real-time on a hardening gel using a refresh rate of one elastogram every 2 s (Fig.2). Temperature and shear modulus [5] were followed in real-time during the laser ablation of a swine liver ex vivo (Fig.3).

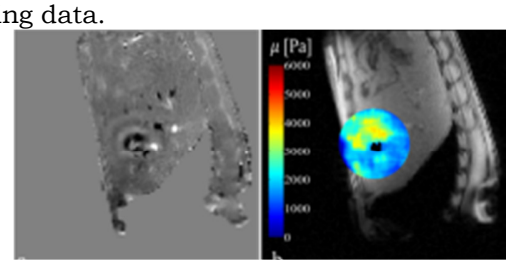

Figure 1: In vivo real-time MRE in swine liver a) unwrapped phase difference image; b) elastogram (reconstructed every 2.56s)

Conclusions: The iMRE system dedicated to the monitoring of percutaneous thermal ablations has shown promising results both ex vivo and in vivo. The compact needle MRE exciter combined with a fast and interactive MRE pulse sequence and online data processing meet the challenging requirements of interventional MRI.

Acknowledgements: This work was supported by French state funds managed by the ANR within the Investissements d'Avenir programme for the Labex CAMI (ANR-11-LABX-0004) and the IHU Strasbourg (ANR-10-IAHU-02).

* *indicates Presenter*

002 **A NOVEL TACTILE SENSOR FOR ELASTOGRAPHY OF SUPERFICIAL ORGANS.**

Ji Fu[1], Faxin Li[1]*
[1] Peking University, Beijing, CHINA

Background: Palpation has long been used as an effective tool in clinical diagnosis. [1] In palpation, physicians sense the reaction force, stiffness, and mobility of the tissues by touching the patient's skin. Actually, the principle of palpation has been used in medical instruments for breast cancer elastography. [2] The tumor induced elasticity changes are detected by measuring the pressure variations through tactile sensors. However in such tactile sensing based techniques, only qualitative pressure results are provided and quantitative elastic properties could not be given.

Aims: A novel tactile sensor is proposed for quantitative elastography of superficial organs such as breast and thyroid.

Methods: The sensor is made of a piezoelectric bimorph cantilever with a strain gauge for deformation monitoring. A cone-shaped tip is fabricated on the cantilever's free end to contact the testing sample. When the tip touches the sample, the sample's elasticity can be derived by tracking the contact resonance frequency of the cantilever-sample system. [3] Consequently, the elastography image can be obtained by a scanning process. The performance of the tactile sensor is validated by elasticity sensing of a Polydimethylsiloxane (PDMS) sample, a silica gel sample, and an injection phantom with both stiff and soft lesions.

Results:

The elasticity sensing results on the PDMS sample and the silica gel sample are plotted in Fig. 1, where the frequency response curves and the elasticity of the samples are given. The contact resonance frequency of the PDMS sample and the silica gel sample were measured as 145.1±7.1Hz and 156.4±11.8Hz, respectively. The obtained average modulus of the PDMS is 3.0±0.2MPa, which is much smaller than that of 25.2±4.5MPa for the Silica Gel. A phantom with a inside plastic tube and a inside longitudinal hole was fabricated to validate the performance of the sensor. The plastic tube is used to simulate the stiffer lesions and the longitudinal hole is used to simulate the lesions softer than normal tissues. As expected, the plastic tube can be recognized by the higher equivalent modulus than the surroundings normal areas. Similarly, the longitudinal hole can be recognized by the abnormal lower equivalent modulus.

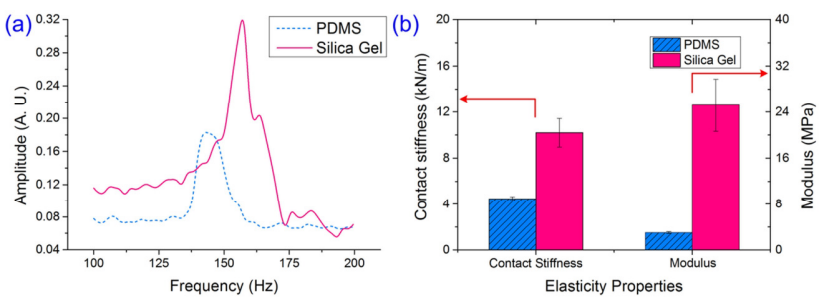

Fig. 1. Elasticity sensing results of PDMS and Silica Gel samples. (a) The frequency response curves of the samples, from which the different contact resonance frequency can be derived. (b) The contact stiffness and the modulus of the samples.

Conclusions: We proposed a novel tactile sensor which can measure the elasticity of soft sample quantitatively. Such a sensor offers a non-destructive and convenient solution for elastography of superficial organs.

Acknowledgements: This work was supported by the NSFC under Grant Nos. 11422216.

References:

[1] P. Wells, *et al.*: Medical ultrasound: imaging of soft tissue strain and elasticity, J. R. Soc. Interface. 8(64), pp. 1521-1549, 2011.

[2] V. Egorov, *et al.*: Mechanical imaging of the breast. IEEE T. Med. Imaging. 27(9), pp. 1275-1287, 2008.

[3] J. Fu, *et al.*: An elastography method based on the scanning contact resonance of a piezoelectric cantilever. Med. Phys. 40(12). pp. 123502, 2013.

027 **SOME INCLUSIONS IN A HARDER SURROUNDING SHOW UP AS THE SO CALLED 'BLACK HOLE PHENOMENON' WITHOUT MEASURED ELASTICITY ON SHEAR WAVE ELASTOGRAPHY (SWE).**

Bowen Jin[1], Andrew Evans[1], Sandy Cochran[1], Katrin Skerl[1].*
[1]University of Dundee, Dundee, Scotland, UNITED KINGDOM.

Background: Shear Wave Elastography (SWE) is an ultrasound imaging modality visualizing the elasticity of tissue. However, the image resolution and the ability of SWE to differentiate smaller areas of different stiffness are controversial.

Aims: Thus, the aim of this project is to investigate the ability of SWE to differentiate areas of different elasticity.

Methods: In this study, seven agar phantom lesions were developed in two breast tissue mimicking phantoms. Three of these lesions were regular shaped lesions (RL) and consisted of halves with different concentrations of agar (1.5% and 1.1%). Four lesions (1.5% agar) were irregular shaped lesions (IL) simulating in-vivo breast lesions and contained soft inclusion (1.1% agar). All lesions were observed with SWE using the ultrasound Aixplorer system, (SuperSonic Imagine, Aix-en-Provence, France).

Results: The boundary between the two parts of the RL is clearly visible (Figure 1a). The shape of the inclusions in the IL is indistinct. Furthermore there is no elasticity measured ('black hole phenomenon') within the larger inclusions (diameter in both dimensions > 2 mm) (Figure 1b). There is no difference if the inclusion is on top or at the bottom of the lesion.

Conclusions: It is possible to reliably differentiate areas of different elasticity with SWE. However, small areas (diameter in both dimensions < 2 mm) are difficult to distinguish. Larger soft inclusions contained in a harder surrounding create areas without elasticity information, the so called 'black hole' phenomenon.

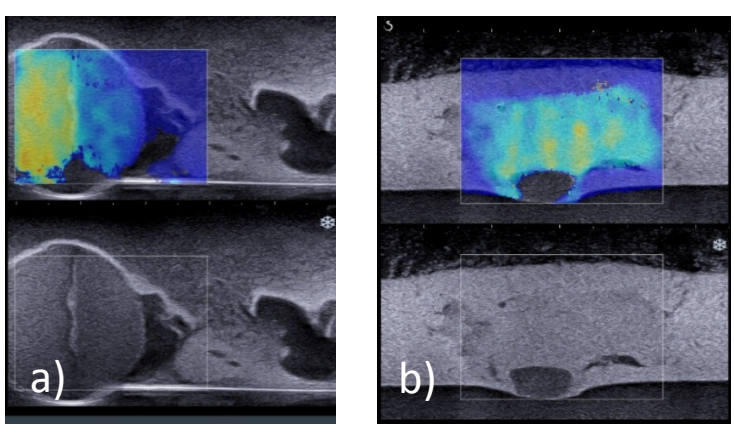

Figure 1a): Halves of different elasticity in a lesion can be identified and the boundary is clearly visible. b): An irregular lesion with two soft inclusions inside; the larger one shows up as a 'black hole' whereas the smaller one is indistinct.

* *indicates Presenter*

031 **SHEAR WAVE ELASTOGRAPHY STIFFNESS CORRELATES WITH FIBRO-GLANDULAR COMPOSITION OF BREAST TISSUE.**

Katrin Skerl[1], Sarah Vinnicombe[1,2], Kim Thomson[2], Andrew Evans[1,2].*

[1]University of Dundee, Dundee, Scotland, UNITED KINGDOM; [2]Ninewells Hospital & Medical School, Dundee, Scotland, UNITED KINDGOM.

Aims: Breast density is the strongest population based risk factor for the development of breast cancer after age. It is usually assessed mammographically, but in younger women, in whom irradiation of the breast is undesirable, an alternative method such as ultrasound would be preferable. Our study investigated the correlation of shear wave elastographic (SWE) measurements of healthy breast tissue stiffness with the ACR BIRADS 5th edition visual breast density assessment to ascertain whether SWE measures could be used as a surrogate.

Methods: The SWE parameter mean elasticity (E_{mean}) of healthy breast tissue in 84 women attending the symptomatic clinic (> 40 years old) was recorded and compared to the manual breast density assessment using BIRADS categories.

Results: The evaluated breasts consisted of 24 BIRADS a, 31 BIRADS b, 26 BIRADS c and 3 BIRADS d breasts. E_{mean} of BIRADS a tissue was significantly lower than the BIRADS b tissue (Fig. 1) using the maximal ROI size ($p=0.03$) but differences were not significant with a 2 mm ROI ($p=0.06$). Furthermore, BIRADS c breasts were stiffer than BIRADS b breasts as were BIRADS d breasts stiffer than BIRADS c breasts (Fig. 1). However, these differences were not significant.

Conclusions: This study shows that the SWE parameter E_{mean} increases with mammographic density and therefore that it shows promise as a proxy for breast density assessment in women who are too young for mammography.

Acknowledgements: This project was performed as part of a PhD project funded by SuperSonic Imagine and the Engineering and Physical Science and Research Council (EPSRC).

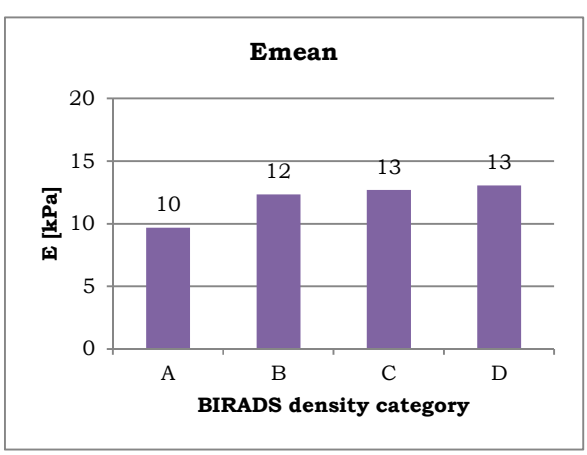

Figure 1: The mean elasticity (E_{mean}) increases with BIRADS breast density category from mammographic assessment.

036 **IN VITRO QUANTIFICATION AND REPRODUCIBILITY OF ELASTICITY MEASUREMENTS USING FIVE DIFFERENT ELASTOGRAPHY PLATFORMS.**

Anesa Mulabecirovic[1], Mette Vesterhus[1,2], Odd Helge Gilja[1,2], Roald Flesland Havre[1].*

[1]National Centre for Ultrasound in Gastroenterology, Department of Medicine, Haukeland University Hospital, Bergen, NORWAY; [2]Department of Clinical Medicine, University of Bergen, Bergen NORWAY.

Background: Several varieties of ultrasound elastography have emerged during recent years, but data on head-to-head comparisons are scarce. We aimed to compare the performance of quantitative elastography measurements using five different elastography platforms on a single elastography liver-mimicking phantom containing four spherical inclusions differing in Youngs modulus from the background material (CIRS no 49). The methods applied included both strain elastography (SE) and shear-wave elastography (SWE).

Aim The aim of this study was to assess the reproducibility of elasticity measurements in a tissue-mimicking phantom.

Methods: We used five different elastography systems in four different scanners: Supersonic Imaging (SSI), Hitachi Ascendus, Philips iu22, GE E9 Strain and shear wave elastography (SWE). In the GE E9 both a strain-based system (GE strain) and a recently released shear-wave based system was applied (GE SWE). The object was a tissue-mimicking phantom with four isoechoic inclusions with different elasticity than the surrounding material within the rage of soft biological tissues. All measurements were performed in parallel by two independent investigators. The five different elastography systems were evaluated for intra- and interobserver variability using variation coefficient, ICC, correlation and limits-of-agreement. Each observer made ten measurements of each inclusion with all systems, and the median value was used for interobserver variability. Linear and curvilinear probes were used if available from the producer.

Results: All five elastography platforms showed high intra- and interobserver agreement (ICC 0.845-0.998). All four inclusions could be differentiated by quantitative elastography by all systems ($p<0.001$). In a Limits-of-Agreement analysis the differences in measurement were larger for harder than for softer inclusions relative to the background stiffness. All systems had a variation coefficient in the range of 0.01-0.19 for all inclusions, equivalent to low variance and high reproducibilty. For most systems the elasticity measurements are more diversified when recorded with a curvilinear probe than with a linear probe. The exception was the SR measurements in Hitachi's system. For the shear wave methods, the curvilinear probes provided lower measurements for the hardest inclusion compared to using linear probes.

Conclusions: All systems provided high reproducibility in elasticity quantitative measurements in a tissue-mimicking phantom. The elastography software of SSI and a new SWE from GE provided elasticity measurements closest to the elasticity values provided by the phantom producer and the best inter- and intraobserver repeatability. For soft inclusions, all the systems showed very good repeatability and low interobserver variability.

Table 1: The table lists the elastography systems, probes, intra- and interobserver variability and measured values. ICC is defined as interrcorellation coefficient.

System	Unit	Probe	ICC A	ICC B	ICC AB	Mean for observer A and B Inlusion 1 (8 +/- 3 kPa)	Mean for Observer A and B inclusion 4 (80 +/- 12 kPa)
Philips	kPa	C5-1	0,983	0,986	0,975	6,22	55,62
GE (pSWE)	kPa	9L	1	0,996	0,998	7,76	90,69
		C1-5	0,986	0,996	0,991	6,63	63,64
Aixplorer	kPa	L10-2	0,997	1	0,996	7,14	88,41
		C1-6	0,995	0,990	0,984	11,24	55,97
GE	Elasticity index (E)	9L	0,992	0,977	0,845	0,77	2,24
		C1-5	0,976	0,956	0,964	0,64	2,61
Hitachi	Strain Ratio (SR)	L-53	0,993	0,998	0,995	0,69	2,64
		C5-1	0,999	0,995	0,997	0,46	2,10

Acknowledgements:
The study was supported by MedViz (http://medviz.uib.no/), an interdisciplinary research cluster from Haukeland University Hospital, University of Bergen and Christian Michelsen Research AS. We express our gratitude to BBS Medical AB, Sweden who let use the Aixplorer scanner during the test period. We also thank GE Healthcare for Providing a new software for shear wave elastography to us before commercial release.

* *indicates Presenter*

039 **HIGH SPEED BEAMFORMING USING FAST FOURIER'S TRANSFORM AND MIGRATION FOR ARBITRARY SIMULTANEOUS PLURAL TRANSMISSIONS AND USING VIRTUAL SOURCE BEHIND TRANSDUCER.**

Chikayoshi Sumi.*
Sophia University, 4 Yonban-cho, Chiyoda-ku, Tokyo, 102-0081 JAPAN.

Background: A high frame rate is required to achieve high accuracy measurement of rapid tissue motion or shear wave propagation, or 3D imaging, which are all important for elastography. It is also a requirement to generate lateral frequencies, i.e., via lateral modulation [1]. For such purposes, we have been evaluating the simultaneous transmissions of plural, steered plane waves, and cylindrically or spherically focused beams. For these transmissions, reception beamforming must be performed with a considerably high speed. Thus far, and only for a single plane wave transmission, several Fourier based beamforming methods were proposed (e.g., [2] and references in [2]).

Aims: For such simultaneous plural transmissions, we evaluated the speed and accuracy of two types of fast-Fourier beamforming methods which used an arbitrary discrete orthogonal coordinate system such as the Cartesian or polar system, in which no approximation is performed with wavelength mapping.

Methods: Two methods, A and B, were respectively implemented on the basis of J.-y. Lu's method and the migration method. In addition, entirely novel methods, Jacobi's method, and steered mono- and multi-static synthetic aperture methods, were developed. Two transmission steering angles, α and β, and a dynamic focused reception steering angle, γ, can be set. In addition to reception echo data obtained from the simultaneous transmissions, those obtained from plural transmissions at the same temporal phase of the target, but at different times, can also be processed via pre-superposing in a spatial domain. The feasibilities were demonstrated through simulations using Field II. For instance, in an ideal case, simultaneous 128 transmissions of 30mm-depth focused beams were performed with a 1D, linear-type transducer (7.5 MHz; rectangular element area, 0.10×5.00 mm^2; 0.12 mm pitch) and 128 effective elements over an ROI having five point scatters (depth, 30 mm). Generated images were compared with those obtained using the corresponding approximate methods A' and B'.

Next, a virtual point source was realized with 30mm distance behind the simulated 1D linear transducer to achieve a cylindrical wave transmission. The result was compared with that obtained using a cylindrical wave transmission from a simulated 1D convex-type transducer (rad = 30mm).

Results: We succeeded in obtaining almost the same image formations using Methods A and B on a simulated linear-type transducer. For instance, Fig. 1 shows radio frequency (RF) images obtained for $\alpha = \beta = 0^\circ$ and $\gamma = 10^\circ$. Table I shows that, for several combinations of α, β and γ, the respectively generated steering angles become approximations of the means of total transmission angles and reception angles. Moreover, the results were more stable than those obtained using the corresponding approximate methods. For instance, see Fig. 2 for Methods A and A' with $\alpha = \beta = \gamma = 0^\circ$. Moreover, we succeeded in imaging the same five scatters using a virtual point source behind the same linear-type transducer; i.e. using a non-focused cylindrical wave transmission, which gave an almost equivalent image to those obtained using a non-focused cylindrical wave transmission and multiple focused beam transmissions from a convex-type transducer (not shown in the figure). The results obtained for simultaneous plural transmissions of focused beams and/or plane waves with different sets of steering angles, or multiple transmission foci, will also be reported.

Conclusions: We have succeeded in implementing and validating fast Fourier image reconstruction algorithms without approximation, using arbitrary transmission beamforming with an arbitrary coordinate system. In particular, various transmission sequences for physically fast imaging were exploited, i.e., simultaneous plural transmissions of focused beams using linear and convex-type transducers, cylindrical wave transmissions using a virtual point source or physical sources, in addition to plane wave transmissions.

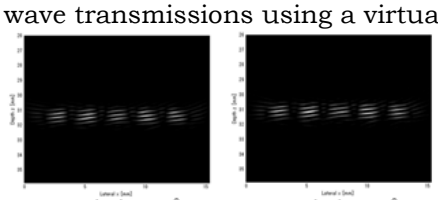

Fig. 1. Rf-images obtained for plural focused beams with steering angles $\alpha = \beta = 0^\circ$ and $\gamma = 10^\circ$.

Table I. Generated steering angles of focused beams with respect to various sets of steering angles α, β and γ. Generated steering angles are evaluated using the 1st moments of spectra.

α	0°	0°	0°	10°	10°	10°	10°
β	0°	10°	0°	0°	10°	0°	10°
γ	0°	0°	10°	0°	0°	10°	10°
Method A	0.14°	5.2°	5.2°	3.4°	9.0°	8.1°	13.9°
Method B	0.14°	5.4°	5.3°	3.2°	9.2°	8.3°	13.9°

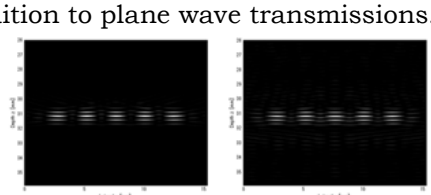

Fig. 2. Rf-images obtained for plural focused beams with steering angles $\alpha = \beta = \gamma = 0^\circ$

References: [1] C. Sumi, Reports in Medical Imaging, vol. 5, 57, 2012. [2] C. Sumi, 2012 ITEC, ID: 046.

040 **ACCURACY COMPARISON OF AXIAL AND LATERAL STRAIN MEASUREMENTS ACHIEVED USING PLURAL STEERED BEAMS AND PLANE WAVES AND SUPER-RESOLUTION IMAGING.**

Chikayoshi Sumi.*
Sophia University, 4 Yonban-cho, Chiyoda-ku, Tokyo, 102-0081 JAPAN.

Background: We have been developing ultrasound (US) tissue displacement vector measurement methods. For instance, simultaneous uses of our previously developed multidimensional autocorrelation method (MAM) and a lateral modulation (LM) with steered beams or plane waves permit a high accuracy measurement [1]. We also generated over-determined systems (e.g., [2,3]) from plural LMs for effectively performing the least squares solution (LST), averaging of measurements (AVE), and coherent superposition of beams or waves (CS). As reported at the last conference [3] (for an US freq., f = 7.5 MHz), both for a scanning with parabolic apodization and spherical dynamic focusing (SP) and plane wave transmissions (PW) with Gaussian apodization, increasing LM frequency up to 3/8f increases the measurement accuracy of axial strain together with that of a lateral strain, even though the axial frequency decreases. This unexpected result is caused by the simultaneous measurements of both components of displacement. With lateral frequencies higher than 3/8f, the accuracy of lateral strain further increases, but axial strain accuracy starts to decrease. The measurement accuracies achieved via these methods were confirmed using lateral strain generated in an agar phantom. In addition, nonlinear processing was performed for displacement vector measurement, and super-resolution and speckle reduction imaging [4]. The accuracy of axial strain measurement is also important for achieving a high accuracy shear modulus reconstruction.

Aims: In this report, the measurement accuracies achieved via these methods are compared using axial strain generated on an agar phantom [3].

Methods: An agar phantom, which had a cylindrical inclusion (10mm diameter) with higher shear modulus than the surrounding, was compressed in a lateral direction (~0.2%). The MAM was used.

Results: (i) SP: In [1], the accurate lateral strain measurement achieved with a single LM of 1/2f had SD of 0.28%. Using a single LM frequency f yielded the more accurate measurement with SD of 0.22%. Thus, by using plural high LM frequency beams, smaller SDs of 0.16%, 0.16% and 0.20% were respectively achieved for 14 beams LST (1/4f to f with an interval of 1/8f), and 10 beams AVE and CS (1/2f to f with an interval 1/8f) [3]. However, using more independent LM frequencies achieved the same accuracies using a fewer beams, i.e., 8 beams LST, and 6 beams AVE and 4 beams CS [3]. Alternatively, for an axial strain measurement, the accurate axial strain measurement achieved with a single LM of 1/2f had SD of 0.10%. Using a single LM frequency f yielded the less accurate measurement with SD of 0.17%. However, by using plural high LM frequency beams, smaller SDs of 0.08%, 0.08% and 0.09% were respectively achieved for 14 beams LST and AVE (1/4f to f with an interval of 1/8f), and 16 beams CS (1/8f to f with an interval 1/8f). However, using fewer, but more independent LM frequencies achieved the same accuracies, i.e., 8 beams LST, AVE and CS. Thus, although lateral frequencies higher than 3/4f yielded less accurate axial measurements, using plural beams yielded the results similar to those in the lateral measurement case. (ii) PW: Single LMs with f/2 and f respectively yielded SDs of 0.50% [1] and 0.42% [3]. Similar combinations for LST, AVE and CS respectively yielded 0.27% (6 waves with f,3/4f,f/2), 0.27% (the same 6 waves) and 0.31% (4 waves with f,3/4f). When using more waves, however, only 14, 12 and 14 (1/4f or 3/8f to f with interval 1/8f) waves respectively yielded more accurate measurements for LST, AVE and CS, i.e., SDs of 0.19, 0.20 and 0.21%. The results were different from those of SP, and also note that the accuracies are higher than the best single LM with SP scanning (0.22 %) [3]. Alternatively, for an axial strain measurement, similarly to SP, lateral frequencies higher than 3/4f yielded less accurate measurements (0.23% vs f/2, 0.21%). Similarly to the lateral strain measurement using PW, using plural independent, high LM frequency waves yielded smaller SDs of 0.14%, 0.13% and 0.20%, respectively (8 waves with f,3/4f,f/2,f/4). Similarly, using more waves, however, only 16 waves (1/8f to f with interval 1/8f) yielded more accurate measurements, 0.12%, 0.11% and 0.19%, respectively. Thus, for PW, the number of waves was more important than the independency of waves. At the conference, other phantom data will also be reported together with super-resolution imaging performed using nonlinear processing [4] as well as coherent superposition [2].

Conclusions: Similarly to the lateral strain measurement, for axial strain measurement with SP, the independency of beams was more important than the number of beams; and for with PW, vice versa.

References: [1] C. Sumi, IEEE Trans. UFFC, vol. 55, pp. 2607–2625, 2008. [2] C. Sumi et al, Procs of 2011-13 ITEC. [3] C. Sumi, Proc 2014 ITEC, ID. 030. [4] C. Sumi, Proc of 2014 ITEC, ID. 025.

* *indicates Presenter*

055 **USING A CONTROLLED ACCELERATION OF THE HEAD TO ACCESS VISCOELATIC PROPERTIES OF BRAIN TISSUE.**

Jakob Bindl[1], Anna-Lisa Kofahl[1], Sebastian Theilenberg[1], Sylvia Napiletzki[1], Jürgen Finsterbusch[2], Carsten Urbach[1], Karl Maier[1].*

[1]University of Bonn, HISKP, Nussallee,Bonn, GERMANY;[2]University Medical Center Hamburg-Eppendorf, Department of Systems Neuroscience, Martinistr Hamburg, GERMANY.

Background:

Knowledge about viscoelastic properties of brain tissue is of great interest in the context of dementia such as Alzheimer's disease or multiple sclerosis [1][2]. Accessing these properties however is quite complicated due to the surrounding cranial bone. By applying a controlled acceleration of the head brain tissue is globally excited with a high bandwidth providing access to the viscoelastic properties of brain tissue with a high special resolution [3][4].

Aims:

The aim of the work presented is to show the feasibility of acceleration-induced excitation of brain-tissue using a new prototype allowing a highly controlled motion inside an MRI-system using a stepper motor.

Methods:

For the head at rest the brain is in a mechanical equilibrium determined by gravitational force on one side and restoring forces from inner tensions on the other (t_1). Using a controlled acceleration of the head the gravitational force can effectively be reduced leading to a new equilibrium. Therefore the brain will perform a relaxation movement into the new equilibrium (t_2). After the acceleration the gravitational force acts on the brain again leading to a second relaxation movement into the primary state. Using a motion sensitive MR-sequence the displacements between two motion-encoding magnetic field gradients (G_1 and G_2) can be observed. For the interpretation of the obtained images a highly controlled excitation motion with a simple progression is desirable. Using a stepper motor different trajectories can be implemented as desired with high control over the duration and slope of the acceleration. To avoid interference with the imaging sequence the stepper motor is electromagnetically decoupled from the MRI-system. To sample the whole relaxation movement of the brain the movement was shifted relatively to the imaging sequence.

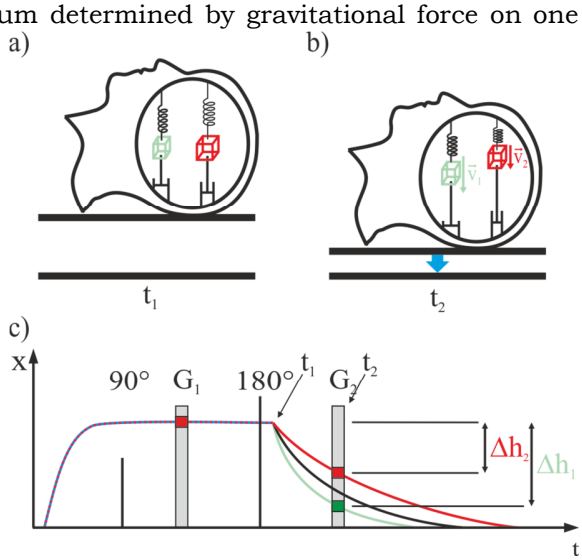

Results:

Measurements were taken using a Siemens Magnetom Avanto 1.5 T on phantoms made of agar-based hydrogel as well as healthy volunteers. Different trajectories were induced leading to different, distinguishable images of the tissues response.

Conclusions:

Using the new prototype the motion of a stepper motor can be transferred onto the head without interference with the imaging process, providing high control over the acceleration exciting the brain tissue.

References:

1. Mariappan, Y.K. et al.: Clin. Anat. 23: pp. 497-511 (2010)
2. Murphy, M.C. et al.: J. Magn. Reson. Imaging 34: pp. 494-498 (2011)
3. Kofahl, A.-L. et al.: Joint Annual Meeting ISMRM-ESMRMB 1689 (2014)
4. Theilenberg, S. et al.: Joint Annual Meeting ISMRM-ESMRMB 1690 (2014)

057 **AUTOMATIC SELECTION OF REPRESENTATIVE FRAMES FROM AXIAL-SHEAR STRAIN ELASTOGRAM (ASSE) CINE-LOOP.**

Bhaskara Rao Chintada [1],Vikram Subramani[1], Arun K. Thittai[1].*
[1]Indian Institute of Technology Madras, Chennai, TN, INDIA.

Background: Ultrasound axial shear strain elastography maps the axial component of the local shear strains of the tissue under study. Typically, an expert breast radiologist selects a representative frame from the sonogram cine-loop to diagnose the lesion. While this approach may not seem burdensome when done on sonograms, which is an established modality and practitioners are well-trained to identify good-quality frames quickly and save only few frames (< 10) in the cine-loop for evaluation, it may not be the case when evaluating cine-loop containing large numbers (several hundred) of newer kind of images, like ASSE, obtained by freehand compression technique.

Aim: To develop an algorithm that automatically selects representative ASSE frames that are of superior quality among the cine-loop of ASSE frames obtained by freehand compression of breast *in vivo*.

Methods: Axial strain elastograms (ASE) and ASSE were generated from cine-loop of RF-frames acquired using a recently-described algorithm that dynamically pairs the pre- and post- compression frames to obtain elastograms having frame-averaged axial strain from ASE of ~1% [1]. The *in vivo* data used in this work were acquired by Dr. Garra and his team at the University of Vermont using an Ultrasonix(R) scanner (RP-500, Richmond, BC, CA) with a L9-14 probe operating at 10 MHz center frequency. Instead of selecting just one representative frame the algorithm is tailored to select a section of contiguous frames (e.g. 10 frames) from the cine-loop that has the best scored- quality. This way, the neighbouring frames are available to provide visual continuity. We have identified correlation coefficient, angle of compression and the mean axial strain as indicative of elastogram quality. Each frame is given a score (linearly) separately between 0 and 1 for (1) correlation coefficients between 0.8 and 1 and (2) compression angles between 10^{o} to 0^{o} . Further, each frame is given a strain score (binary)of either 1 or 0, based on whether the mean strain value in the ASE is within or outside the range 0.5%-2%. The quality score for each frame is the sum of these three scores. First, the algorithm identifies five non-overlapping sections of contiguous frames from the cine-loop that possess the top five cumulative quality scores. Next, the image contrast to noise ratio (CNR) of the corresponding ASEs was employed as a parameter to further refine our selection. The algorithm determines the cumulative CNR of the five sections selected by the previous step, and identifies the final representative section as the one with highest cumulative CNR.

Results: It was seen that the frames selected objectively by the algorithm were the most noise-free frames in the cine-loop that demonstrated clearly the two important ASSE features:"fill-in" & NASSA [2]. The cumulative quality score for 10- consecutive frame segments, the quality factor for individual frame from the highest and lowest scoring segments, and a representative frame from each of these segments are shown in figure 1 for an example *in vivo* benign breast lesion case where "fill-in" in ASSE is expected. Conclusions: The developed algorithm provides an objective way of quantifying the elastographic quality and shortlists representative frames for evaluation thus saving radiologist time. The individual frame "quality indicator" developed here can also be used to provide real-time feedback to guide elastographic data acquisitions (see quality indicator bar in figure 1c and 1d). Further, the automatic selection of a representative frames must be compared to those from subjective observer selection. We are currently in the process of performing such an observer study.

References: [1] Rongmin Xia, Guazhi Tao, and Thittai, A.K.: Dynamic Frame-Pairing in Real Time Freehand Elastography, IEEE Transactions on Ultrasonics, Ferroelectrics, and Frequency Control, 61(6), 979-985, 2014. [2] Ophir, J., Srinivasan, S., Righetti, R., and Thittai, A.K.: Elastography: A decade of progress (2000-2010), Cur. Med. Img. Rev. Special Issue on Elasticity Imaging, 7 (4), 292-312, 2011.

Figure 1: (a) The cumulative quality score for 10- consecutive frame segments (b) Quality factor for Individual for highest and lowest scoring segments (c) representative frame for highest quality score (d) representative frame for lowest quality score. The image dimension is 30mm(depth) x 40 mm(width).

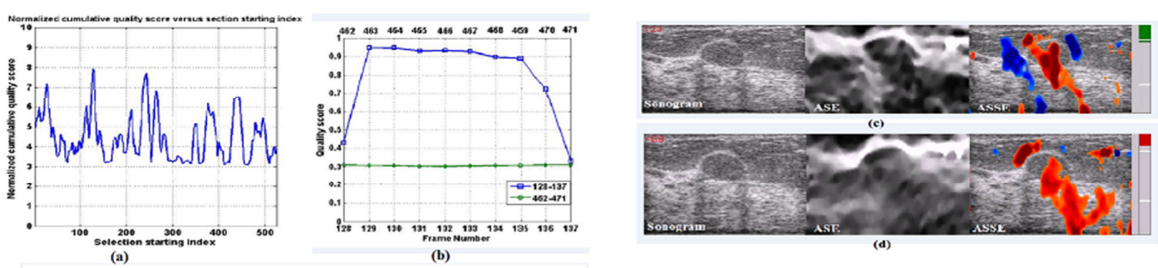

* *indicates Presenter*

047 **THE SIMULATION STUDY TO EVALUATE THE EFFECT OF LIVER VISCOSITY ON SHEAR WAVE PROPAGATION BY THE TRANSIENT ELASTOGRAPHY.**

JH Shao[1], F Zhai[1], JW Luo[1], HC Xing[2], JX Zhao[2], J Cheng[2], Q He[1], L Tong[1].*

[1]Tsinghua University, Beijing, CHINA; [2]Beijing Ditan Hospital, Beijing, CHINA.

Background: Viscosity is closely related to a variety of liver diseases including liver fibrosis. More comprehensive information of liver can be obtained by measuring the viscosity. Elastography technology based on ultrasound is non-invasive. Ultrasound can captures the propagation of mechanical waves in the liver tissue generated by external mechanical vibration and liver elasticity can be gotten the data of the returned ultrasonic. The traditional solving simultaneous equations' method quantifies both elasticity and viscosity by applying different frequencies' vibrations to generate the shear wave in different velocities. And it is limited by frequencies in clinical use. This method did not make full use of propagation properties.

Aims: To study the effect of liver viscosity on shear wave propagation in the transient elastography by numerical simulation.

Methods: Idealized 2-D axisymmetric finite element models with different viscoelasticity of liver tissue was built to simulate the shear wave propagation in the tissue. The each model consists of liver tissue and probe. The transient elastography probe can generate mechanical vibration. Sinusoidal mechanical vibration which perpendicular to the material surface can induce the shear wave. The frequency, period and amplitude of mechanical vibration were set as 50 Hz, one period and 0.001m. This mechanical vibration was imposed on the probe position. Simulation time was set as 0.15s and time step was set as 5.0E-5s. To analyze and discuss the effect of viscosity at transient elastography, five viscosity values and four elasticity value was choose in our numerical simulations. The paper studies the numerical results of displacement in 2-D cross section.

Results: 1, Amplitude of shear wave get smaller with the rising of viscosity. 2, As the value of viscosity increases, the distance between adjacent two peaks increased at every model. 3, Viscosity cannot influent wave velocity in single frequency and the velocity of shear wave are same at different viscosity quantities.
4, In the same set depth. The bigger tissue viscosity, the bigger the vibration amplitude attenuation. 5, One defined shear wave amplitude attenuation value, which can be obtained by existing data, decrease when depth increase. Moreover the slope of the decrease curve is inversely proportionate to viscosity.

Conclusions: Vibration amplitude is relevant to tissue viscosity because increase of viscosity lead to the energy loss increase when relative motions inside the liver tissue. At the clinical practice, tissue elasticity (shear wave velocity) can be gotten by using existing medical system (FibroScan or FibroTouch). And viscosity can be gotten by dealing with the data of vibration amplitude. The study based on viscosity parameters will be able to provide new attribute information and evaluating indexes in the diagnostic of the liver disease.

Acknowledgements: This work is supported by the National Natural Science Foundation of China under Grant No. 81201160; China's Post-doctoral Science Foundation Grant No. 2012M510463. Also support for this study is provided by Tsinghua University and Beijing Ditan Hospital was built to simulate the shear wave propagation in the tissue. The each model consists of liver tissue and probe. The transient elastography probe can generate mechanical vibration. Sinusoidal mechanical vibration which perpendicular to the material surface can induce the shear wave. The frequency, period and amplitude of mechanical vibration were set as 50 Hz, one period and 0.001m. This mechanical vibration was imposed on the probe position. Simulation time was set as 0.15s and time step was set as 5.0E-5s. To analyze and discuss the effect of viscosity at transient elastography, five viscosity values and four elasticity value was choose in our numerical simulations. The paper studies the numerical results of displacement in 2-D cross section.

Results: 1, Amplitude of shear wave get smaller with the rising of viscosity. 2, As the value of viscosity increases, the distance between adjacent two peaks increased at every model. 3, Viscosity cannot influent wave velocity in single frequency and the velocity of shear wave are same at different viscosity quantities.
4, In the same set depth. The bigger tissue viscosity, the bigger the vibration amplitude attenuation. 5, One defined shear wave amplitude attenuation value, which can be obtained by existing data, decrease when depth increase. Moreover the slope of the decrease curve is inversely proportionate to viscosity.

Conclusions: Vibration amplitude is relevant to tissue viscosity because increase of viscosity lead to the energy loss increase when relative motions inside the liver tissue. At the clinical practice, tissue elasticity (shear wave velocity) can be gotten by using existing medical system (FibroScan or FibroTouch). And viscosity can be gotten by dealing with the data of vibration amplitude. The study based on viscosity parameters will be able to provide new attribute information and evaluating indexes in the diagnostic of the liver disease.

Acknowledgements: This work is supported by the National Natural Science Foundation of China under Grant No. 81201160; China's Post-doctoral Science Foundation Grant No. 2012M510463. Also support for this study is provided by Tsinghua University and Beijing Ditan Hospital.

048 **DISCUSSION ABOUT THE EFFECT OF LIVER ELASTICITY IN ASSESSMENT OF LIVER FIBROSIS IN PATIENTS WITH CHRONIC HEPATITIS B AND THE INFLUENCE OF FACTORS ON IT.**

JH Shao[1], HC Xing[2], JW Luo[1], F Zhai[1], JX Zhao[2], J Cheng[2], Q He[1], L Tong[1].*
[1]Tsinghua University, Beijing, CHINA; [2]Beijing Ditan Hospital, Beijing, CHINA.

Background: Liver fibrosis is generally caused by excessive accumulation of extracellular matrix proteins and often occurs in most types of chronic liver diseases. It can ultimately lead to liver cirrhosis and has long serious consequence for patient's morbidity and mortality. It is very important to diagnose liver fibrosis early, promptly and accurately. Transient elastography (TE), which is a non-invasive method widely used in hospitals, offers high diagnostic accuracy for the assessment and detection of liver fibrosis and cirrhosis. The use of non-invasive monitoring was considered by researchers to be preferable to invasive testing. TE is the most useful tests for assessing the stage of liver disease.

Aims: To investigate liver elasticity measured by TE in assessment of liver fibrosis in patients with Chronic Hepatitis B and to explore which factors influence it.

Methods: We performed a prospective performance analysis of TE for the diagnosis of liver fibrosis stages in a diagnostic cohort of 263 patients with chronic hepatitis B, from Beijing Ditan Hospital Capital Medical University, between April 2014 and February 2015. All patients were diagnosed CHB according to the 2010 guidelines for prevention and treatment for chronic hepatitis B, and had undergone liver biopsy, reliable TE and routine blood tests. TE measurements were performed with a FibroScan (Echosens, Paris) and FibroTouch (Hisky, Wuxi).

Results: The liver stiffness measure (LSM) of each liver fibrosis stage were significantly different, ($p<0.05$); LSM was well correlated with liver fibrosis stage, r=0.556. The area under receiver operating characteristic (ROC) curves of LSM were 0.836 (95%CI：0.781-0.890), 0.891(95%CI：0.831～0.952) and 0.972(95%CI：0.948～0.997) for ≥S2, ≥S3 and =S4 respectively. Diagnostic optimal cut-off of liver stiffness in discriminating fibrosis stages ≥S2, ≥S3 and =S4 were 7.45 KPa, 9.07 KPa and 10.8 KPa, respectively. A Spearman's correlation analysis showed that the LSM value was significantly associated with the liver inflammation grade besides liver fibrosis. Body mass index (BMI) correlated with LSM values as well as the grade of inflammation of liver. At the same stage, high alanine aminotransferase (ALT) resulted in high value of LSM. When ALT<50u/l, AUROCs of LSM for ≥ S2, ≥ S3 and S4 were 0.881, 0.924 and 0.983 respectively. Cut-off value were 6.85 kPa、9.06 kPa、10.7 KPa respectively. In the ALT 50-100U/L group, area under the ROC curve (AUROC) of LSM for ≥S2, ≥S3 and S4 was 0.675, 0.792 and 0.986. Cut-off values were 10.2 kPa、8.3 KPa and12.4 respectively.
Total bilirubin (TBIL) also influenced the value of LSM. In TBIL<17.1μmol/L group, AUROC of LSM for ≥ S2, ≥S3 and S4 were 0.834, 0.864, 0.968; cut-off values were 10.2 kPa、8.3 kPa和12.35 respectively. In TBIL 17.2-34.2 μmol/L group, AUROCs of LSM for ≥S2, ≥S3 and S4 were 0.820, 0.941, 0.983; cut-off values were 7.75 kPa、10.1 kPa和17.5 KPa respectively.
As for the AST influence, in AST<40U/L group, AUROCs of LSM for ≥S2 and S4 were 0.830, 0.981; cut-off values were 6.85 kPa、10.65 KPa respectively. In AST>40U/L group, AUROCs of LSM for ≥S2 and S4 were 0.840, 0.936; cut-off values were 7.70 kPa、12.4 KPa, respectively.

Conclusions: 1. TE is a reasonable noninvasive tool for the assessment of liver fibrosis. 2. LSM value was affected by many liver function indicators. BMI was correlated with LSM values as well as grade of inflammation of liver. 3. According to different level of ALT and TBIL, the specific cut-offf value of LSM should be made up to evaluate the diagnosic merits. 4. Liver viscosity value was significantly associated with liver fibrosis, and influenced by the level of a number of liver function indicators. 5. TE can to make a distinction for liver fibrosis ≥ S2 stages.

Acknowledgements: This work is supported by the National Natural Science Foundation of China under Grant No. 81201160; China's Post-doctoral Science Foundation Grant No. 2012M510463. Also support for this study is provided by Tsinghua University and Beijing Ditan Hospital.

* *indicates Presenter*

051 **REAL-TIME STEERING FOR INDUCING AND MONITORING HIFU ABLATION USING HARMONIC MOTION IMAGING**

Yang Han[1], Thomas Payen[*1], Shutao Wang[1], Elisa Konofagou[1,2]*
[1]Department of Biomedical Engineering, Columbia University, New York, NY, USA; [2]Department of Radiology, Columbia University, New York, NY, USA.

Background: Harmonic motion imaging (HMI) utilizes an amplitude-modulated HIFU beam to induce and simultaneously estimate the resulting localized focal oscillatory motion.

Aims: The objective of this study is to develop and demonstrate initial feasibility of 2D HIFU beam steering for HMI using a HIFU phased array.

Methods: A 93-element, ceramic HIFU phased array (individual element diameter = 10 mm, overall diameter = 110 mm, inner diameter = 41 mm, fc = 4.5 MHz, and focal depth = 70 mm) was used in this study. The -3 dB focal size was equal to 0.3 mm (transverse) by 1.1 mm (axial) in water. The geometric and acoustic parameters of the HIFU transducer were designed for clinical application of the localized HIFU treatment on superficial organ applications. The diagnostic transducer was a 64-element phased array (fc = 2.5 MHz) confocally fitted through a circular void of the HIFU transducer aperture. The HIFU phased array operated through a four-board VDAS system and the diagnostic probe is operated through another four-board VDAS system. A Fiber Optic Hydrophone was used to measure the pressure field and access steering range in water. HMI using steered HIFU beam was acquired in gel phantoms and *ex vivo* canine liver specimens. The output acoustic power was 12.46 W, and the duration 1 s for imaging and 90 s for HIFU ablation.

Results: A pressure profile after steering was acquired in free field to calculate the focal pressure loss due to beam steering. A safe steering range was assumed when the highest grating lobe was under -6 dB. The HMI displacement was imaged within the steering range of +/-1.65 mm in the lateral direction in both phantoms and liver specimens and found to be 33.5 μm and 28.9 μm in phantom and liver respectively. 8 HIFU lesions were generated in liver specimens using the steered HIFU beam sequence with HMI ablation monitoring. An average decrease of 60.1% was found in the HMI displacement amplitude due to ablation.

Conclusions: Using the steered HIFU beam, HMI can be used to image and ablate a larger tissue volume with higher efficiency and without requiring physical movement of the transducer.

Acknowledgements: This study was supported by the National Institutes of Health grant R01EB014496.

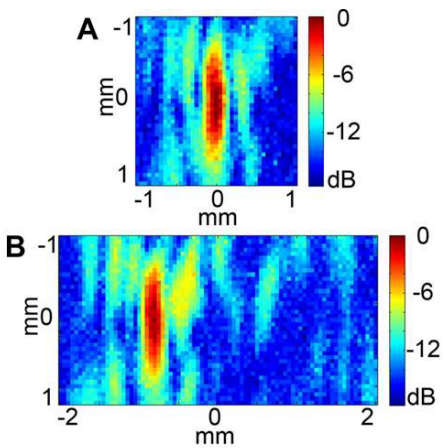

Figure. (A) shows the HIFU geometric focus in free field, and (B) shows the HIFU focus steered to 0.9 mm in the lateral direction.

004 **CONTACTLESS REMOTE INDUCTION OF SHEAR WAVES IN SOFT TISSUES USING A TRANSCRANIAL MAGNETIC STIMULATION DEVICE.**

Pol Grasland-Mongrain[1], Erika Miller-Jolicoeur[1], An Tang[2,3], Stefan Catheline[4,5], Guy Cloutier[1,2,6].*

[1]Laboratory of Biorheology and Medical Ultrasonics, University of Montreal Hospital Research Center (CRCHUM), Montréal, Québec, CANADA; [2]Department of Radiology, Radio-Oncology and Nuclear Medicine, University of Montreal, Montréal, Québec, CANADA; [3]University of Montreal Hospital Research Center (CRCHUM), Montréal, Québec, CANADA; [4]Inserm, U1032, LabTau, Lyon, France; [5]Université de Lyon, Lyon, France; [6]Institute of Biomedical Engineering, University of Montreal, Montréal, Québec, CANADA.

Background: Current methods of shear wave elastography use an external vibrator or an acoustic radiation force to produce shear waves. However, these techniques are limited in situations where the organ of interest is located behind an attenuating medium. The brain, notably, is protected by the skull, which strongly attenuates the propagation of compression and shear waves, thus reducing their spread. Recently, it was demonstrated that the combination of an electrical current and a magnetic field could create shear waves in biological tissues [1]. If the electrical current is induced using a remote coil, this could allow a technique to remotely induce shear waves.

Aims: The goal of this study was to induce remotely shear waves using a coil and a magnet.

Methods: An experiment was built with the following key components: a coil to induce an electrical current j in the sample; a magnet to create a magnetic field B; and an ultrasound probe to track displacements u propagating as shear waves in the sample. The coil was a Transcranial Magnetic Stimulation device using a 2x75 mm diameter butterfly coil (MagPro R100 device with C-B60 Butterfly coil, MagVenture, Farum, Danemark). The magnetic field was induced by a 5x5x5 cm^3 N48 NdFeB magnet (BY0Y0Y0, K&J Magnetics, Pipersville, PA, USA). The first tested sample was a 4x8x8 cm^3 water-based tissue-mimicking phantom with 5% salt (electrical conductivity σ of 5 S/m). Alternatively, a 3x5x5 cm^3 chicken breast sample previously immersed in saline water (σ = 1 S/m) was used. Each sample was observed with a 5 MHz ultrasonic probe made of 128 elements (ATL L7-4, Philips, Amsterdam, Netherlands) and a Verasonics scanner (V-1, Redmond, WA, USA). Great care was given to ensure that the coil and the magnet were fixed independently, without contact with the sample. A three dimensional simulation based on a physical model of the experiment was also performed using Matlab (version 2012b, The MathWorks, Inc., Natick, Massachusetts, USA) in an area of 15x9x9 cm^3 with spatial steps of 1 mm.

Results: We observed displacements reaching amplitudes of 5 µm in the polyvinyl alcohol cryogel phantom and 0.5 µm in the chicken breast sample. These displacements propagated as shear waves at respective speeds of 4.0 ± 1.0 m/s and 6.5 ± 1.5 m/s. Different positions of magnet and coil were tested numerically and experimentally, and amplitudes of displacement were in excellent agreement.

Conclusions: These results indicate the possibility of inducing remotely shear waves using a standard clinical device and a simple magnet. It has an interest to induce shear waves in organs like the brain. In this case, displacements should be measured with an MRI instead of an ultrasound device.

Acknowledgements: Pol Grasland-Mongrain was recipient of a post-doctoral fellowship (PDF) award of the Fondation pour la Recherche Médicale (#SPE20140129460), and is now supported by a PDF of the Natural Sciences and Engineering Research Council of Canada. Dr An Tang is supported by a clinical research scholarship of the Fonds Québécois de la Recherche en Santé and by the Fondation de l'Association des Radiologistes du Québec (#26993).

References: [1] Grasland-Mongrain P, Souchon R, Zorgani A, Cartellier F, Chapelon J-Y, Lafon C, Catheline S(2014). Imaging of shear waves induced by Lorentz force in soft tissues. Physical Review Letters, 113(3):038101.

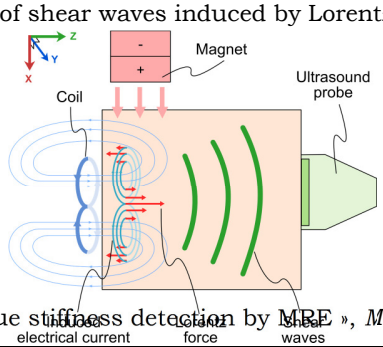

Fig1.
Principle of the experiment: a coil (violet blue circles) induces an electrical current (turquoise circles) in the sample (orange square). Due to the magnetic field (pink arrows), a displacement is induced (red arrows), which propagates as shear waves (green lines).

and tissue stiffness detection by MRE », *MRM*, vol. 5

* *indicates Presenter*

018 **ASSESSMENT OF CORNEAL BIOMECHANICAL PROPERTIES BASED ON MODIFIED RAYLEIGH-LAMB FREQUENCY EQUATION.**

Salavat R. Aglyamov[1], Zhaolong Han[2], Jiasong Li[2], Manmohan Singh[2], Shang Wang[2,3], Srilatha Vantipalli[4], Chen Wu[1], Chih-hao Liu[1], Michael D. Twa[4], Kirill V. Larin[1,3].*

[1]University of Texas at Austin, Austin, TX, USA; [2]University of Houston, Houston, TX, USA; [3]Baylor College of Medicine, Houston, TX, USA; [4]University of Alabama, Birmingham, AL, USA.

Background: The biomechanical properties of the cornea can have a profound influence on the health, and normal function of the eye. The biomechanics of the cornea can be significantly altered by keratoconus and other similar ectatic diseases of the cornea [1]. Currently, keratoconus is one of the leading causes of corneal transplant in the United States and in the developed world. Hence, it is critically important to assess corneal biomechanical properties and understand the interplay between physiological function and the mechanical properties of the cornea. Optical coherence elastography has great potential for noninvasive measurements of the local biomechanical properties of the cornea with high spatial and temporal resolutions. Previously, we developed a method to assess corneal biomechanics based on the measurements of the elastic wave propagation in the cornea using phase-sensitive OCT imaging system after micro air-puff stimulation of the cornea [2,3]. However, quantification of tissue viscoelastic properties from OCE measurements requires the selection of a proper model that can accurately map the viscoelastic parameters. We consider the elastic waves in the cornea as Lamb waves in thin viscoelastic plate when one surface of the plate is free from stress, while second surface is submerged in the liquid. Such model requires modification of the classical Rayleigh-Lamb frequency equation, where both surface are considered as free from stress.

Aims: In this study we demonstrate, application of a modified Rayleigh-Lamb frequency equation which accounted for the fluid effect on the corneal posterior surface to quantify the viscoelastic properties of tissue-mimicking phantoms and porcine corneas from OCE measurements.

Methods: In the model we assumed a Kelvin-Voigt viscoelastic body. The boundary conditions were assumed as zero stress on the corneal anterior surface and equal stresses and vertical displacements between the corneal tissue and aqueous humor on the posterior surface. The modified Rayleigh-Lamb frequency equation was derived and used to calculate the dispersion of the Lamb wave. The home-built OCE system was composed of a focused air-pulse delivery system [2] and a phase-stabilized swept source optical coherence tomography (PhS-SSOCT) system [2,3]. The system utilized a broadband swept laser source (HSL2000, Santec, Inc., CA) with a central wavelength of ~1310 nm, bandwidth of ~150 nm, scan rate of 30 kHz, and experimentally measured phase stability of ~40 nm during experiments. The focused air-pulse delivery system was comprised of a controller with a signal input for synchronization, a solenoid-controlled air gate, and an air-pulse port with a flat edge and diameter of ~150 μm. The system is capable of delivering a short duration focused air-pulse (≤1 ms) with a Gaussian profile to induce a small amplitude deformation (order of μm) on the surface of a sample. Experiments were performed on 2% agar phantoms and porcine corneas *ex vivo*.

Results: Young's modulus values of the tissue-mimicking phantoms obtained from OCE measurements (~160 kPa) were compared with the results of uniaxial mechanical compressional tests (Model 5943, Instron Corp., Massachusetts) and demonstrated good agreement. The Young's modulus of porcine corneas at 20 mmHg IOP was estimated to be ~60 kPa and shear viscosity as ~0.33 Pa·s.

Conclusions: The results indicate that the combination of PhS-SSOCE and the modified Rayleigh-Lamb characteristic equation may be potentially useful for assessing corneal viscoelasticity noninvasively.

Acknowledgements: This work was supported, in part, by grants 1R01EY022362, 1R01HL120140, and U54HG006348 from the NIH and PRJ71TN from DOD/NAVSEA.

References:

[1] Ruberti JW et al.: Corneal Biomechanics and Biomaterials. *Annu Rev Biomed Eng* 2011;13:269–95.
[2] Wang S et al.: A focused air-pulse system for optical coherence tomography-based measurements of tissue elasticity. *Laser Physics Letters* 2013;10:075605.
[3] Li J et al.: Air-pulse OCE for assessment of age-related changes in mouse cornea in vivo. *Laser Physics Letters* 2014;11(6):065601.

020 **DETECTION OF STEATOHEPATITIS IN A RAT MODEL: LOW VERSUS HIGH FREQUENCY ULTRASOUND ELASTOGRAPHY FOR ASSESSMENT OF LIVER SHEAR STIFFNESS.**

Siavash Kazemirad[1,2], Eric Zhang[1,2], Boris Chayer[1,2], François Destrempes[1,2], Bich Nguyen[3], Marc Bilodeau[4], Paule Bodson-Clermont[2], Guy Cloutier[1,2], An Tang[2].*

[1]Laboratory of Biorheology and Medical Ultrasonics, Montreal, Quebec, CANADA; [2]University of Montreal Hospital Research Center, Montreal, Quebec, CANADA; [3]Department of Pathology, University of Montreal Hospital Center, Montreal, Quebec, CANADA; [4]Liver Unit, University of Montreal Hospital Center, Montreal, Quebec, CANADA.

Background: Nonalcoholic fatty liver disease (NAFLD) is a highly prevalent disease identified in 20-30% of adults in Western nations, making NAFLD the most common chronic liver condition. The advanced form, nonalcoholic steatohepatitis (NASH) is found in 2-5% of the general population. If undetected and untreated, NASH may be complicated by liver fibrosis and cirrhosis. Only a few studies have investigated the early detection of NASH [1, 2]. Key knowledge gaps in noninvasive NASH diagnosis include the detection of inflammation, differentiation from early fibrosis, and monitoring of disease progression [3].

Aims: To compare low- vs. high-frequency ultrasound elastography for detection of NASH in a rat model.

Methods: This study was approved by the institutional animal care committee. Sixty male Sprague-Dawley rats divided in 5 cohorts of 12 rats each were either fed a standard chow for 4 weeks or fed a methionine and choline deficient diet for 1, 4, 8, or 12 weeks to obtain a range of NASH disease severity. At the end of each cohort duration, liver shear stiffness was assessed *in vivo* by shear wave ultrasound elastography over a frequency range from 40 to 220 Hz, which was divided into low-frequency (40 to 130 Hz) and high-frequency (130 to 220 Hz) ranges. NASH scoring in 4 categories (no NASH, borderline, NASH without fibrosis, NASH with fibrosis) was assessed *ex vivo* by histopathology and used as the reference standard. Kruskal-Wallis rank sum test, post-hoc Dunn's test with Bonferroni correction, and receiver operating characteristic (ROC) analysis were performed.

Results: In the low-frequency range, liver shear stiffness was significantly different (p = 0.022) between groups of rats categorized by NASH diagnosis (Fig. 1(a)). However, post-hoc tests only revealed a trend for higher liver stiffness in definite NASH with fibrosis compared with borderline (p = 0.081). In the high-frequency range, liver shear stiffness was significantly different (p < 0.001) between groups of rats categorized by NASH diagnosis (Fig. 1(b)). Post-hoc tests revealed significantly higher stiffness for NASH without fibrosis than borderline (p = 0.017), and NASH with fibrosis than NASH without fibrosis (p = 0.042). Area under the ROC curves between consecutive stages of NASH continuum was higher at high-frequency (0.910, 0.923, 0.926) than low-frequency range (0.799, 0.824, 0.688).

Conclusions: Ultrasound elastography showed liver shear stiffness separation between different stages of NASH disease continuum. The measured shear stiffness values provided better discrimination between NASH disease categories at the high-frequency than the low-frequency range.

Acknowledgements: Siavash Kazemirad was supported by a postdoctoral fellowship award from the FRQNT. Dr An Tang was supported by a clinical research scholarship of the FRQS and by the FARQ (#26993).

References:

[1] Salameh N, Larrat B, et al.: Early Detection of Steatohepatitis in Fatty Rat Liver by Using MR Elastography. *Radiology*, 253, 90-7, 2009.

[2] Chen J, Talwalkar JA, et al.: Early Detection of Nonalcoholic Steatohepatitis in Patients with Nonalcoholic Fatty Liver Disease by Using MR Elastography. *Radiology*, 259, 749-56, 2011.

[3] Sanyal AJ, Brunt EM, et al. Endpoints and clinical trial design for nonalcoholic steatohepatitis. *Hepatology*, 54, 344-53, 2011.

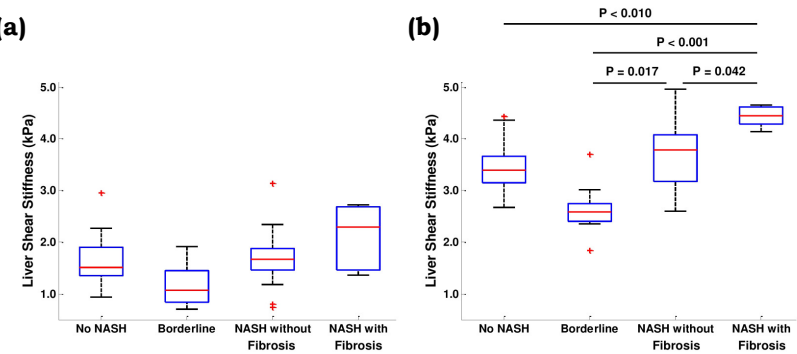

Fig1: Box plots showing interquartile range (box), median (line within box), range (whisker), and outliers (dot) of liver shear stiffness for different NASH categories obtained by shear wave ultrasound elastography over a **(a)** low frequency range from 40 to

* *indicates Presenter*

023 **SHEAR WAVE ULTRASOUND VISCOELASTOGRAPHY FOR MODEL-INDEPENDENT QUANTIFICATION OF COMPLEX MODULUS.**

Siavash Kazemirad[1,2], Abderrahmane Ouared[1,2], An Tang[2], Guy Cloutier[1,2].*
[1]Laboratory of Biorheology and Medical Ultrasonics, Montreal, Quebec, CANADA; [2]University of Montreal Hospital Research Center, Montreal, Quebec, CANADA.

Background: Shear wave elastography methods are developed to assess mechanical properties of soft tissues. A limitation of most current methods is that only shear wave speed is measured, and thus only the storage modulus (G') can be directly estimated from the inverse problem solution. However, other properties such as loss modulus (G'') may be required for tissue characterization [1]. Approximate rheological models may be fitted to measured wave speeds to obtain the complex modulus, $G^*(\omega) = G'(\omega)+iG''(\omega)$. Yet, these models may not accurately describe the behavior of different types of normal and pathological soft tissues. Hence, the development of a noninvasive model-independent characterization method remains of great interest. Only a few model-independent methods have been proposed, each with their own limitations and *a priori* assumptions, which have hindered their clinical adoption [2].

Aims: To develop an ultrasound viscoelastography method with no *a priori* assumption for model-independent quantification of frequency-dependent viscoelastic complex shear modulus from the semi-cylindrical shear wavefronts generated by most clinically used elastography systems.

Methods: Two *in-vitro* tissue mimicking gelatin-agar phantoms and two *ex-vivo* porcine liver samples were tested. An implantation of beam sequence similar to Supersonic Shear Imaging (SSI) was used for shear wave generation [3]. An analytical complex model was developed for the inverse wave propagation problem of the generated semi-cylindrical shear wavefronts, considering both shear wave speed and amplitude decay versus propagation distance. The complex inverse problem was solved numerically using an optimization method to obtain the real and imaginary parts of the shear wavenumber at each frequency, resulting in the estimation of G' and G'' over a broad range of frequencies (up to 500-600 Hz). Results were compared to shear elasticity of SSI and to rheology measures obtained with the longitudinal wave propagation method and hyper-frequency viscoelastic spectroscopy.

Results: Good agreements were obtained between G' and G'' of the proposed method and benchmark measures. *In-vitro*, differences between G' of the proposed method and SSI or rheology measures were smaller than 7% or 20%, respectively (Fig. 1(a)). Differences for G'' were smaller than 30% for comparisons with benchmark rheology results. For *ex-vivo* porcine livers, G' of the proposed method were close to SSI values, whereas G'' depicted small variations over the studied bandwidth (Fig. 1(b)).

Conclusions: For both phantom and liver experiments, differences between the proposed method and SSI can be explained by the assumption of zero dissipation (*i.e.*, neglecting the imaginary part of the shear wavenumber) in standard elastography. Errors with rheology measures are likely related to experimental variability. To conclude, the developed ultrasound viscoelastography method can provide reliable estimates of G* over a broad range of frequencies. This method may improve classification of diseases with shear wave elastography imaging.

Acknowledgements: Postdoctoral fellowship award of FQRNT, clinical scholarship awards of FQRS and FARQ (#26993), and grant support from FQRNT (#PR-174387).

References:

[1] Garteiser P et al. : *Eur Radiol*, 22: 2169-77, 2012. [2] Montagnon E et al., *IEEE UFFC*, 61: 277-87, 2014. [3] Bercoff J et al. : *IEEE UFCC*, 51: 396-409, 2004.

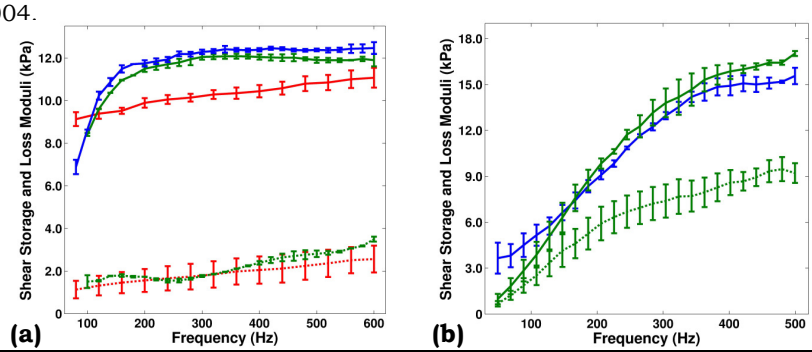

Fig1: **(a)** Shear storage and loss moduli for a 4% gelatin – 5% agar phantom; solid lines: storage modulus; dotted lines: loss modulus; green: proposed method; red: benchmark rheology results; blue: benchmark SSI results. **(b)** Shear storage and loss moduli of two porcine liver samples tested *ex-vivo*; solid lines: storage modulus; dotted line: loss modulus; green: proposed method; blue: benchmark SSI

001 **STORAGE AND LOSS MODULI IMAGING IN SOFT SOLIDS USING SUPERSONIC SHEAR IMAGING TECHNIQUE.**

Ji Fu[1]*, *Faxin Li*[1].

[1] Peking University, 5 Yiheyuan Road, Beijing, CHINA.

Background: The material's vibration response to dynamic excitation can be regarded as a function of elasticity. Therefore, the vibration amplitude or the resonance frequency of soft tissue can been tracked for elastography. Actually at nanoscale, a scanning probe microscopy technique which is called atomic force acoustic microscopy (AFAM) has been proposed for modulus mapping of nanomaterials. [1] AFAM detects the ultrasonic contact resonance frequency (CRF) of a micro cantilever at each testing point and calculates the sample elasticity by a resonance model, leading to modulus mapping within the whole scanning area.[2] Intuitively, such a technique can also be employed for macroscopic elastography.

Aims: Enlightened by the modulus mapping principle of AFAM, we propose a novel elastography method that can be used for modulus imaging of superficial organs.

Methods: This method is based on the scanning contact-resonance of a unimorph piezoelectric cantilever. The cantilever vibrates in its bending mode with the tip pressed tightly on the sample. The contact resonance frequency (CRF) of the cantilever-sample system is tracked at each scanning point, from which the sample's modulus can be derived based on a beam dynamic model. The depth information can be qualitatively obtained by varying the pressing force. Scanning is performed by a three-dimensional motorized stage and the whole system is assembled in a homemade software program based on LabVIEW.

Results: The elastography result on an *in vitro* beef sample is presented in Fig. 1, where the shape and the interface of the tissues are very clear. The modulus of the fat and the muscle were measured as 1.25MPa and 0.29MPa, respectively, which are consistent with that measured by nanoindentation. The detection limit of this elastography method was specially examined both experimentally and numerically. Results show that it can detect the typical lesions in superficial organs with the depth of several centimeters. The lateral resolution of this elastography method/system is better than 0.5mm, and could be further enhanced by using more scanning points.

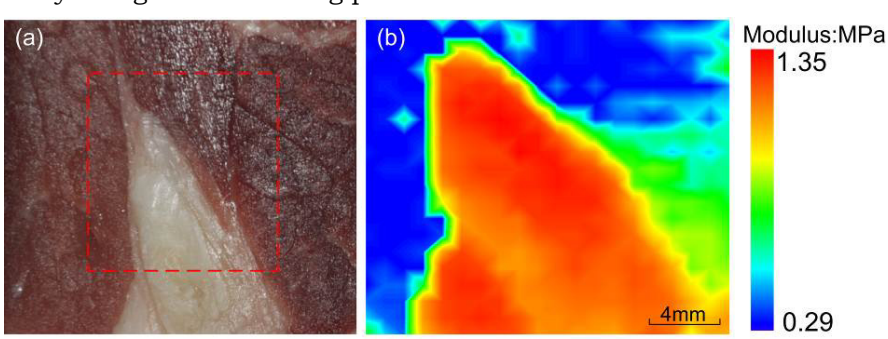

Fig. 1. Elastography on an *in vitro* beef sample. (a)Photograph of the beef tissue where the deep color area is the muscle and the white area is the fat. (b) Modulus image.

Conclusions: The proposed elastography system can be regarded as a sensitive palpation robot, which may be very promising in early diagnosis of tumours in superficial organs such as breast and thyroid. Our improvement work on this homemade elastography system is still undergoing and we believe that it may enter hospitals/families and benefit the suspected patients in near future.

Acknowledgements: This work was supported by the National Natural Science Foundation of China under Grant Nos. 11090331 and 11002002.

References:

[1] U. Rabe et al.: Acoustic microscopy by atomic force microscopy, Appl. Phys. Lett. 64 (12), pp. 1493-1495, 1994.
[2] X. Zhou et al.: Contact resonance force microscopy for nanomechanical characterization: Accuracy and sensitivity. J. Appl. Phys. 114, pp. 064301, 2013.

* *indicates Presenter*

016 **A PILOT COMPARISON BETWEEN ELASTIC REGISTRATION AND RADIO-FREQUENCY-BASED BLOCK MATCHING IN TRANSVERSELY ISOTROPIC MEDIA.**

He Li[1], Wei-Ning Lee[1].*
[1]The University of Hong Kong, Hong Kong, CHINA.

Background: The mechanical properties and view-dependent ultrasonic backscattering of anisotropic soft tissues have been extensively demonstrated, but to our knowledge, whether and how such tissue anisotropy impacts ultrasound elastographic methods has not been substantiated. Radio-frequency-based block matching (RF-BM) and elastic registration (ER) are two representative techniques frequently used in ultrasound motion estimation, but little is known about the performance of these methods in different imaging planes of an anisotropic tissue.

Aims: We aim to investigate the effect of tissue mechanical and acoustic anisotropy due to underlying myofiber arrangement on the theoretical performance of two-dimensional (2D) ultrasound strain imaging (USI) under quasi-static compression. Specifically, we aim to compare the performance of RF-BM and ER in strain estimation of transversely isotropic media in the following scenarios: 1) in fiber planes where the ultrasound beam is either parallel (TIS_{para}) or perpendicular (TIS_{perp_fb}) to the fiber orientation, and 2) in transverse fiber plane (TIS_{perp_cfb}) where the beam is perpendicular to the fiber orientation.

Methods: An axial strain of 3% was applied to compress a finite element (FE) tendon model (Abaqus®), and the pre- and post-deformed radio-frequency (RF) signals of the above scenarios were simulated using Field II [1] in a linear array configuration, with the acoustic anisotropy incorporated [2]. Porcine skeletal muscle embedded in a gelatin-agar phantom was deformed by the ultrasound array probe (L7-4) in the three compression scenarios. The RF data were acquired using a Verasonics® Vantage system. For RF-BM, RF frames were processed using an improved approach derived from [3]. For ER, signal envelopes converted from RF frames were processed using a modified technique from [4]. The 2D strain tensor was then computed from the estimated 2D displacements using a 2D least-squares strain estimator [5].

Results: In the simulation, both RF-BM and ER yielded comparable lateral elastographic signal-to-noise ratio (SNR_e) values in TIS_{perp_fb} (14.0 vs. 15.6 dB) or TIS_{perp_cfb} (27.5 vs. 30.1 dB), and the higher SNR_e value in TIS_{perp_cfb} confirmed the effect of mechanical anisotropy on both methods. This was also revealed by the lower quality of lateral strains in TIS_{perp_fb} *in vitro* (Fig. 1(b) and (d)), which deviated from expected positive strains (i.e., extension) in the muscle. In contrast, RF-BM yielded a lower SNR_e value than ER in TIS_{para} (17.8 vs. 28.9 dB), and presented peak hopping artifacts in the *in vitro* strain fields (Fig. 3(a) and (b)).

Conclusions: The pilot comparison between RF-BM and ER demonstrated that tissue anisotropy affected the performance of USI techniques. Both methods generated lower lateral strain quality in the fiber than transverse fiber planes. RF-BM underperformed when the tissue fiber orientation was parallel to the ultrasound beam, while ER was less vulnerable to such an anisotropic acoustic effect.

Acknowledgements: This study is supported by Hong Kong Research Grants Council (HKU 739413E).

References:

[1] J. Jensen, "Simulation of advanced ultrasound systems using Field II," in *Proc. IEEE Int. Symp. Biomedical Imaging: Nano to Macro*, vol. 1, pp. 636–639, 2004. [2] J. Crosby et al.: "The effect of including myocardial anisotropy in simulated ultrasound images of the heart," *Ultrasonics, Ferroelectrics and Frequency Control, IEEE Transactions on*, vol. 56, pp. 326–333, 2009. [3] W.-N. Lee et al.: "Theoretical Quality Assessment of Myocardial Elastography with In Vivo Validation," *Ultrasonics, Ferroelectrics and Frequency Control, IEEE Transactions on*, vol. 54, pp. 2233–2245, 2007. [4] D. Rueckert et al.: "Nonrigid registration using free-form deformations: application to breast MR images," *Medical Imaging, IEEE Transactions on*, vol. 18, pp. 712–721, 1999. [5] R. G. Lopata et al.: "Comparison of one-dimensional and two-dimensional least-squares strain estimators for phased array displacement data," *Ultrasonic Imaging*, vol. 31, pp. 1–16, 2009.

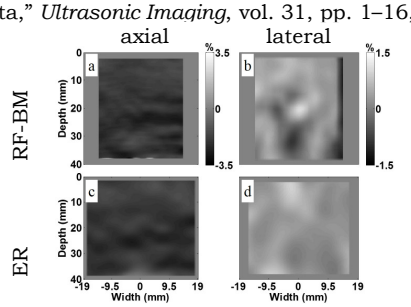

Fig. 1 *In vitro* strain images of TIS_{perp_fb}

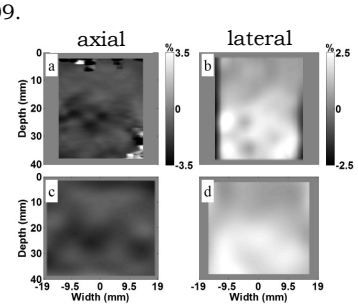

Fig. 2 *In vitro* strain images of TIS_{perp_cfb}

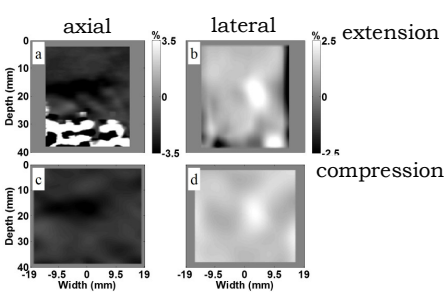

Fig. 3 *In vitro* strain images of TIS_{para}

050 **INCORPORATING SECOND-ORDER DERIVATIVES INTO REAL-TIME REGULARIZED ULTRASOUND ELASTOGRAPHY.**

Hassan Rivaz[1]*

[1]Department of Electrical and Computer Engineering and PERFORM Centre, Concordia University, Montreal, QC, CANADA.

Background: Ultrasound elastography [1] involves imaging tissue while it undergoes deformation, and estimating its mechanical properties from the deformation pattern. Many elastographic methods have been developed, commercialized and successfully tested on patients. At the heart of all elastography techniques is estimation of tissue deformation, where more accurate and fast estimates are required to obtain high quality elastography in real-time. We focus on methods that optimize a regularized cost function to obtain the displacement estimates. An excellent review of these techniques is provided in [2].

Aims: Our first aim is to improve our previous work on real-time optimization of a regularized cost function to obtain 2D displacement estimates [3,4]. A first-order Taylor expansion of the cost function is used in [3,4] to obtain a linear system of equations that can be solved in real-time. We modify this expansion to incorporate second-order derivative terms into the cost function to improve the quality of tracking estimates. Our second goal is to keep the method computationally efficient and real-time.

Methods: Let I_1 and I_2 be RF data from two ultrasound frames acquired from the same but deformed tissue. Let $i = 1\ldots m$ denote indices of all samples of RF-line j, and assume that the current estimate of axial and lateral displacement of all samples in RF-line j are respectively a_i and l_i. The goal is to find update values Δa_i and Δl_i, so that $(a_i+\Delta a_i,\ l_i+\Delta l_i)$ is a better approximation of the 2D displacements. The algorithm can then iterate until convergence is achieved. To find Δa_i and Δl_i, we optimize the following regularized cost function with two terms: data D and regularization R.

$$C = D + R, \text{ where } D = \Sigma\,[\, I_1(i, j) - I_2(i+a_i+\Delta a_i,\ j+l_i+\Delta l_i)\,]^2 \text{ and } R = f(a_1+\Delta a_1,\ldots,a_m+\Delta a_m) + f(l_1+\Delta l_1,\ldots,l_m+\Delta l_m) \quad (1)$$

The summation in D is performed over samples $i=1\ldots m$, and f is a simple quadratic function that specifies the regularization (see [3] for more details). To optimize C, we linearized D using Taylor expansion [3]:

$$I_2(i+a_i+\Delta a_i,\ j+l_i+\Delta l_i) \approx I_2(i+a_i,\ j+l_i) + \Delta a\, I'_{2,a} + \Delta l\, I'_{2,l} \quad (2)$$

where $I'_{2,a}$ and $I'_{2,l}$ are respectively axial and lateral derivatives of I_2 at sample $(i+a_i,\ j+l_i)$. Inserting Eq. (2) in Eq. (1) will make Eq. (1) quadratic, and its derivative linear, meaning that Eq. 1 can be solved efficiently by solving the linear system of equations. The issue is that if we include higher order derivatives in Eq. (2), the derivative of Eq. (1) will not become linear. To overcome this, we propose the novel cost function:

$$D = \Sigma\, w[\, I_1(i, j) - I_2(i+a_i+\Delta a_i,\ j+l_i+\Delta l_i)\,]^2 \quad w = 1/(\alpha+|I''_{2,a}|+|I''_{2,l}|) \quad (3)$$

where α is a small positive constant to prevent the denominator to become zero, and $|I''_{2,a}|$ and $|I''_{2,l}|$ are the absolute values of second-order derivatives in the axial and lateral directions respectively. The weight w reduces the contribution of highly nonlinear parts of the RF-data (where Eq. (2) does not hold).

Results: We have tested the new technique on simulated and patient data. The simulation data consists of 2D compression of a uniform phantom of fully developed speckle by 2%. Ultrasound images are simulated using Field II software. The new method improved the signal to noise ratio (SNR) of the resulting strain image by 14%. We also test the algorithm on a patient data with liver cancer (Fig. 1). The results show that, compared to [3], the new method improves contrast to noise ratio (CNR) by 11%.

Conclusions: We showed that direct incorporation of second-order derivatives into the cost function makes the optimization computationally intractable. We therefore proposed the novel cost function in Eq. (3), which penalizes areas with large second derivative. The increased computational complexity is negligible and the code runs in real-time.

Acknowledgements: We thank Drs. Boctor and Choti for sharing the patient data. H. R. is supported by NSERC DG.

References:

[1] Ophir, J et al.: Elastography: a quantitative method for imaging elasticity biological tissue, Ultras. I. 1991 111-34
[2] Hall, T et al.: Recent results in nonlinear strain and modulus imaging. Current med imag. reviews 7.4 (2011): 313
[3] Rivaz, H, et al.: Real-Time Regularized Ultrasound Elastography, IEEE Trans. Med. Imag. 2011, vol 30 pp 928-945
[4] Rivaz, H, Boctor, E, Choti, M, Hager, G, Ultrasound Elastography Using Multiple Images, Medical Image Analysis, 2014, vol. 18 pp 314-329

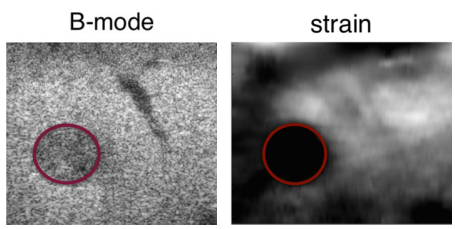

Fig. 1. Ultrasound and strain images of a patient with liver cancer. The tumor, delineated with a red circle, is not visible in the B-mode image, but is visible in strain image.

* *indicates Presenter*

044 **VOXEL-WISE FRACTIONAL-SPRINGPOT SOFT TISSUE VISOCOELASTIC PARAMETER MAPPING WITH MULTIFREQUENCY MAGNETIC RESONANCE ELASTOGRAPHY.**

E. Barnhill[1], P. Kennedy[1], I. Sack[2], J. Braun[2], N. Roberts[1].*
[1]University of Edinburgh, Edinburgh, UK; [2] Charité Universitätsmedizin Berlin, GERMANY.

Background: MR Elastography [1] uses phase contrast MRI imaging in conjunction with time-harmonic shear wave propagation to measure tissue elastic properties *in vivo*. MRE at a given frequency of vibration yields a complex shear modulus |G*|, however soft tissue shows power-law frequency dependence [2], rendering linear tissue elasticity models inadequate. Previous work has fit MRE acquisitions at multiple frequencies to a spring-pot model (e.g. [3][4][5]), deriving one elasticity (μ) and one viscosity (α) value for the region of interest. However new de-noising techniques, combined with serial multifrequency acquisitions, indicate voxel-wise mapping of this spring-pot model is now possible rather than obtaining a single global value.

Aims: Here an algorithm was developed for rapid, voxel wise spring-pot mapping of MRE acquisitions acquired at multiple frequencies. The algorithm was applied to cohorts of brain, liver, and skeletal muscle to determine variability and relative valuations.

Methods: Cohorts of ten healthy volunteer acquisitions for brain, liver, and skeletal muscle were acquired. Shear modulus G* was determined at each frequency for each acquisition using Algebraic Helmholtz Inversion (AHI) [6]. The fit of the spring-pot formulation $G^*(\omega) = \mu(i\omega\eta/\mu)^{\alpha}$ to the shear modulus vector was optimised by minimisation of the root mean squared error (RMSE).

Results: μ results showed liver (3939 +/- 289) slightly stiffer than brain (3809 + / - 202), and brain stiffer than muscle (3243 + / - 149), as is typical for the MRE literature. α results were highest for brain (0.53 +/- 0.01) followed by thigh (0.47 +/- 0.02) and liver (0.44 +/- 0.02). Figure 1 shows example elastograms (brain only due to space constraints), first using averaged AHI results, then using the spring-pot fit. The α values correlate to ϕ values, while |G*| values correlate to both μ and η values.

Conclusions: While spring-pot parameter fitting is frequently undertaken to characterise homogeneous materials, to our knowledge this is the first voxel-wise mapping of the spring-pot to soft tissue. Images are well-resolved and values for the different organs are consistent and in expected relation. Spring-pot mapping is a promising new way to characterise soft tissue that incorporates fractional modelling and powerlaw frequency dependence.

Acknowledgements: The authors gratefully acknowledge funding from the Scottish University Physics Alliance, the Scottish Imaging Network and the Mentholatum Company.

References: [1] Muthupillai et al.: Science 269(5232):pp.1854–1857. [2] Szabo & Wu 2000 J. Acoust. Soc. Am. 107 2437. [3] Klatt et al.: Phys. Med. Biol. pp. 55 6445. [4] Asbach et al 2008 Magn. Reson. Med. 60 373–9. [5] Sack 2008 NMR Biomed. 21 265–71 [6] Papazoglou et al.: Phys. Med. Biol. pp. 53 3147.

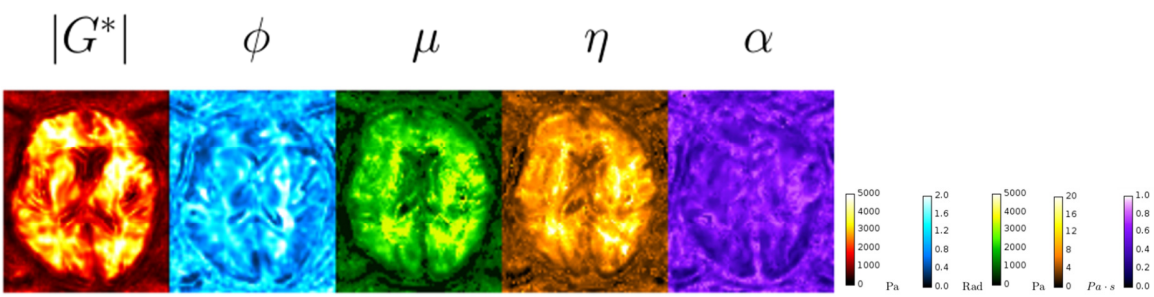

Fig 1. Averaged shear modulus (|G*| and ϕ) and spring-pot parameters (μ, η, and α) for the brain acquisitions.

060 **3D FRACTIONAL VISCOELASTICITY TO MODEL ARTERIAL BEHAVIOUR.**

O Barrera[1], G Alotta[1,2].*

[1]University of Oxford, Oxford, UK; [2]University of Palermo, Sicily, ITALY.

Background: Nowadays over one million of stents are implanted to reopen artherosclerotic vessel and restore their original lumen [1]. It is essential to understand and predict how the arteries deform during stent deployment and when the stent is in place and it is subjected to cyclic loading due to the systolic and diastolic pressure of the blood. Arteries, like other biological tissues exhibit viscoelastic behavior. Classical viscoelastic models are not suitable to capture both the relaxation and the creep behavior of tissues. One of the limitations is that these models are unable to describe the long-time memory of real viscoelastic materials such as tissues.

Aims: We propose a 3D fractional viscoelastic constitutive model to reproduce the time dependent behavior of arteries among other soft tissues and its implementation in a finite element code. Fractional viscoelastic models are characterized by the presence of the so-called fractional derivatives and integrals, namely derivatives and integrals of non-integer order [2, 3]. The constitutive laws governing the time dependent behaviour of the material do not correspond to a spring or a dashpot or a simple combination of springs and dashpots but involve an element labeled as a springpot characterized by a non-integer order derivative. The advantages of fractional viscoelasticity versus classical viscoelasticity are:
a) Fractional operators have a long "fading" memory. In this context the term "hereditariness" is usually used in the sense that the actual response of the arterial tissue in terms of stress/displacement depends on the previous stress/strain history. b) Only few parameters are needed to capture both the creep and relaxation behavior. Figure 1 shows how the fractional viscoelastic model that we propose captures accurately the behavior of human arterial segments [4].

Methods: The 3D fractional viscoelastic constitutive law that we propose has been successfully implemented into the finite element software Abaqus 6.14 [5] by using the discretized version of fractional derivatives provided by Grünwald-Letnikov. Comparisons between analytical and numerical benchmark problems discussed in [5] show the accuracy of these models.

Results: The proposed fractional viscoelastic model is currently being extended to study the viscoelastic behavior of blood vessels in order to be able to analyze the effect of stenting. Here we analyze a 3D finite element model of the stent-vessel subjected to cyclic pressure (figure 2). The Abaqus mesh of the stent has been taken from the Ghent Stent Research Unit link (https://www.stent-ibitech.ugant.be).

Conclusions: The detail form of the fractional viscoelastic model that we propose is derived by fitting creep or relaxation data of human arteries as shown in Figure 1. We can then analyze the time-dependent behavior of the stent- artery system subjected to cyclic loading due to the systolic and diastolic pressure of the blood.

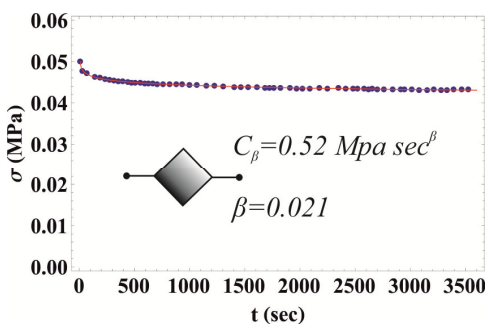

Figure 1. Fitting of arterial stress-relaxation data [4] using the springpot.

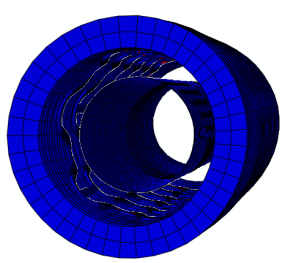

Figure 2. Abaqus model of the stent inside the artery.

Acknowledgements: G.A. wish to acknowledge support from the University of Palermo to visit the University of Oxford during which period this research was conducted. O. B. would like to acknowledge the Engineering and Physical Sciences Research Council [Programme grant number EP/L014742/1].

References:

[1] American Heart Association. American Heart Association, pp. 1–43, 2007. [2] Podlubny I., Fractional Differential Equations. San Diego: Academic Press; 1999. [3] Samko G.S., Kilbas A.A., Marichev O.I., Fractional integrals and derivatives. Amsterdam: Gordon and Breach Science; 1993. [4] Craiem D.O., Rojo F.J., Atienza J.M., Guinea G.V, Armentano R.L. Latin American applied research 38: pp.141-145, 2008. [5] Alotta G., Barrera O., Cocks A.C.F., Di Paola M., Communications in Nonlinear Science and Numerical Simulation, under review.

* *indicates Presenter*

061 **CHARACTERIZATION OF ARTEFACTS IN SHEAR WAVE ELASTOGRAPHY FOR IMPROVED BREAST CANCER ASSESSMENT**

Ramona De Luca[1,2,3], Jérémie Fromageau[1], Franco Marinozzi[3], Jeffrey Bamber[1]*
[1]Institute of Cancer Research and Royal Marsden NHS Foundation Trust, Sutton, England, UK.
[2]Italian Foundation for Cancer Research, Milan, ITALY
[3]Sapienza University of Rome, Mechanical and Aerospace Engineering, Rome, ITALY.

Background: Shear wave elastography (SWE) has the potential advantages over strain elastography of providing quantitative images of Young's modulus (E) and reducing operator dependence. When used in combination with conventional ultrasound it provides additional and clinically relevant information, improving the specificity of breast cancer diagnosis over B-mode alone [1]. Nevertheless, this potential may not be fully realized, as incorrect elasticity patterns, caused by artefacts, are frequently observed in the images. The causes of some of these artefacts are not fully understood, which therefore limits the usefulness of SWE.

Aims: The eventual aim of this project is to study the causes of these artefacts with the hope of improving the interpretation of shear wave elastograms. In this presentation, we report an investigation of the vertical bands of apparent stiffness which are most easily seen in homogeneous tissue-mimicking phantoms when scanned with the SuperSonic Imagine Aixplorer®, although they may also be seen in tissues, especially those overlying stiff tumours.

Methods: The ultrasound emission sequence implemented on the Aixplorer® scanner (SuperSonic Imagine, France) to generate shear waves, has been measured using a needle hydrophone (Precision Acoustics, UK) to identify the spatial pattern and intensity of the Acoustic Radiation Force (ARF) pushes and the duration and frame rate of the plane wave imaging mode. This information was then used to generate load boundary conditions for simulating shear wave generation within a 2D Finite Element Method (FEM) model created in MARC/Mentat (MSC Software, USA). The subsequent propagation of the shear waves was imaged by following their arrival in the local displacement map, and the elasticity pattern was deduced from the speed distribution. The material was assumed to be nearly incompressible (i.e. a Poisson's ratio of 0.49) with a density of 1000 kg/m^3, and the Young's modulus was varied from 9 to 100 kPa, according to the values characterizing breast tissues [2].

Results: Good agreement was found between the FEM model and experiments, as expected: for example, the elasticity was E_{FEM}=10.19±0.13 kPa and $E_{AIXPLORER}$=9.46±0.89 kPa respectively. The simulations show that the reconstructed elasticity maps exhibit the highest values of E in regions approaching the ARF location. We have also shown experimentally that the bands of stiffness correspond to the area where the supersonic emission sequence is applied, and that they are emphasized when an acoustic reflecting and stiff object is placed behind the region imaged.

Conclusions: The FEM model developed, which contained realistic ARF conditions for generating shear waves, allowed the comparison of numerical and experimental results in order predict and to better understand the behavior of the bands of artefactual stiffness. This understanding may help to improve the interpretation of breast SW elastograms, particularly to distinguish the artefact from genuine heterogeneity in stiffness.

Acknowledgements: Ramona De Luca was supported by a fellowship from FIRC (the Italian Foundation for Cancer Research)

References:

[1] Berg WA, Cosgrove DO, Doré CJ, Schäfer FKW, Svensson WE, Hooley RJ, et al. Shear-wave elastography improves the specificity of breast US: the BE1 multinational study of 939 masses, Radiology, 2012 Feb; 262(2):435-49
[2] Evans A, Whelehan P, Thomson K, McLean D, Brauer K, Purdie C, et al. Quantitative shear wave ultrasound elastography: initial experience in solid breast masses. Breast Cancer Res. 2010 Jan;12(6):R104

063 **LONGITUDINAL SHEAR WAVE AND TRANSVERSE COMPRESSIONAL WAVE IN ELASTIC SOLIDS.**

S. Catheline[1]*, R.Souchon[1], J-Y. Chapelon[1], N. Benech[2].
[1]LabTau, INSERM, University of Lyon, Lyon, FRANCE; [2] Laboratorio de Acústica Ultrasonora, Instituto de Física, Facultad de Ciencias, Montevideo, URUGUAY.

Aims: What general definition can one give to elastic P-wave and S-wave, especially when they are transversely and longitudinally polarized respectively? This question is the main motivation of the analysis of the Green's function in elastic solids reported in this letter.

Methods: The anomalous polarization of S-wave was observed in seismology [1] in non-destructive testing [2] and medical imaging [3]. It is in this latter field called elastography, that this special wave has been systematically studied [4,5] and even commercialized [6] for fibrosis diagnostic. In this paper, it is shown that this latter longitudinal S-wave has a symmetrical counterpart: the transverse P-wave.

Results: These unexpected waves are shown to be special parts of the solution of the wave equation known as coupling terms. Similarly to surface water wave, they are divergence and rotational free. Their special motion is carefully described and illustrated.

Conclusions: Some practical applications of this work could consist in using a longitudinal transducer or a laser to measure both P-wave and S-wave arrivals from a point source. Equivalently a transverse transducer is able to detect both waves if placed in the correct direction. Thus one measurement only can supply elastic properties of solids.

Acknowledgements: This work is supported by the French research minister within the ECOS-Sud programs under references U09E01.

References:

[1] K. Aki and P. Richards, "Quantitative seismology: Theory and methods" 2nd Edition, University Science Books, chapter 4 "Elastic waves from a point dislocation source", pp. 63-121, (2002).
[2] P.Gendreu, M.Fink, D.Royer "Optical imaging of transient acoustic fields generated by piezocomposite transducers", IEEE Trans.Ultrason. Ferroelec.Freq.Contr., 42, pp. 135-143 (1995).
[3] Y. Yamakoshi, J. Sato, and T. Sato, "Ultrasonic imaging of internal vibration of soft tissue under forced vibration," IEEE Trans. Ultrason. Ferroelectr. Freq. Control UFFC-37, pp. 45–53 (1990).
[4] S.Catheline, F. Wu, and M. Fink, "A solution to diffraction biases in sonoelasticity: The acoustic impulse technique," *J. Acoust. Soc. Am.*, vol. 105, no. 5, pp. 2941–2950 (1999).
[5] S. Catheline, J. L. Thomas, F.Wu, and M. Fink, "Diffraction field of a low frequency vibrator in soft tissues using transient elastography," IEEE Trans. Ultrason. Ferroelectr. Freq. Control 46, pp. 1013–1019 (1999).
[6] L. Sandrin, S. Catheline, M. Tanter, X. Hennequin and M. Fink, Ultrasonic Imaging 21, 259 (1999).

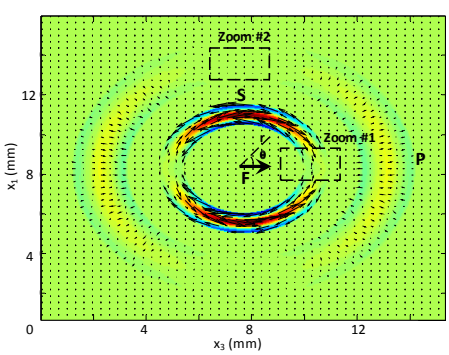

Fig.1 Elastic Green's function. The P and the S wave are clearly visible at $\theta=0$ and $\theta=\pi/2$. The longitudinal S-wave and the transverse P-wave are located inside dashed boxes called Zoom #1 and #2.

* *indicates Presenter*

014 **ON THE RESPONSE OF LIVER STIFFNESS TO BLOOD PERFUSION REVEALED BY TIME HARMONIC ELASTOGRAPHY IN HEALTHY VOLUNTEERS AND PATIENTS WITH HEPATIC HYPERTENSION.**

Selcan Ipek-Ugay[1], Heiko Tzschätzsch[1], Christian Althoff[1], Thomas Fischer[1], Christian Hudert[2], Jing Guo[1], Jürgen Braun[3], Ingolf Sack[1].*
[1]Departments of Radiology, [2]Pediatric Endocrinology, and [3]Medical Informatics,
Charité - Universitätsmedizin Berlin, Charitéplatz 1, Berlin, GERMANY.

Background: Time harmonic elastography (THE) has recently been introduced for the measurement of liver stiffness (LS) in large tissue windows in patients with obesity or ascites [1,2]. The method exploits continuous harmonic vibrations at several frequencies between 30 and 60 Hz measured by fast A-line motion sampling integrated into a commercial ultrasound device [2]. In the current study, we implemented real-time postprocessing and instant quality feedback (Fig.1a) in order to measure subtle elasticity changes due to hepatic compression due to water consumption and decompression following the placement of a transjugular intrahepatic portosystemic shunt (TIPS) in patients with portal hypertension [3].

Aims: i) To provide THE-measured reference values for LS with consideration of the volunteer's fasting and hydration state; ii) to test if THE is sensitive to the LS reduction following TIPS intervention.

Methods: For external wave stimulation to the liver, a loudspeaker was integrated into the patient bed [2]. The excitation waveform was a superposition of 7 harmonics with frequencies from 30 to 60 Hz. The method was implemented into a commercial ultrasound device (SonixMDP, Ultrasonix). Elastographic postprocessing followed the pipeline in [2], however, in real-time and by an online-display as illustrated in Fig. 1a. 12 healthy volunteers were scanned five times: (b1) after overnight fasting, (b2) after lunch meal, (c1) after two hours fasting, (c2) after drinking 1.5 liters of water and (c3) after two-hours following up. 7 patients with elevated hepatic venous pressure gradients subjected to TIPS intervention were scanned before TIPS placement and 48 h after the intervention. Only one patient was scanned immediately after the treatment. All patients suffered from ascites.

Results: Results are shown in Figs1b-d. Mean wave speed values were measured in healthy livers with 1.68 ± 0.18 m/s (b1), 1.84 ± 0.19 m/s (b2), 1.75 ± 0.18 m/s (c1), 1.94 ± 0.25 m/s (c2), 1.77 ± 0.15 m/s (c3) (numbers in brackets refer to the experiment numbers above) corresponding to 9.78 ± 7.65 % (p = 0.0024) LS increase due to eating and 11.00 ± 8.02% (p = 0.002) LS increase due to drinking. In patients, a mean reduction of LS of 16.23 ± 8.90% (p = 0.031) was observed from 3.87 ± 0.57 m/s to 3.34 ± 0.50 m/s which is similar to recent observations made by MR elastography [3].

Conclusions: Our study reproduces previous observations of postprandial LS-increase [4,5] and shows for the first time that LS increases due to water consumption alone. This indicates that LS depends on the perfusion state of the liver which increases by an increased fluid volume received through the portal vein. Bypassing venous blood flow through shunts in patients with portal hypertension resembles LS relaxation observed in healthy volunteers. THE can accurately measure LS relaxation in patients with ascites and obesity towards THE-based assessment of the success of TIPS interventions.

References: [1] Tzschätzsch H et al.: Phys Med Biol. 59: 1641–1654, 2014. [2] Tzschätzsch H et al., Ultrasound Med Biol. 41(3): 724-33, 2015. [3] Guo J et al.: Invest Radiol. 2015 doi: 10.1097/RLI.0000000000000136. [4] Popescu et al. Ultrasound Med Biol. 39(4): 579-584, 2013. [5] Jajamovich et al. PLoSOne, 9(5): e97355, 2014.

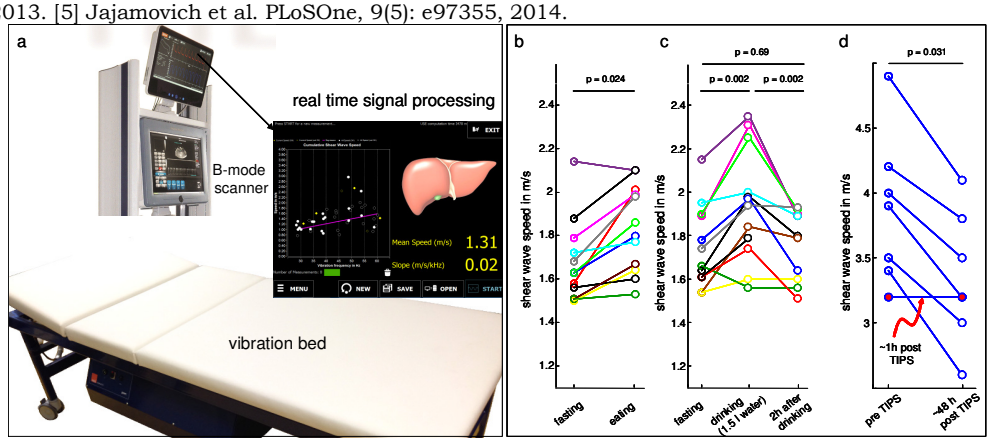

Figure 1: THE scanner (a), results of obtained in 12 healthy volunteers under different metabolic conditions (b,c) and in patients (d)

045 **VALIDATION OF SHEAR-WAVE ELASTOGRAPHY CUTOFF VALUES FOR LIVER FIBROSIS STAGING.**

Joseph R. Grajo[1], Manish Dhyani[1], Atul K. Bhan[1], Anthony E. Samir[1].*
[1]Massachusetts General Hospital, 55 Fruit St, White 270, Boston, MA, USA.

Background: Fibrosis is the common pathway for many different types of liver insults. Hepatitis C Viral (HCV) disease, Hepatitis B Viral (HBV) disease, Non-alcoholic Steatohepatitis (NASH) and Autoimmune Hepatitis (AIH) are all characterized by progressive liver fibrosis. The current gold standard for fibrosis measurement is non-focal liver biopsy. Shear-wave elastography (SWE) as a non-invasive test has been validated as a biomarker for the differentiation of higher grades of fibrosis from no/early fibrosis. A number of studies have proposed cutoff values for the diagnosis of METAVIR fibrosis stage F2 or greater or F4. However, to date, these cutoff values have not been validated in data sets independent of those from which they were derived.

Aims: To determine the validity of known estimated liver Young's modulus (eYM) cut-off values for liver fibrosis staging.

Methods: In this IRB approved, HIPAA compliant study, patients undergoing liver biopsy at our institution underwent elastography measurements with the Aixplorer (Supersonic Imagine, France) prior to the biopsy procedure. Sets of 10 elastograms were acquired in the right upper lobe through an intercostal approach at the end of normal expiration. Median eYM values were taken as the representative Young's modulus for each subject. A total of 192 subjects were enrolled; 9 subjects were excluded for poor-quality elastograms. A single blinded sub-specialist pathologist performed METAVIR fibrosis staging on all biopsy samples. Receiver-operating characteristic curves were constructed, and the area under the curve was computed for differentiating higher grades of fibrosis (F2-F4) from lesser grades of fibrosis (F0, F1).

Results: A total of 183 subjects with a mean age of 48 years (range: 18-78) were analyzed. There were 108 females (n=103, 56.3%) and 84 males (n=80, 43.7%). The reason for biopsy was diagnostic in 55.7% of patients (n=102) and for the follow-up of known liver disease in 44.3% of patients (n=81). On pathological examination, a total of 145 subjects had either no fibrosis (F0; n=61, 33.3%) or F1 fibrosis (n=76, 41.5%). There were 21 subjects with F2 fibrosis (11.5%), 20 subjects with F3 fibrosis (10.9%) and 5 subjects with F4 fibrosis (2.7%). Spearman's correlation showed moderate correlation of fibrosis with elastography values ($r=0.44$, $p<0.001$). A cutoff value of 7.25 kPa provided a sensitivity and specificity of 89% and 47%, respectively, validating our prior study, in which a similar cut-off value of 7.29 kPa provided sensitivity and specificity of 91.4% and 52.5%, respectively [1].

Conclusions: A cutoff value of 7.25 kPa has been validated in an independent patient sample to have high sensitivity of ~ 90% and relatively low specificity of ~ 50% for the diagnosis of METAVIR fibrosis stage >= F2 in patients with chronic diffuse liver disease.

References:

[1]. Samir AE, Dhyani M, et al.: Radiology. Mar, 274(3), pp. 888-896, 2015.

* *indicates Presenter*

025 **ASSESSMENT OF AXILLARY LYMPH NODES WITH SHEAR WAVE ELASTOGRAPHY: PRELIMINARY *IN VIVO* HUMAN STUDY**

M. Denis[1], A. Gregory[1], M. Bayat[1], D.D. Meixner[1], R.T. Fazzio[1], M. Fatemi[1], A. Alizad[1].*
[1]Mayo Clinic, Rochester, MN, USA.

Background: Axillary lymph node status node status of breast cancer patients at the time of their initial clinical diagnosis is generally considered one of the most important prognostic factors [1]. Sentinel lymph node biopsy is the standardized staging procedure in patients with low risk of axillary nodal metastases [2]. However, noninvasive imaging procedures are currently used to examine the axillary lymph node status in order to reduce the number of biopsies [3]. Shear wave elastography is noninvasive ultrasound modality that has shown the ability to delineate benign and malignant tissues based on their mechanical properties [4].

Aims: The purpose of this study was to determine the diagnostic value of shear wave elastography in combination with conventional ultrasound in the diagnosis of benign versus metastatic disease for abnormal axillary lymph nodes in breast cancer patients.

Methods: Breast cancer patients with suspicious metastatic axillary lymph nodes on conventional ultrasound who were scheduled for fine-needle aspiration biopsy (FNAB) of indicated lymph node were included in this study. The shear wave elastography evaluation was conducted using the GE LOGIQ E9 (GE Healthcare, Wauwatosa, WI) system with a linear array transducer 9L-D (GE Healthcare). The reconstructed 2D shear wave speed map was evaluated for the Young's modulus from the region-of-interest (ROI) mean shear wave speed in the lymph node. The performance of SWE evaluation of lymph node status will be assessed by comparing the results to pathology. All patient study procedures were conducted according to the protocol approved by Mayo Clinic Institutional Review Board (IRB).

Results: A total of 16 patients with axillary lymph nodes were examined; 3 nodes were benign, and 13 had metastases. Our results indicate an increase in the Young's modulus in malignant lymph nodes compared to benign lymph nodes (Figures 1). The Young's moduli in benign and malignant nodules were found to be 14.88 ± 5.80 kPa and 61.63 ± 29.96 kPa, respectively.

Conclusions: Added SWE improves the diagnostic ability of conventional ultrasound when evaluating abnormal axillary lymph nodes.

Acknowledgements: This work is supported in part by the grant 3R01CA148994-04S1 and 5R01CA148994-04 from NIH.

References:

[1] Fisher ER, Costantino J, Fisher B, and Redmond C (1993) Pathologic findings from the National Surgical Adjuvant Breast Project (Protocol 4). Discriminants for 15-year survival. National Surgical Adjuvant Breast and Bowel Project Investigators. Cancer, 71 (6 Suppl), pp. 2141-2150.

[2] Verpnesi U, et al.: (1999) Sentinel lymph node biopsy and axillary dissection in breast cancer: results in a large series. J. Natl. Cancer Inst., 91, pp. 368-373.

[3] Ueda, S., Tsuda, H., Asakawa, H., Omata, J., Fukatsu, K., Kondo, N., ... Mochizuki, H. (2008). Utility of ^{18}F-fluoro-deoxyglucose emission tomography/computed tomography fusion imaging (^{18}F-FDG PET/CT) in combination with ultrasonography for axillary staging in primary breast cancer. *BMC Cancer*, *8*, 165. doi:10.1186/pp. 1471-2407-8-165.

[4] Denis M, et al.: (2002) Comb-Push Ultrasound Shear Elastography of Breast Masses: Initial Results Show Promise." Ed. François Hug. *PLoS ONE* 10.3 (2015):e0119398. *PMC*. Web. 1 Apr. 2015.

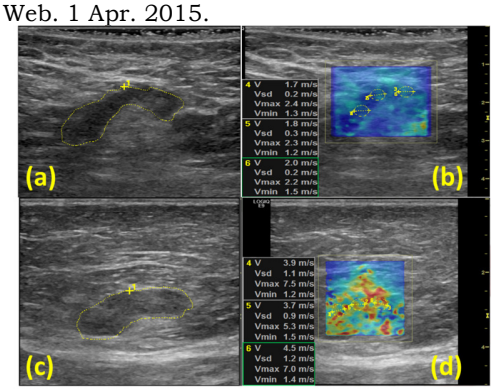

Figure 1. (a, b) B-mode US of a benign reactive lymph node and shear wave speed map, respectively. (c,d) B-mode US of a metastatic adenocarcinoma lymph node and shear wave speed map, respectively. These figures display a high mean shear wave speed for a metastatic lymph node compared to the benign lymph nodes.

026 **MALIGNANT BREAST TISSUE CHANGES CREATE ANISOTROPY ON SHEAR WAVE ELASTOGRAPHY.**

Katrin Skerl[1], Sarah Vinnicombe[1], Kim Thomson[1], Denis McLean[1], Elisabetta Gianotti[1,2], Andrew Evans[1].*

[1]University of Dundee, Dundee, Scotland, UNITED KINGDOM; [2]"Mario Serio" University of Florence, Firenze, ITALY.

Background and Aims: Anisotropy is the directional dependence of the measurement of a property. As breast tissue and some breast diseases (DCIS) are anisotropic in structure, we aimed to evaluate the frequency, degree and diagnostic value of shear wave elastography (SWE) anisotropy in solid breast lesions.

Methods: Study-group A comprised 244 solid breast lesions imaged with SWE between April 2013 and May 2014. Each lesion was imaged in two orthogonal planes related to the breast anatomy (radial and antiradial). The mean elasticity Emean was recorded for each plane at the stiffest point and the difference between them calculated (AD). AD was squared to achieve the degree of anisotropy (AF). The results were correlated with lesion histology. This was repeated for a study-group B of 968 solid breast lesions imaged in two orthogonal planes unrelated to the breast anatomy. Paired Student t-tests and Chi-square tests were performed to establish statistical significance of the relationships.

Results: Neither benign nor malignant lesion anisotropy is plane dependent. However, malignant lesions are more anisotropic than benign lesions ($p \leq 0.001$). Anisotropy correlates with stiffness, BIRADS assessment categories, core biopsy result and tumor grade. Large cancers are significantly more anisotropic than small cancers ($p \leq 0.001$).

Conclusions: Stiffness of solid breast lesions at shear wave elastography is not directly related to the examination plane. Malignant lesions show more anisotropy than benign lesions. Therefore, adding anisotropy to other shear wave parameters has the potential to improve the ability of this modality to differentiate benign from malignant solid breast lesions.

Acknowledgements: This project was performed as part of a PhD project funded by SuperSonic Imagine and the Engineering and Physical Science and Research Council (EPSRC).

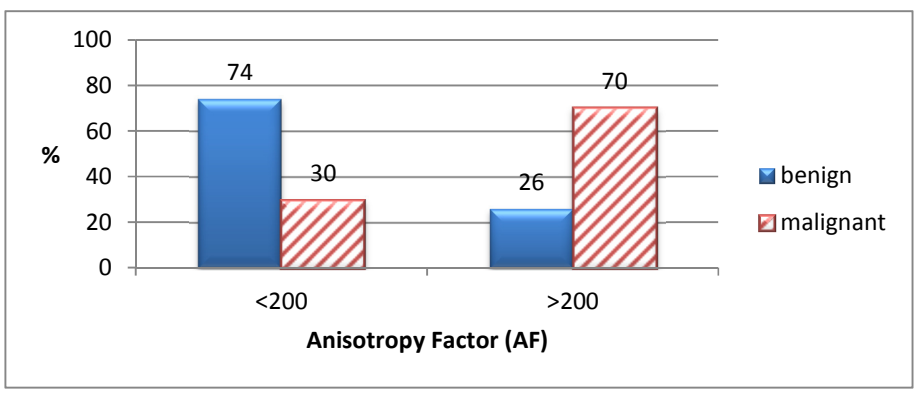

Figure 1: The anisotropy factor AF (squared difference of both planes) is larger for malignant lesions than for benign lesions.

* *indicates Presenter*

029 ***IN VIVO* SHEAR WAVE ELASTOGRAPHY OF THE RHESUS MACAQUE CERVIX: PRELIMINARY RESULTS AND CHALLENGES.**

Ivan M. Rosado-Mendez[1], Lindsey C. Carlson[2], Quinton W. Guerrero[1], Bin Huang[1], Mark L. Palmeri[2], Helen Feltovich[1,3], Timothy J. Hall[1].*

[1]Department of Medical Physics, 1111 Highland Ave., Rm. 1005, Madison, Wisconsin, USA; [2]Biomedical Engineering Department, Durham, North Carolina, USA;
[3]Maternal Fetal Medicine Department, Intermountain Healthcare, Provo, Utah, USA.

Background: The uterine cervix is a dynamic organ that changes its stiffness during pregnancy, significantly softening at term. Our long-term goal is to use Shear Wave Elastography (SWE) to objectively quantify these changes and potentially assess abnormalities that may lead to spontaneous preterm birth. Previous small studies in human subjects have demonstrated the feasibility of this technique.[1] Animal models with similar anatomy, physiology, and mechanical loading during pregnancy to that of humans can provide deeper insight into this problem. This work presents preliminary results of the application of SWE to assess cervix stiffness in a non-pregnant rhesus macaque nonhuman primate (NHP) model.

Aims: This work investigates the use of SWE to establish the baseline stiffness of the non-pregnant cervix of a rhesus macaque NHP model.

Methods: This study includes 10 non-pregnant (5 nulliparous, 5 multiparous) NHP subjects, scanned at eight time points during two sequential ~26-day long menstrual cycles. Shear waves were generated by an Acoustic Radiation Force Impulse (ARFI) excitation and tracked in the anterior and posterior sides of the cervix with a Siemens Acuson S2000 (Siemens Healthcare, Mountain View, CA, USA) using the 9L4 transducer while scanning transabdominally with the subject in the supine position. Each cervix side was scanned twice, performing five ARFI measurements per scan. Displacements were calculated using the Loupas' routine.[2] Shear wave speed (SWS) was estimated using a RANSAC [3] linear fit to the time-to-peak displacement as a function of the distance from the ARFI excitation. A Radon-sum method [4] that selects the largest displacement-projection trajectory on a time vs. distance plane was also used for comparison. We evaluated the agreement between both estimates as well as their variation within the menstrual cycle, NHP age, parity, and weight.

Results: Average RANSAC SWS was 14.9m/s (range 5.2-25.7m/s) on the anterior side of the cervix, and 19.9m/s (range 14.6-26.2m/s) on the posterior side. These values are larger than *ex vivo* SWS estimates in the NHP cervix (5-7m/s) and *ex vivo* SWS of the human cervix (2-3.5m/s).[5, 6] Comparable results were obtained with the Radon sum method. No trends with menstrual cycle day, age, parity or weight were observed. This suggests that the non-pregnant NHP cervix is very stiff. Stiff materials pose complications on SWE that might challenge the accuracy and sensitivity limits of the technique. Some of these complications are related to incomplete tracking of the wave and the high variance in SWS estimation caused by the uncertainty in time-to-displacement-peak estimation. To test this, we are comparing our results with Finite Element Analysis simulations.[7] Initial results suggest the presence of a viscous component might further complicate the analysis and the interpretation of the results.

Conclusions: The stiffness of the non-pregnant NHP cervix imposes important challenges in SWE and requires further investigation of the accuracy and sensitivity limits of this technique.

Acknowledgements: This work was supported by National Institutes of Health Grant R01HD072077 from the Eunice Kennedy Shriver National Institute of Child Health and Human Development. We are also grateful to Siemens Healthcare Ultrasound Division for equipment loans and technical support.

References: [1] Carlson LC, *et al.*: "Changes in shear wave speed pre and post induction of labor: a feasibility study," Ultrasound in Obstetrics and Gynecology, 2014. [2] Pinton GF, *et al.*: "Rapid tracking of small displacements with ultrasound," IEEE Trans. Ultrason. Ferroelect. Freq. Control, 53, 1103-1117, 2006. [3] Wang MH, *et al.*: "Improving the robustness of time-of-flight based shear wave speed reconstruction methods using RANSAC in human liver in vivo," Ultrasound Med. Biol., 36, 802-813, 2010. [4] Rouze NC, *et al.*: "Robust estimation of time-of-flight shear wave speed using a Radon Sum transformation," IEEE Trans. Ultrason. Ferroelect. Freq. Control, 57, 2662-2670, 2010. [5] Huang B, *et al.*: "Quantifying rhesus monkey cervical softness with shear wave speed estimation," SRI 6nd Ann. Sci. Meeting, San Francisco, CA, USA, March 25-28, 2015. [6] Carlson LC, *et al.*: "Estimation of shear wave speed in the human uterine cervix," Ultrasound Obstet. Gynecol., 43, 452-458, 2014. [7] Palmeri ML, *et al.*: "A finite-element method model of soft tissue response to impulsive acoustic radiation force," IEEE Trans. Ultrason. Ferroelect. Freq. Control, 52, 1699-1712, 2005.

042 **ULTRASOUND STRAIN MAPPING FOR MEASURING ACHILLES TENDON COMPRESSION IN PATIENTS WITH INSERTIONAL ACHILLES TENDINOPATHY.**

Ruth L. Chimenti[1], A. Samuel Flemister[2], John Ketz[2], Mary Bucklin[1], Mark R. Buckley[1], Michael S Richards[2].*

[1]University of Rochester, Rochester, NY, USA; [2]University of Rochester Medical Center, Rochester, NY, USA.

Background: One of the most frequent sites of tendon pathology is the Achilles, which connects the calf muscles (gastrocnemius, soleus) to the heel bone (calcaneus). It is estimated that the cumulative lifetime incidence of Achilles tendon pathology in the general population is between 6 and 15% [1]. Approximately 1/3 of cases of Achilles tendon pathology involve the tendon insertion [2] and are classified as insertional Achilles tendinopathy (IAT). IAT causes intense foot pain focused near the heel that is exacerbated by activity and more than 50% of people with IAT fail conservative care and require surgery. To improve clinical outcomes for IAT patients, there is a need to develop new and effective conservative treatments for IAT and we hypothesize that understanding the role of tendon compression will aid in the development of these therapies.

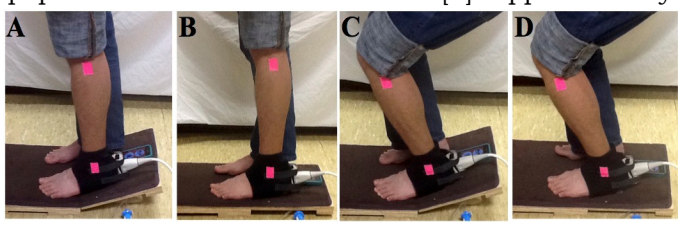

Aims: The purpose of this study was to: 1) to quantify tendon compression using ultrasound and examine the effects of heel lifts on tendon compression during dorsiflexion; 2) Assess the compressive strain at the Achilles tendon insertion in individuals with IAT during dorsiflexion compared to healthy subjects.

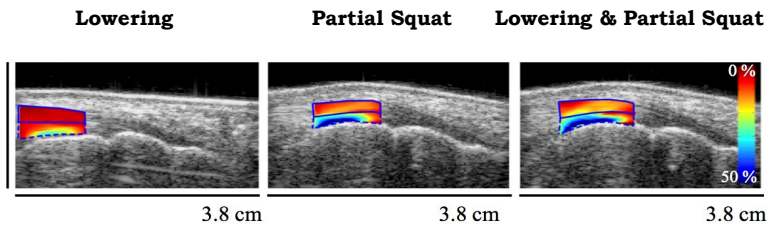

Methods: Tendon compression in ten adults with no Achilles tendinopathy was measured during three weight-bearing tasks: 1) Lowering via a controlled removal of a heel lift, 2) Performing a partial squat to a tibial inclination of 15°, and 3) Combined lowering and partial squat (Fig 1). Subjects Achilles tendons were imaged with a Sonix Touch Ultrasound system (Analogic, Boston, MA) with RF image capabilities (Fig 1,2). An image registration algorithm [3] was adapted to cumulatively (over 50-100 image frames) measure the total strain over each exercise using the US image sequences. The tendon compression was defined as the absolute value of the minimum principal strain in the region of Achilles tendon overlying the bursal prominence, which was subdivided into superficial and deep regions (Fig 2). Tibial inclination during the partial squat was independently measured via video. Ten adults with IAT were also tested during task 3 to compare to healthy subjects.

Results: There was significantly greater compression during task 3 compared to the individual tasks and greater compression on the deep tendon compared to the superficial region for all tasks (Fig 3a). Note that heel lowering to a neutral ankle position induces substantial compression, comparable to a partial squat. Compressive strains were lower in the IAT group and lowest in the subjects who experience pain (Fig 3b).

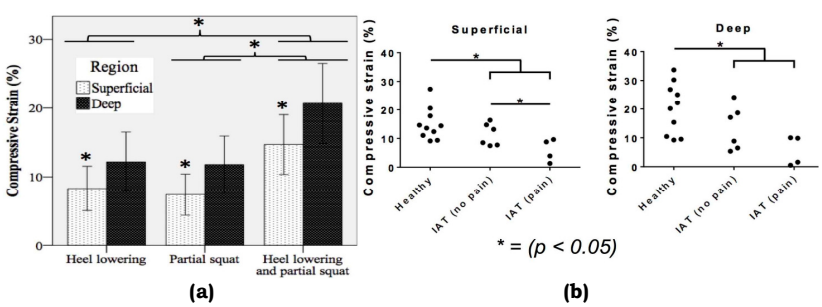

Figure 3. (a) Compression in deep and superficial Achilles tendon regions for three tasks in healthy subjects. (b) Compressive strain during task 3 in Achilles tendon comparing healthy controls to individuals with IAT. *IAT (pain)* denotes subjects who experienced pain during task.

Conclusions: These preliminary findings suggest that IAT tendons experience lower compression due to some biomechanical stiffening induced within the tendon and that it may be transferred compression in the surrounding tissues which causes pain during dorsiflexion.

Acknowledgements: This work was partially supported by NIH-funded study (R03 AR067484).

References: [1] Kujala UM, et al.: Cumulative incidence of AT rupture and tendinopathy in male former elite athletes. *CJSM.* 2005;15(3):133-5. [2] Karjalainen PT, et al.: MR imaging of overuse injuries of the Achilles tendon. *AJR*, 2000;175(1):pp.251-60. [3] Richards MS, et al.: Non-rigid image registration based strain estimator for IVUS elastography. *Ultrasound Med Bio*, 2013;39(3):pp.515-33.

* *indicates Presenter*

062 **HIGH RESOLUTION PROSTATE MR ELASTOGRAPHY USING EXTRACORPORAL ACTUATION. INITIAL RESULTS.**

A. Hoang Dinh[1], R. Souchon[1], S Lounis[3], JM Ménager[3], S Catheline[1], JY Chapelon[1], O.Rouvière [1,2].*
[1]INSERM U1032, LabTAU, University of Lyon, Lyon, FRANCE; [2]Hospice civil of Lyon, Lyon Est Hospital, Lyon, FRANCE; [3]IRM Lyon-Villeurbanne, Villeurbanne, FRANCE.

Abstract Body: We report the initial results of high frequency prostate MR elastography. The use of high frequency shear waves is inherently related to high resolution given the reconstruction algorithms used in Magnetic Resonance Elastography (MRE). In this work, a 200Hz shear wave is observed in the prostate. It should be compared to a maximum of 70Hz reported in the literature. This was possible firstly because efficient piezoelectric actuators were used and secondly because a transperineal approach was chosen. These high resolution elastography images of the prostate are discussed.

Background: Prostate MRE is still challenging because of the size, the position and probably the viscous nature of the gland. Intracorporal approaches (endorectal, intraurethral) [1,2] are delicate because of their invasive characteristic. Extracorporal approach uses low frequency excitation (under 70 Hz) [3, 4, 5, 6] resulting in a low resolution and probably misevaluation of prostate mechanical properties.

Aims: In this study, we used high frequency shear waves at 100 Hz and 200 Hz to confirm or infirm these latter prostate mechanical properties.

Methods: This study was conducted in a calibrated elasticity phantom to start with (CIRS® 049). Then healthy volunteers were submitted to transperineal vibrations using a MR compatible piezoelectric Cedrat® actuator.

Results:

In the calibrated phantom, at 100 Hz, the amplitude of shear wave is 16±2, 19±1.7, 17±0,5, 12±2.1 and 8.7±1.4 µm and at 200 Hz, this amplitude is 4.4±0.18, 9.4±1.3, 5.7±0.3, 6.9±1.1 and 2.9±0,3 µm for lesion type I, II, background, type III and IV, respectively. Shear wave velocity is 1.9±0.06, 2.1±0.02, 2.6±0.01, 2.6+0.03 and 3±0.12 m/s at 100 Hz and 1.9±0.07, 2.1±0.05, 2.6±0.02, 2.8±0.05 and 3.3 m/s at 200 Hz for lesion type I, II, background, type III and IV, respectively. A well-differentiated wave speed is obtained between lesion types and background. In a healthy volunteer, the wave amplitude is 20±13, 19±12, 22±16 and 15±11 µm at 100 Hz and 3.1±2.1, 3.1±2.1, 4.7±4.2, 1.9±0.8 µm at 200 Hz for Right peripheric zone (ZP/D), Left peripheric zone (ZP/G), Transition zone (ZT) and central zone (ZC), respectively. An important loss of wave amplitude between base, middle and apex part of prostate, is partly due to the attenuation of the shear wave in the prostate. Wave speeds is 1.5+0.2, 1.4±0.1, 1.6±0.3 and 1.9±0.3 m/s at 100 Hz and 1.9±0.14, 1.8±0.17, 1.9±0.18 and 2.1±0.15 m/s at 200 Hz for for Right peripheric zone (ZP/D), Left peripheric zone (ZP/G), Transition zone (ZT) and central zone (ZC), respectively. Significative difference of wave speed between peripheric zone and transition zone were observed either at 100 Hz or 200 Hz (Figure 1).

Conclusions: MRE is shown to be able to discriminate peripheric zone from transition zone of the prostate at high frequency excitation using an extracorporal approach.

References:

[1] Arani. A et al.: The feasibility of endorectal MR elastography for prostate cancer localization. Magnetic Resonance in Medicine 2011; 66(6):1649-1657. [2] Chopra. R et al.: *In vivo* MR elastography of the prostate gland using a transurethral actuator. Magnetic Resonance in Medicine 2009; 62(3):665-671. [3] Kemper. J et al.: MR elastography of the prostate: initial in-vivo application; ROFO 2004; 176(8): 1094-1099. [4] Sahebjavaher. R.S et al.: Transperineal prostate MR elastography: initial in vivo results. Magnetic Resonance in Medicine 2013; 69(2):411-420. [5] Sahebjavaher. R.S et al.: MR elastography of prostate cancer: quantitative comparison with histopathology and repeatability of methods. NMR in biomedicine. 2015; 28(1): 124-139. [6] Sahebjavaher. R.S et al.: Prostate MR elastography with transperineal electromagnetic actuation and a fast fractionally encoded steady-state gradient echo sequence. NMR in biomedicine. 2014; 27(7): 784-794.

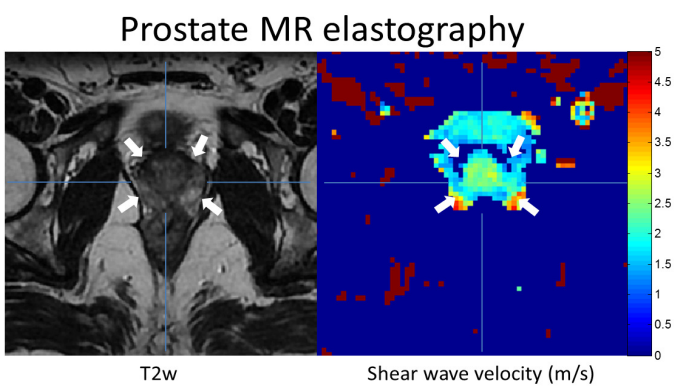

Figure 1- Left: T2w image of the prostate in a healthy volunteer. Right: Corresponding shear wave speed reconstruction.

032 **VISUALIZING PRINCIPAL STRAINS OF THE COMMON CAROTID ARTERY USING PLANE WAVE IMAGING.**

Rohit Nayak[1], Steven Huntzicker[1], Giovanni Schifitto[2], Marvin M. Doyley[1].*

[1]University of Rochester, Dept. of Electrical & Computer Engineering, Rochester, New York, USA;
[2]University of Rochester Medical Center, Dept. of Neurology, Rochester, New York, USA

Aims & Background: Rupture of lipid-rich plaque in the carotid artery may lead to stroke – a leading cause of death and long-term disabilities. The rupture propensity of plaques is governed by the material properties of the plaque components. Clinicians may use strain elastograms to identify life-threatening plaques in the carotid artery. In this study, we investigate the feasibility of using plane wave imaging to visualize principal strains in vascular tissues. Our hypothesis is that principal strain elastograms can detect the early onset of atherosclerosis. Principal strains represent the largest strain component at any spatial location [1]. To corroborate this hypothesis, we computed principal strain elastograms from axial, lateral, and shear strains estimated with a compounded plane wave imaging protocol consisting of 15 transmits [2].

Methods: To validate principal strain imaging, we conducted simulation and *in vivo* studies. The simulation study was performed with homogeneous and heterogeneous finite element (FE) vessel models with inner and outer radii of 1.5 mm and 6 mm, respectively and arterial wall stiffness of 45 kPa. The heterogeneous vessel contained an eccentric plaque with a soft lipid core and thin (350 μm) fibrous cap of stiffness 1 kPa and 700 kPa, respectively. The simulated ultrasound system was equipped with a linear transducer array that had 128 elements, each of size 0.2 mm (width) x 4 mm (height); pitch of 0.03 mm, and center frequency of 5 MHz. The *in vivo* study was conducted on 10 healthy volunteers. All echo imaging was performed by an experienced sonographer using a commercial ultrasound scanner (Ultrasonix RP, Analogic, Canada) that was equipped with a 5 MHz, 128 element transducer array and a parallel data acquisition system (Ultrasonix DAQ, Canada). Beamforming was performed off-line using the delay-and-sum technique [2]. Displacement elastograms were computed by applying a 2D cross-correlation-based echo-tracking technique to the pre- and post-dilated RF echo frames. The principal strains were estimated by computing the eigenvalues of the full 2D strain tensor. Further, the elastographic contrast-to-noise ratio (CNRe), signal-to-noise ratio (SNRe), and root mean square error (RMSE) were computed to evaluate the quality and accuracy of the principal strain elastograms.

Results: Fig. 1(a) shows a representative example of a principal strain elastogram obtained from a simulated homogeneous vessel. Fig. 1(d) shows the corresponding circumferential strain elastogram, which demonstrates that in the absence of shear strain principal (major) and circumferential strains are equivalent—both were radially symmetric, and decayed inversely with increase in radial distance. In both cases the SNRe was approximately 16.2 ± 0.44 dB. Fig. 1(b) shows an example of a principal strain elastogram obtained from a heterogeneous vessel. The corresponding circumferential strain elastogram is shown in Fig. 1(e) Principal strain elastograms revealed high strain within the plaque and the at the interface between the vessel wall and the fibrous cap, which was expected because in these regions the principal strain was dominated by shear strain. Figs 1(c) and 1(f) show principal and circumferential strain elastograms obtained from a healthy volunteer. The principal strain elastogram displays a radially symmetric strain distribution – as expected for a healthy, homogenous vessel (Fig. 1a); however, this was not apparent in the circumferential elastograms because in this case the principal strain elastograms were dominated by radial strains.

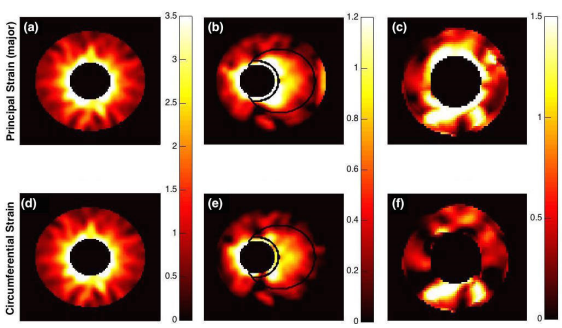

Figure 2 Principal and circumferential strain elastograms obtained from (a) homogeneous vessel, (b) heterogeneous vessel and (c) healthy subject (in vivo). Results are shown only for one of the two components of principal and polar strain because the trends were observed to be similar.

Conclusions: The results from this preliminary study suggest that (1) principal strain can improve the efficacy of non-invasive vascular elastography (NIVE), and (2) compounded plane wave imaging can produce clinically useful principal strain elastograms.

Acknowledgements: This work was supported by NIH RO1 HL123346. We thank Nancy Carson for assisting with the ultrasound scans.

References: [1] Zervantonakis et. al.: "A novel, view-independent method for strain mapping in myocardial elastography: eliminating angle and centroid dependence," PMB, 2007. [2] S. Korukonda et. al.: "Non-invasive vascular elastography using plane wave and sparse array imaging," IEEE UFFC, 60(2), pp. 332-342, 2013.

* *indicates Presenter*

043 **ULTRASOUND ELASTOGRAPHY FOR ASSESSING ABDOMINAL AORTIC ANEURYSMAL RUPTURE RISK.**

Ling Yang[1], Camille C. Johnson[2], Nathan Couper[1], Ben Zarras[1], Doran Mix[3], Michael S. Richards[3].*
[1]University of Rochester, Rochester, NY, USA; [2]Rochester Institute of Technology, Rochester, NY, USA; [3]University of Rochester Medical Center, 601 Elmwood Avenue, Rochester, NY, USA.

Background: Abdominal aortic aneurysms (AAA) are a focal enlargement of the aorta that occurs preferentially in the infrarenal location. According to a recent study [1], the prevalence of AAA disease is 8.8% in the population above 65 years of age and 13th leading cause of death in this country [2]. Aneurysmal sizes of 50 to 55 mm in diameter are routinely recommended for surgical repair, while smaller aneurysms are placed under surveillance. Diameter alone, however, is only a rough estimate of rupture potential as many patients rupture and die with AAA diameters smaller than 50 mm while other patients survive and present with AAA diameters 60 mm or greater. Ultrasound elastography (USe) allows us to measure, *in vivo* biomechanical tissue changes, such as stiffness or stress distribution changes, that may improve a patients rupture risk assessment.

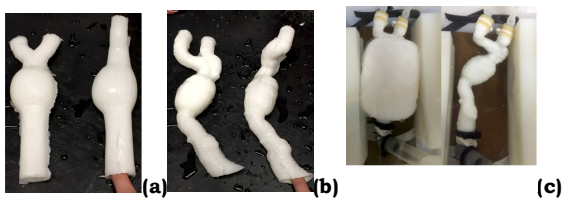

Figure 1.(a) Idealized geometry phantom. (b) Patient-specific phantom. (c) Patient-specific phantom connected to hemodynamic simulator in a water bath (shown without background for visualization only).

Aims: The goal of this project was to: 1) Create tailored, geometrically similar AAA phantoms and an experimental imaging setup to determine if USe can measure the total strain over a cardiac cycle of AAA in cross section; 2) Determine if these USe measurements can be used to detect changes in the mechanical properties of AAA tissue with identical geometries.

Methods: Two AAA geometries were created; an idealized geometry designed using CAD software (Solidworks, Dassault Systemes, Providence, RI) and a patient specific geometry created using clinical CT images and image segmentation software (Mimics Innovation Suite, Materialise NV, Leuven, Belgium). Phantom molds were created from the inverse of the vessel geometries using CAD software and 3D printed. The molds were filled with a 10% by mass concentration polyvinyl alcohol (PVA) cryogel and subjected to 5 freeze-thaw cycles to create the homogeneous phantoms (Fig 1). Additional phantoms with identical geometries but a stiffer anterior portion of the aneurysmal bulge using 25% concentrated PVA. Phantoms were placed in a low stiffness PVA block (5% PVA, 2 FT cycles) and a water bath to mimic surrounding organs and connected to a flow simulator able to induce physiologically pulsatile flow with programmable pressure profiles with ~80 mmHg mean arterial pressure (Fig 1c). Phantoms were imaged with a Sonix Touch Ultrasound system with RF image capabilities (Analogic, Boston, MA). An image registration algorithm [3] was adapted to cumulatively (~55 image frames) measure the total strain for an entire cardiac cycle (Fig 2).

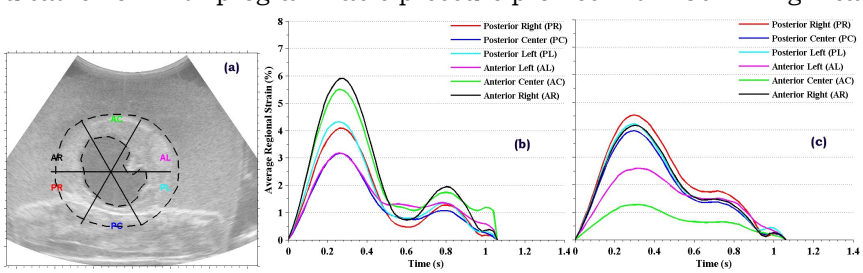

Figure 2. (a) B-mode US of patient specific AAA cross-section and regional sections posterior (bottom), anterior (top) and left/center/right. (b) Averaged regional minimum principal strain measurements for all sections of homogeneous phantom (%) over entire cardiac cycle. (c) Regional measurements for all sections of the aneurysmal stiffened phantom.

Results: The strain at systole of the heterogeneous, patient-specific phantoms in the anterior center (stiffened region) of the phantoms showed a decrease of approximately ~4.4% from ~%5.5 in the homogeneous phantoms. The idealized geometry, heterogeneous phantoms show a similar decrease of ~2.8% from ~%5.5 in anterior center region relative to homogeneous. In addition an increase in the posterior sections of the heterogeneous phantoms showed a relative increase in the strain magnitude.

Conclusions: These results suggest that our USe technique can measure the relative strain in geometrically tissue mimicking phantoms under physiologic pressures and may be used to detect stiffness changes in patients with AAA. Further validation of this technique will be presented.

Acknowledgements: This work was partially supported by NIH-funded study (R21 EB018432-01A1)

References: [1] Newman AB, et al.: Cardiovascular disease and mortality in older adults with small abdominal aortic aneurysms detected by ultrasonography: the cardiovascular health study. *Ann Intern Med*, 2001; pp. 134:182-190. [2] Upchurch Jr., et al.: Abdominal aortic aneurysm. *Am Fam Physician*, 2006;73: pp. 1198-11204. [3] Richards MS, et al.: Non-rigid image registration based strain estimator for IVUS elastography. *Ultrasound Med Biol*, 2013;39(3): pp. 515-33.

008 **4D ULTRAFAST SHEAR WAVE IMAGING.**

Jean-Luc Gennisson[1]*, Jean Provost[1], Thomas Deffieux[1], Clément Papadacci[1], Marion Imbault[1], Mathieu Pernot[1], Mickaël Tanter[1].
Institut Langevin, ESPCI ParisTech, PSL, INSERM, Paris, FRANCE.

Background: 2D shear wave elasticity imaging has been developed within the last ten years and allows mechanical characterization of tissues in order to improve the diagnosis of several pathologies such as breast cancer or liver fibrosis. It is based on ultrafast imaging of shear waves with an ultrafast ultrasound scanner, typically limited to 128 channels and thus to 1D array. Using a full 3D ultrafast ultrasound scanner with a 2D array has many advantages: 3D elastic volume can be reconstructed in a single acquisition in order to limit motion artifacts or track fast changing elastic properties such as in the heart. It could yield an increase of overall SNR by using ultrasonic 2D plane waves as well as 2D plane shear waves to limit diffraction. It allows for better shear wave attenuation and dispersion measurement by either limiting or taking into account the full 3D shear wave diffraction in the volume.

Aims: The aim of this study was to demonstrate the feasibility to achieve 3D ultrafast shear wave elastography in quasi real time, *in vitro* and *in vivo*.

Methods: A customized, programmable, 1024-channel ultrasound system was designed to perform 3D ultrafast imaging (10000 volumes/s) and shear wave tracking. Using a 32x32, 3 MHz matrix phase array (Vermon, france), shear waves were generated inside the medium using acoustic radiation force organized on a grid with different delays and volumes were beamformed by coherently compounding successive emissions from virtual sources. As a comparison, shear waves were also generated using an additional 1D linear array to test different configurations. 3D elastic volumes were reconstructed using the conventional time-of-flight algorithm based on local multiscale cross correlation of shear wave profiles in the three main directions with directional filters and shear wave synthetic compounding.

Results: In figure results are presented at different time step in an isotropic and homogeneous phantom. The shear wave speed was found to be 0.8 m/s in the imaging volume (40x40x40 cm3). Results show that 3D ultrafast shear wave imaging is possible using either a single 2D matrix array or a combination of 2D matrix array and 1D array. With 2D matrix array, 2D plane shear wave were generated using different focusing strategies (synthetic or physical compounding), with different angles and higher SNR compared to cylindrical shear wave. They could also be used to improve image quality using shear compounding. Diffraction biases could be estimated in order to retrieve 2D shear attenuation and dispersion measurements leading to a full 3D rheological characterization. At last first initial *in vivo* results on healthy breast are presented.

Conclusions: Such new full 3D ultrafast ultrasound systems have great potential to assist the understanding of elastic wave physics and improve shear wave elastography in medical device.

Acknowledgements: This work was supported by the Agence Nationale de la Recherche under the program "Future Investments" with the reference ANR-10-EQPX-15 and by the European Research Council under the European Union's Seventh Framework Programme (FP/2007–2013) / ERC Grant Agreement n°311025. J.P. was funded by a FP7 Marie Curie International Incoming Fellowship.

References:

[1] J. Provost et al.: "3D ultrafast ultrasound imaging in vivo." Phys. Med. Biol., 59(19), pp. L1-L13, 2014.
[2] J.L. Gennisson et al.: "4D ultrafast shear wave imaging.", IEEE_UFFC, in press, 2015.

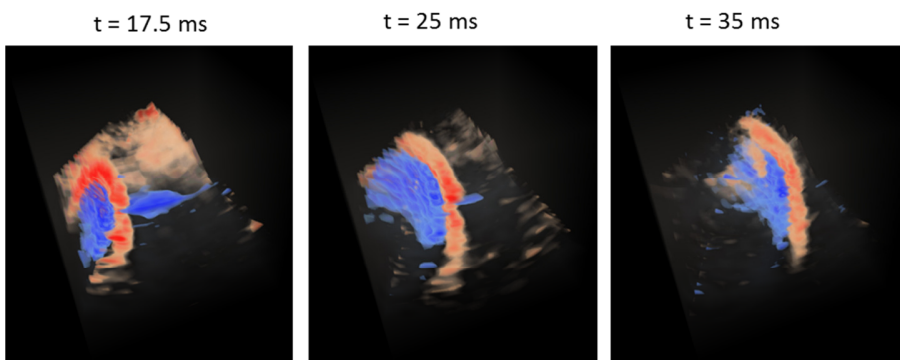

Fig.1 : Shear wave propagation in a volume of interest at different times.

* *indicates Presenter*

017 **ESTIMATION OF POROELASTIC PARAMETERS OF LYMPHEDEMATOUS TISSUE.**

Mariusz Kaczmarek[1], Joanna Nowak[1], Waldemar L. Olszewski[2], Marzanna Zaleska[2].*
[1]Kazimierz Wielki University, Kopernika 1, Bydgoszcz, POLAND; [2]Medical Research Center, Polish Academy of Sciences, Pawinskiego, Warsaw, POLAND.

Background: Development of lymphedematous tissues results from disturbances in lymph transport from interstitial space through lymphatic system to blood [1]. The accumulation of lymph in subcutaneous tissues of e.g. limbs or trunks limits functionality of individuals, may be accompanied by serious infections and other health problems. Thus, it must be diagnosed in order to apply appropriate treatment. The optimization of treatment requires knowledge of tissue properties [2].

Aims: The paper discusses procedures of estimation of parameters of lymphedematous tissue described as two-phase poroealistic material using simple diagnostic techniques to measure creep or relaxation of the tissue.

Methods: Three experimental techniques: indentation (tonometry) method [3], skinfold caliper method [4], and inflation-deflation chamber method [5] applied in vivo are considered as sources of data on mechanical properties of lymphedematous tissues. The ultrasound is used to monitor instant of loading and tissue's deformation (independently of displacement sensor). The poroelastic model with parameters of drained/undrained stiffness and permeability of tissue [6, 7] along with numerical simulations of the considered diagnostic modalities are applied in order to describe poroelastic creep or relaxation. The results for tissue's deformation are then approximated by appropriate surrogate models which are used to estimate poroelastic parameters. A simplified material and geometrical characteristics (homogeneous and isotropic layers of tissues with or without skin cover) along with a set of idealized initial and boundary conditions are assumed.

Results: Capabilities and limitations of the considered techniques are discussed. The role of stiffness of skin in evaluation of parameters of the subcutaneous tissue is evaluated. Basic measures which refer to properties of poroelastic material and useful to distinguish normal and edematous tissue are specified. The results for small and finite strain poroelastic models are elaborated taking into account the evolution of tissue deformations and dissipation of interstitial fluid pressure. Peculiarities of tissue behavior under external loads as well as its sensitivity to changes of crucial hydro-mechanical tissue parameters (permeability or stiffness) are analyzed.

Conclusions: The studies prove the need of complementarity in application of diagnostic methods for estimation of poroelastic parameters of lymphedematous tissue. Particularly important is separation of skin effect, which stiffness may interfere with stiffness of subcutaneous layer. Further works are necessary to establish a form of effective stress law.

Acknowledgements: This study was supported by the National Science Centre in Poland under grant UMO-2013/11/B/ST8/03589.

References:

[1] Olszewski W. L. Physiology - lymph flow, in Lymphoedema. A concise compendium of theory and practice, eds. B.-B. Lee, J. Bergan, S. G. Rockson, Springer 2011, Chap. 9.
[2] Kaczmarek M., et al.: The hydromechanics of edema fluid in lymphedematous limb during intermittent pneumatic compression, Lymph Res Biol., 2015, in press.
[3] Bates D. O., et al.: Quantification of rate and depth of pitting in human edema using an electronic tonometer, Lymphology, 27: pp.159-172, 1994.
[4] Roberts C. C. et al.: Assessment of truncal edema following breast treatment using modified skinfold calipers, Lymphology, 28, pp. 78-88, 1995.
[5] Zaleska M. et al.: A novel clinical test for setting intermittent pneumatic compression parameters based on edema fluid hydromechanics in the lymphedematous calf, Lymp. Res. Biol., 2015 in press,
[6] Biot M. A., General theory of three-dimensional consolidation, J. Appl Phys. 12, pp.155-164, 1941.
[7] Borja R. I., On the mechanical energy and effective stress in saturated and unsaturated porous continua, Int. J. Solids Struct, 43, pp. 1764-1786, 2006.

021 **PARA-SPINAL MUSCLES STIFFNESS DISTRIBUTION ON NORMAL SUBJECTS IN STANDING POSITION.**

Connie LK Cheng[1], YP Zheng[1].*

[1]Interdisciplinary Division of Biomedical Engineering, The Hong Kong Polytechnic University, Hong Kong, CHINA.

Background: Muscle stiffness change is commonly associated with musculoskeletal pathologies. In clinical examination, muscle stiffness change is assessed by manual palpation for diagnosis. Therapists compare stiffness of the affected side with the unaffected side to confirm any asymmetrical change. Alteration in muscle stiffness is also used to indicate muscle response to treatment. Meanwhile, a baseline value of normal muscle stiffness is needed to distinguish possible pathological cases from normal cases. However, study on back muscles' stiffness, related to gender, age groups and physical conditions, is very limited compared with limb muscles.

Aims: To quantify stiffness distribution of para-spinal muscles, along and across the vertebral column in normal subjects.

Methods: A total of 10 normal asymptomatic subjects (4 females and 6 males, Mean age: 24.3 years) were recruited. All subjects were not involved in rigorous training targeted on spinal muscles. Subjects were required to stay in standing posture during measurement. Para-spinal muscle stiffness was measured on top of bilateral laminar at 1.5cm from spinous process at four vertebrae (T3, T7, T11 and L4). Muscle thickness at each measurement point was measured by ultrasound imaging beforehand. Stiffness measurement was performed with a hand-held indentation system developed by our group previously [1]. The flat-end indenter was hand-driven to load and unload tissue at the point of measurement for multiple cycles as one trial. Force applied and subsequent tissue deformation were recorded by a load cell and an electromagnetic spatial sensor embedded in indenter respectively. Young's modulus (kPa) was then calculated from force, deformation and thickness information using Hayes' indentation model to represent stiffness of underlying muscle layers. Three trials were performed on each point for an average measurement. Lateral symmetry of para-spinal muscle stiffness was further analyzed using a ratio (PSR) of right over left stiffness. 3 subjects were invited to take another measurement at T3 and L4 after one day for repeatability study.

Results: Average para-spinal muscle stiffness at T7 and T11 on either side compared with T3 and L4 were slightly higher but not significantly different ($p > 0.05$) (Figure 1). Mean PSR ratios were between 0.9 and 1 indicating overall para-spinal muscle stiffness was lower on the right (Figure 2). However, only asymmetry at T7 was found significant using one-sample t-test with test value of 1. There were no significant differences ($p > 0.05$) between the measurements taken with one day apart.

Conclusions: Para-spinal muscle stiffness on normal asymptomatic subjects was quantified in this study. Although the sample size was small, preliminary results showed that muscle stiffness at various levels along spine in standing posture was not significantly different. Muscle stiffness across lateral sides was found generally symmetrical except at T7. Results from this study provided a reference value for future understanding of the para-spinal muscle stiffness change in pathological conditions.

Acknowledgements: This project was partially supported by Hong Kong Grant Council (PolyU152220/14E)

References:

[1] LU, M.H., et al.: 2009. IEEE Transactions on Instrumentation and Measurement 58, pp. 3079-3085.

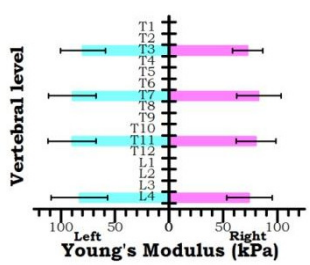

Figure 1: Average para-spinal muscle stiffness.

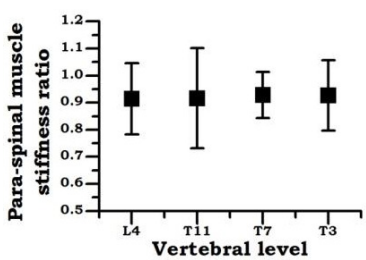

Figure 2: Para-spinal muscle stiffness ratio.

* *indicates Presenter*

030 **INFLUENCE OF APPLIED PRESSURE ON 2D SHEAR WAVE ELASTOGRAPHY (SWE) IN A PHANTOM STUDY.**

Katrin Skerl[1], Bernd Eichhorn[2], Romans Poltorjanoks[1], Bowen Jin[1], Sandy Cochran[1], Andy Evans[1].*
[1]University of Dundee, Dundee, Scotland, UNITED KINGDOM; [2]Schuler-Konstruktionen GmbH, Nuremberg, GERMANY.

Background: Applied pressure influences 2D Shear Wave Elastography (SWE) measurements and variation should be avoided during observations [1]. However, the correlation between the applied pressure and SWE outcomes is unknown.

Aims: The work reported here aimed to investigate, in a preliminary phantom study, the relationship between applied pressure and SWE measurement of stiffness.-

Methods: We have developed a device to measure the pressure applied by the front face of the ultrasound probe, area 488 mm^2. The device is attached as a shell around the handle of the probe and the observer holds this shell instead of the probe. The shell also presses onto a pressure transducer which produces a voltage that is amplified and displayed. Calibration of the voltage with applied pressure was obtained by applying weights in the range 1 g - 1 kg repetitively. Then an agar-based phantom (0.6% agar) with 5 agar lesions (lesions 1, 2, 4 and 5: 1.1% agar, lesion 3: 1.5% agar) was evaluated with SWE with applied pressures of 0, 2, …, 8 kPa. The lesion size was in the range 25 – 83 mm. SWE images of poultry breast were also obtained, under pressures of 0, 2, …, 14 kPa. All images were recorded using the Aixplorer ultrasound imaging system, (SuperSonic Imagine, Aix-en-Provence, France). The images were evaluated using a 2 mm region of interest and the mean elasticity, E_{mean}, was recorded for each image.

Results: E_{mean} increases with pressure in lesions 1 – 4 and the poultry breast. However, no increase was observed in the largest lesion (lesion 5, diameter 83 mm). Pressure of more than 2 kPa damaged the phantom. The smaller lesions 1 – 3 were damaged by an applied pressure of 4 kPa and were thus unable to be used at higher pressures. Pressure of 10 kPa also damaged lesion 4. Hence, all phantom measurements were done only once. No damage was done to the poultry breast by the pressure and the elasticity was observed to increase on average by 10 kPa/2 kPa applied pressure (Fig. 1).

Conclusion: With the device developed during this work, it is possible to measure applied pressure in real time. This enables analysis of the influence of the applied pressure on SWE stiffness measurements. The applied pressure measurements support a standardized procedure to eliminate the natural variance in applied pressure caused by handheld methodology. A study *in vivo* has previously shown that the apparent stiffness of malignant tissue varies more strongly with applied pressure than benign tissue [2]. Thus, monitoring the applied pressure has the potential to improve the differentiation of benign from malignant tissues.

Acknowledgements: This project was performed as part of a PhD project funded by SuperSonic Imagine and the Engineering and Physical Science and Research Council (EPSRC).

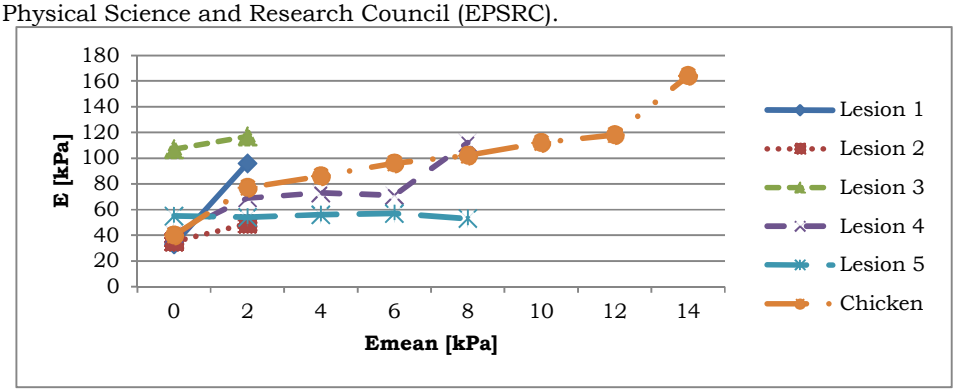

Figure 1: Elasticity increases with pressure in an agar-based phantom containing 5 lesions

References: [1] W. Berg, D. Cosgrove et al.: Shear-wave Elastography Improves the Specificity of Breast US: The BE1 Multinational Study of 939 Masses. Radiology: Volume 262: Number 2, February 2012. [2] A. Sayed, G. Layne et al.: 3-D Visualization and Non-Linear Tissue Classification of Breast Tumors Using Ultrasound Elastography *in Vivo*. Ultrasound in medicine & biology 40, no. 7 (2014).

052 ***IN VIVO* QUANTIFICATION OF THE NONLINEAR SHEAR MODULUS IN BREAST LESIONS: FEASABILITY STUDY.**

M. Bernal[1], F. Chamming's[2], M. Couade[3], J. Bercoff[3], Mickaël Tanter[1], Jean-Luc Gennisson[1].*
[1]Institut Langevin, ESPCI ParisTech, PSL, , INSERM U979, Paris, FRANCE; [2]Radiology Department, Hôpital Européen Georges Pompidou, Paris, FRANCE; [3]Supersonic Imagine, Aix en Provence, FRANCE.

Background: Detection of the breast cancer at its earlier stages is a key factor in the prognosis and treatment. The study of the mechanical properties of breast tissue (shear elasticity, strain imaging) have been used for the diagnosis of malignancies. Nevertheless, there are still some misdiagnosed, and therefore there is a need for new parameters to increase specificity.

Aims: The aim of this study was to develop a technique that allows the quantification of the nonlinear shear modulus (*A*) *in vivo* and show its utility to distinguish breast lesions from healthy tissue.

Methods: The technique relies on the acoustoelasticity theory in quasi-incompressible media. By using static elastography (strain measurements) and supersonic shear imaging (shear elasticity) we were able to determine the stress field using the Hooke's Law in the tissue due to compression. The nonlinear shear modulus (NLSM) *A* (third order Landau coefficient), can be recover from the relationship between the stress (σ) and the shear wave speed (V_S) expressed as follow [1]: $\rho V_S^2=\mu_0-\sigma.A/12\mu_0$, where ρ is the density and μ_0 the shear modulus at zero stress. In this study, a series of 5 nonlinear phantoms using agar-gelatin and pork liver were built and tested to evaluate the sensitivity of our methodology. Furthermore, *in vivo* characterization of the nonlinear shear properties of breast were done in 11 patients, presenting with malignant and benign masses.

Results: The phantom results showed a very good differentiation of the liver inclusions when measuring *A* with a mean value of -114.1 kPa compared to -34.7 kPa for the gelatin. Meanwhile values for the shear modulus for the liver and the gelatin were very similar, 3.7 kPa and 3.4 kPa, respectively. *In vivo* NLSM mean value for the healthy breast tissue was of -95 kPa, while mean values of the benign and the malignant lesions were -619 kPa and -806 kPa with a strong variability respectively.

Conclusions: This study shows the potential of the acoustoelasticity theory in quasi-incompressible medium to bring a new parameter for breast cancer diagnosis.

Acknowledgements: This work was supported by the Agence Nationale de la Recherche under the program "Future Investments" with the reference ANR-10-EQPX-15 and ANR-10-IDEX-0001-02 PSL*.

References:

[1] J.L. Gennisson et al.: "Acoustoelasticity in soft solids: assessment of the nonlinear shear modulus with the acoustic radiation force." JASA, 122(6), pp. 3211-3219, 2007.

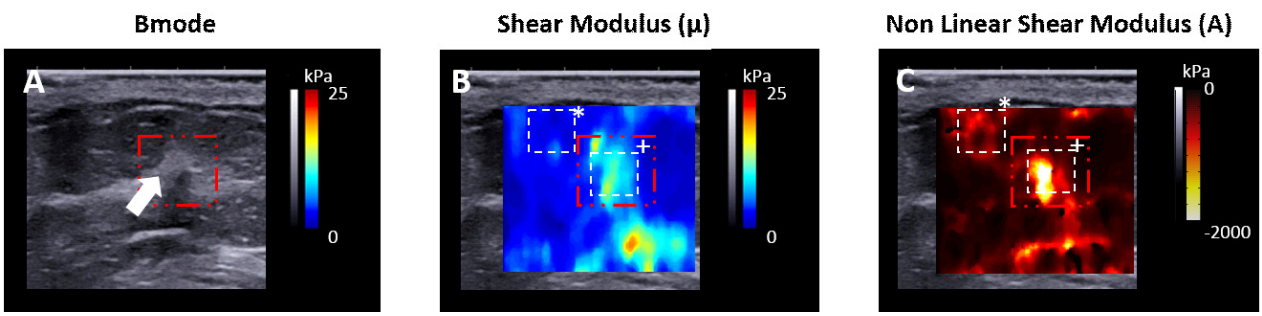

Figure. Results obtain for a patient with a breast cancer. Panel A shows the Bmode images while Panel B shows the shear modulus image in kPa. Panel C shows the Nonlinear shear modulus A, in kPa. The red square shows the location of the mass, while the white ones represent the areas from where the values for statistical analysis were taken.

* *indicates Presenter*

034 **COMPARING MR AND ULTRASOUND SHEAR WAVE ELASTICITY MEASUREMENTS IN HETEROGENEOUS MEDIA.**

JL. Yue[1 2], M Tardieu[1], F Julea[1], L Leenhardt[3], X Maître[1], C Pellot-Barakat[2].*
[1]Univ Paris-Sud, Imagerie par Résonance Magnétique Médicale et Multi-Modalités, CNRS, Orsay, FRANCE; [2]Imagerie Moléculaire *in vivo*, Inserm/CEA/Univ Paris-Sud-CNRS, Orsay, FRANCE; [3]Médecine Nucléaire, APHP, Pitié-Salpétrière, Paris, FRANCE.

Background: Ultrasound Elastography (UE) and Magnetic Resonance Elastography (MRE) have complementarily attractive prospectives for clinical applications. There has been some researches dedicated to the cross-validation of the global elasticity measurements obtained using these two modalities in assumed homogeneous media [1, 2]. Supersonic Shear Wave Elastography (SSWE) allows a 3D quantitative assessment of elasticity maps. A 3D comparison of SSWE and MRE optimizing the registration between the elastograms in a heterogeneous medium is thus possible.

Aims: Compare 3D SSWE and MRE elasticity maps obtained in a tissue-like heterogeneous phantom.

Methods: A realistic heterogeneous breast phantom with embedded inclusions (model 073, CIRS, Norfolk, VA, USA) was used for the comparison. First, the whole phantom was imaged and mechanically characterized at 85 and 152 Hz on a 1.5 T MR Scanner (Achieva, Philips Healthcare, The Netherlands) with a dual flexible coil. The voxel size was (2 x 2 x 2) mm^3. The 3D maps of shear elastic modulus μ were inferred by inversion of the equation of motion [3]. According to the relation E = 3*μ, the corresponding elasticity maps were obtained. Next, four dense inclusions identified from the magnitude images of MRI were imaged using a 3D probe (SLV16-5 MHz) of the Aixplorer ultrasound system (Supersonic Imagine, France). The excitation frequency range was 70-800 Hz (central excitation frequency around 350 Hz). The pixel size was (0.2 x 0.2) mm^2 and the angular resolution 0.16°. A manual segmentation of the inclusions was performed. The mean elasticity E_{mean} and standard deviation *SD* in these regions were computed. The E_{mean} for different parts of the background were averaged to obtain a representative value for the phantom background.

Results: Fig 1 shows the segmentation of a slice of one of the inclusions. The correlations between E_{mean} values of SSWE and MRE at 85 and 152 Hz were 0.91 (P = 0.01) and 0.86 (P = 0.02) respectively. The linear regression between the two modalities showed SSWE elasticity values about four and two times higher than MRE values at 85 and 152 Hz respectively (Fig 2). *SD* ranges in inclusions were 10.8-17.3 kPa and 0.6~2.8 kPa 4.9-7 kPa for SSWE and MRE respectively. *SD* ranges of background were 4.9-7 kPa and 0.2~0.6 kPa for SSWE and MRE respectively.

Conclusions: This preliminary study demonstrated the correlation between quantitative 3D SSWE and MRE in a tissue-like heterogeneous medium. The scaling is related to the difference of excitation frequencies between the two modalities. The study is challenged by the low spatial resolution of MRE as well as the mixed frequency spectrum of SSWE.

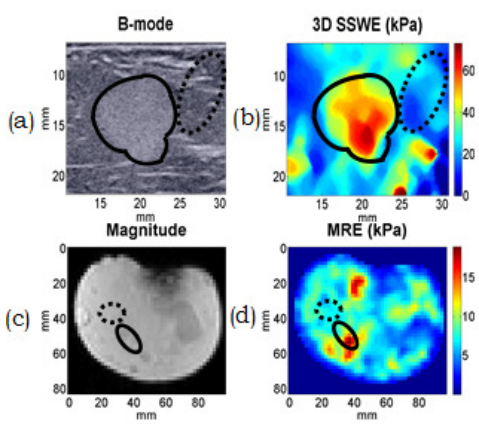

Fig 1: (a) B-mode image (b) SSW elastogram (c) Magnitude image (d) MR elastogram. The solid and dashed lines represent the segmented inclusion and an adjacent region of

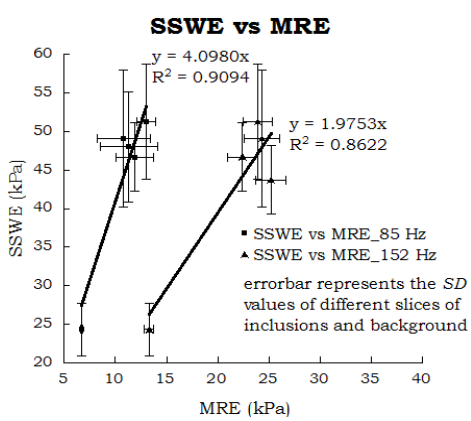

Fig 2: Correlation graph of E_{mean} values measured with MRE (85 and 152 Hz respectively) and SSWE on four inclusions and the background.

References:

[1] Bensamoun SF, et al.: J Magn Reson Imaging, 28, pp. 1287–1292, 2008.
[2] Oudry J, et al. : J Magn Reson Imaging, 30 (5), pp. 1145–1150, 2009a.
[3] R.Sinkus, et al. : Magnetic Resonance Imaging, 23, pp. 159-165, 2005.

041 **THERMAL PROPERTY RECONSTRUCTION VIA REDUCING ULTRASONIC TEMPERATURE MEASUREMENT NOISE USING POLYNOMIAL FITTING METHOD.**

Chikayoshi Sumi.*
Sophia University, 4 Yonban-cho, Chiyoda-ku, Tokyo, 102-0081 JAPAN.

Background: A robust non–invasive technique for reconstructing the thermal properties of living tissues – thermal conductivity, capacity and diffusivity – and thermal quantities such as thermal source/sink and perfusion, for diagnosis, monitoring and planning thermal treatments such as high-intensity focused ultrasound (HIFU) and interstitial radio frequency or microwave coagulation therapy, have been reported by us [1,2]. Internal tissue temperatures can be measured using ultrasonic (US) strain imaging (Ebbini's model) [3] or magnetic resonance imaging. Estimating the point spread function at the high intensity focus position can be used for determining the shape of thermal source [4]. Now, an effective tool for reducing US temperature measurement noise is required in order to increase the accuracy and stability of the thermal property reconstructions, particularly a perfusion coefficient. In the field of US elasticity imaging, the polynomial fitting method is known as a more powerful tool for reducing strain measurement noise rather than a low-pass filtering.

Aims: Through simulations and phantom experiments, the effectiveness of the polynomial fitting method is evaluated for reducing US temperature measurement noise.

Methods: The method's effectiveness was confirmed on (i) simulations and (ii) ultrasonic phantom experiments. In (i), the same cubic tissue phantoms (50.0mm sides) were simulated as in [2]. They contained a spherical region (diameter = 6.0mm), which had a conductivity and a specific heat twice those of the surrounding medium, i.e., 1.0 vs 0.5W/(mK), and 8,400 vs 4,200J/(Kkg) (uniform density, 1,000kg/m^3). As shown in Figure 1a in [2], a spherical perfusion region (dia = 6.0mm) was set at t=0 s such that it overlapped with the inclusion. The Pennes' model was used (blood temperature, 36.0℃; perfusion coefficient w, 2.00kg/m^3s; specific heat cb, 3,770J/Kkg). The phantom had a uniform temperature of 36.0℃ originally, and the temperature of one surface of the phantom was increased by 6.0℃. The time series of temperature distribution was calculated by the successive over–relaxation (SOR) method. White noise data were added to temperature data (SNR = 40dB). In (ii), an agar phantom (height, 50 mm) with a circular cylindrical region (dia. = 15 mm; depth, 30 mm) having different thermal properties realized by adding a small amount of copper powder. An ROI was set (19.8 × 13.2 mm) centered at a depth of 19.7 to 39.5 mm [1]. The phantom (21.4℃) was heated by hot water (46℃) from underneath. The 2D temperature distributions were evaluated by measuring strains generated due to the thermal effects [3] using our previously developed cross-spectrum phase gradient method and phase matching method (US equipment: Aloka, SSD5500; US frequency, 7.5 MHz) and differential filters having cutoff frequencies of 0.05 Hz and 0.511 mm^{-1}.

To achieve the spatial 2nd order partial differentiation of measured temperature data, the fitting method with a spatial quadratic polynomial was used. In simulations, the three thermal properties were reconstructed together with a perfusion coefficient (w × cb), whereas in experiments, only the three thermal properties were reconstructed.

Results: (i) Simulations: With no regularization in reconstruction, the polynomial fitting method yielded higher accuracy and stability than the corresponding low-pass filtering (LPF). Particularly, only the polynomial fitting method succeeded in visualizing the spherical distributions of thermal capacity and perfusion. For instance, using rad = 2mm and the corresponding LPF respectively yielded means (and SDs) as follows: 0.686 (0.041) vs 0.756 (0.195)W/mK; 8.37(0.85) vs 3.59(0.97)x10^6J/m^3K; 7.18(1.56) vs 5.24(7.03)x10^3 J/m^3sK. A too large local spherical size for polynomial fitting (rad > 2mm) yielded less accurate reconstructions with low spatial resolutions. In terms of reconstruction accuracy, the most appropriate size is smaller than that for temperature noise reduction. (ii) Ultrasonic phantom experiments: Also in experiments, so long as regularization methods were employed, the polynomial fitting method yielded higher accuracy and stability than the corresponding LPF (omitted).

Conclusions: For reducing temperature measurement noise, the polynomial fitting method was more effective than low-pass filtering. It significantly increased the accuracy and stability of thermal reconstructions, in simulations and ultrasonic experiments.

References: [1] C. Sumi et al., Phys. Med. Biol. 52, 2845, 2007. [2] C. Sumi et al., Therm. Med. 26, 31, 2010. [3] C. Sumi et al., Jpn. J. Appl. Phys. 46(7b), 4790, 2007. [4] C. Sumi et al., Full paper version proc and abstract of ITEC, ID: 068, 2012.

* *indicates Presenter*

006 **2D TIME HARMONIC ULTRASOUND ELASTOGRAPHY AT LOW FRAME RATES.**

Heiko Tzschätzsch[1], Jürgen Braun[2], Ingolf Sack[1].*
[1]Charité - Universitätsmedizin Berlin, Departments of Radiology, Charitéplatz 1, Berlin, GERMANY; [2]Medical Informatics, Hindenburgdamm 30, Berlin, GERMANY.

Background: Time harmonic ultrasound elastography exploits continuous harmonic vibrations at several frequencies between 30 and 60 Hz for measuring the liver's viscoelastic response in large tissue windows [1,2]. The method has been demonstrated by fast motion sampling based on 1D A-mode ultrasound [1,2]. Alternative approaches to image-resolved time harmonic shear wave elastography utilize crawling waves [3] or multi-periodic wave bursts synchronize to high-frame rate sampling (in the order of 1kHz per image) [4]. We hypothesize that time harmonic elastography (THE) would benefit from combining high penetration depths achievable by uninterrupted harmonic vibrations with motion sampling by low frame rates (FR) obtained in standard medical ultrasound scanners (in the order of tens of Hertz per image).
Aims: To test and demonstrate image resolved THE by multiple continuous vibrations with frame rates as low as 80 Hz provided by our clinical ultrasound scanner.
Methods: For external wave stimulation, a loudspeaker was integrated in the patient bed [2] and fed with a superimposed waveform comprising 6 frequencies (27, 33, 39, 44, 50, 56 Hz) centered on FR/2 (according to Nyquist's theorem for the maximum phase offset between FR and external vibration). Moreover, our frequency selection ensured that stroboscopic sampling by FR = 80 Hz yielded the harmonic wave patterns of six distinct aliasing frequencies after motion extraction and Fourier-decomposition. After correction of temporal wave phases in each of the 64 lines of sights, the resulting six complex-valued wave images were processed by *k*-space bandpass filters (for suppression of noise and compression wave components) combined with spatio-directional filters (for extracting plane waves) followed by wave number recovery (later converted to wave speed values) based on first-order spatial gradients [5]. The method was implemented in a commercial ultrasound device (SonixMDP, Ultrasonix) and tested in phantoms and livers of healthy volunteers and a patient with hepatic fibrosis.
Results: Figure 1 demonstrates the capability of the method to detect elevated liver stiffness (high wave speed values) in a patient with fibrosis of grade F4 (cirrhosis). The increased stiffness in the patient's liver is already seen from larger wavelengths compared to the waves in healthy tissue. Mean values obtained in healthy and diseased liver agree well to reports in the literature [1,2]. Moreover, the wave-speed map in the volunteer demonstrates the resolution of elastic heterogeneities by display of vessels and boundaries.
Conclusions: The preliminary demonstration of image resolved THE is encouraging in that this method provides consistent maps of wave speed values based on multiple harmonic driver frequencies without the need of probe angulations as required by our previous setup [1,2]. Furthermore, the possibility to obtain mechanical parameter images as large as the entire liver (up to 13 cm penetration depth) in high spatial resolution paves the way for a wider range of clinical applications including investigations of heterogeneous tissues such as the kidney or characterization of tumor lesions.
References: [1] Tzschätzsch H et al.: Phys Med Biol, 59(7): 1641–1654, 2014. [2] Tzschätzsch H et al.: Ultrasound Med Biol, 41(3): 724-33, 2015. [3] Wu Z et al.: Physics Med Biol, 49: 911-922, 2004. [4] Zhao H et al., IEEE Trans Med Imaging, 33(11): 2140-8, 2014. [5] Manduca A et al.: Med Image Anal 5: 237-254, 2001.

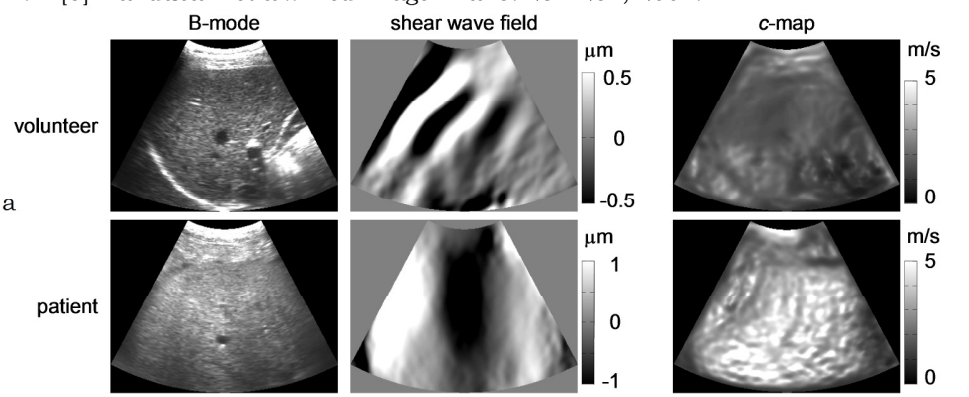

Figure 1. Image-resolved THE in a healthy volunteer and a patient with cirrhosis: B-mode, one direction of the wave propagation pattern (real part for 44 Hz) and shear wave speed maps.

065 **ACOUSTIC PARTICLE PALPATION: A NOVEL STRESS SOURCE FOR ELASTICITY IMAGING.**

Hasan Koruk[1,2], Ahmed El Ghamrawy[1], Antonios N Pouliopoulos[1], James J Choi[1].*
[1]Imperial College London, Royal School of Mines Building, South Kensington Campus, London, UNITED KINGDOM; [2]MEF University, Istanbul, TURKEY.

Background: Acoustic radiation force (ARF) is currently the major noninvasive stress source used for palpating tissue and is the basis for clinically used elasticity imaging technologies including acoustic radiation force impulse imaging [1] and shear wave elasticity imaging [2]. Despite its success, the vast majority of diseases with known mechanical changes remain undiagnosable, and this is in part due to intrinsic limitations with the size, distribution, and depth of current stress sources. We propose here, a novel stress source that uses acoustic particles (e.g., microbubbles) driven by ultrasound (US) to push against tissue surfaces deep in our body. In contrast to ARF-based palpation methods, which displace a volume within the US focal beam, acoustic particle palpation (APP) displaces a surface where acoustic particles are located in a manner similar to atomic force microscope and optical tweezers.

Aims: We will demonstrate the feasibility of APP as a stress source for imaging tissue elasticity.

Methods: We administered lipid-shelled microbubbles (MBs) (mean diameter: 1.3±0.8 μm) into a wall-less 0.8-mm-in-diameter tunnel of a tissue-mimicking material (1.2% gelatin) so that they were compartmentally separate from the surrounding tissue. US pulses (f_c: 5 MHz) forced the MB against the tissue wall to cause a transient deformation, which was observed with high-speed optical microscopy. A range of acoustic pressures was evaluated for different concentrations of MBs while optical observations were recorded before, during, and after sonication with and without MBs present.

Results: Without the presence of MBs in the tunnel, no tissue deformation was observed. However, when MBs were administered, a net displacement of MBs was observed in the direction of wave propagation (figure), which ultimately caused the tissue to deform in the same direction. The deformation magnitude increased with peak-rarefactional pressure and MB concentration.

Conclusions: Our results are the first demonstration of APP. Clinically relevant US and MB parameters were used and our future work will incorporate APP into elasticity imaging systems by palpating (impulse, quasi-static, harmonic) and imaging deformations on- and off-site (impulse, shear wave imaging).

Acknowledgements: We would like to acknowledge funding from the Wellcome Trust Institutional Strategic Support Fund to Imperial College London. HK was supported by the Scientific and Technical Research Council of Turkey (TUBITAK) in the context of the 2219-International Postdoctoral Research Fellowship Programme.

References: [1] Nightingale KR, Palmeri ML, Nightingale RW, Trahey GE. On the feasibility of remote palpation using acoustic radiation force. J Acoust Soc Am. 2001 Jul;110(1):625-34. [2] Sarvazyan AP, Rudenko OV, Swanson SD, Fowlkes JB, Emelianov SY. Shear wave elasticity imaging: a new ultrasonic technology of medical diagnostics. *Ultrasound Med Biol.* 1998 Nov;24(9):1419-35.

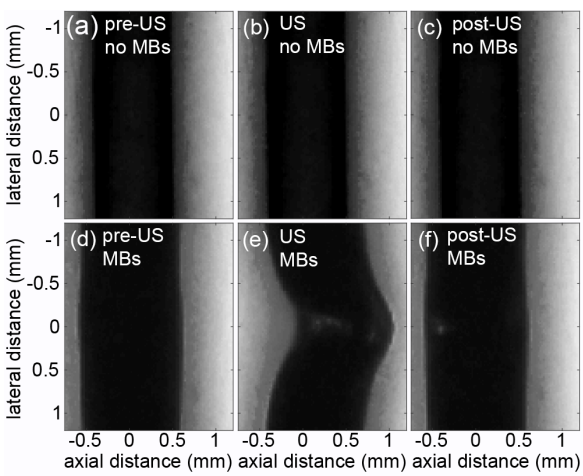

Figure. Feasibility of Acoustic Particle Palpation. A wall-less vessel phantom (1.2% gelatin) contained (a, b, c) water only or (d, e, f) microbubbles. The images are zoomed into the focal volume (a, d) before, (b, e) during, and (c, f) after ultrasound exposure (f_c: 5MHz, P_{neg}: 400kPa). US propagated left to right and produced (b) no displacement with ultrasound alone, and (e) a large displacement with microbubbles.

* *indicates Presenter*

015 **AN AUTOMATIC DIFFERENTIATION OF THE 1D VISCOELASTIC GREEN'S FUNCTIONS FOR MAGNETIC RESONANCE ELASTOGRAPHY RECONSTRUCTION IN ANISOTROPIC TISSUE.**

Simon Chatelin[1,2]*, Nadège Corbin[1], Isabelle Charpentier[1], Jonathan Vappou[1].
[1]ICube, University of Strasbourg, CNRS, 1 place de l'hôpital, Strasbourg1 FRANCE; [2]IHU Institute of Image-Guided Surgery, 1 Place de l'hôpital, Strasbourg, FRANCE.

Aims: Quantitative and accurate measurement of the mechanical properties has been the scope of many research efforts in dynamic elastography over the past two decades [1]. Most of shear-wave-based methods make the assumption of isotropic viscoelasticity, First attempts to extend these methods to anisotropic reconstructions have been limited to transverse isotropy [2,3]. We propose a gradient-based data assimilation approach for Magnetic Resonance Elastography (MRE) to solve the inverse problem in anisotropic viscoelastic soft tissues. The automatic differentiation (AD) tangent method was evaluated on both simulated and experimental MRE data.

Methods: *Numerical data simulation:* The harmonic (130 Hz) displacement field generated by an acoustic radiation force transducer has been simulated by coupling the ultrasound field from the FieldII software and the 3D hexagonal viscoelastic Green's formalism (longitudinal -SV- stiffness: μ_{SV} = 4 kPa; transverse -SH- stiffness: μ_{SH} = 2 kPa; dynamic viscosity: $\eta_{SV} = \eta_{SH}$ = 0.02 Pa.s) [4].
Experimental MRE data: As proposed by [5], the shear waves were generated by a harmonically vibrating (130 Hz) needle inserted in an isotropic gelatin phantom. MRE experiments were performed on a 1.5T MRI system (Siemens Aera, Erlangen, Germany) using a spoiled gradient echo sequence with motion-sensitizing gradients (25 mT/m).
AD reconstruction: A tangent code was generated by the automatic differentiation software (TAPENADE 3.10 [6]) applied to the uniaxial viscoelastic Green's formalism (Figure A). Both shear modulus μ and dynamic viscosity η were quantitatively estimated in the overall direction θ (from 0 to 360° by 10° steps) of space by minimization of a cost function.

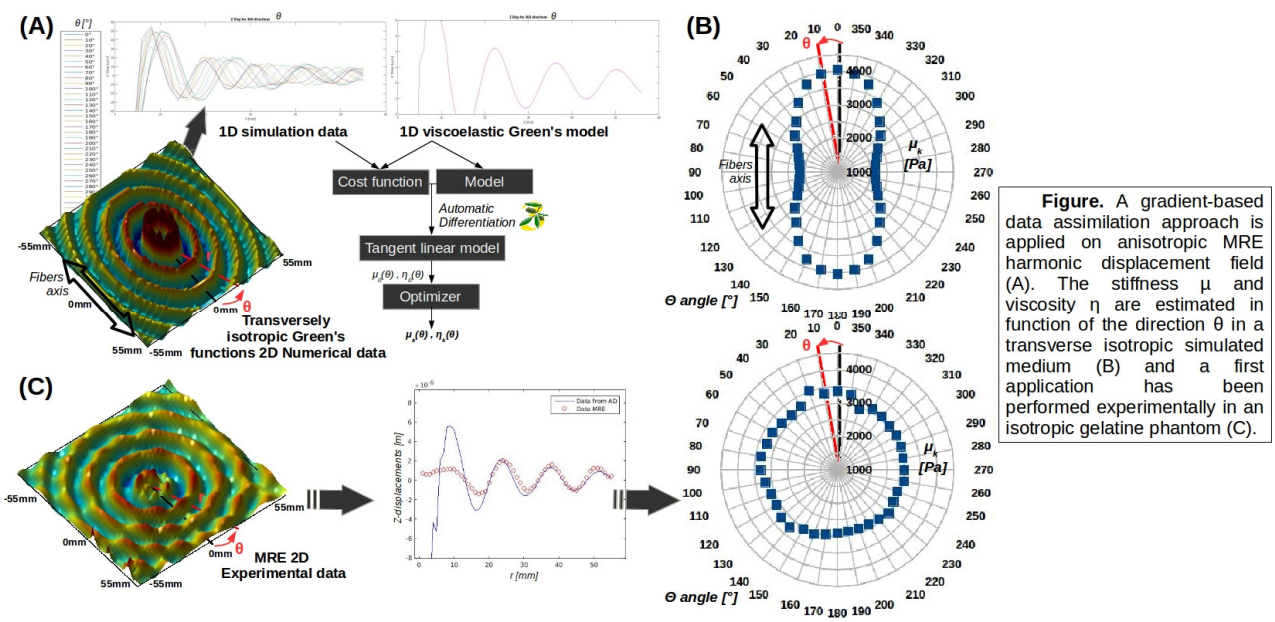

Figure. A gradient-based data assimilation approach is applied on anisotropic MRE harmonic displacement field (A). The stiffness μ and viscosity η are estimated in function of the direction θ in a transverse isotropic simulated medium (B) and a first application has been performed experimentally in an isotropic gelatine phantom (C).

Results: The results on the transversely isotropic numerical data indicates the potential of the method for the identification of both anisotropic stiffness (Figure B) and viscous tensors (μ_{SV} = 4.048 kPa; μ_{SH} = 2.120 kPa; η_{SV} = 0.022 Pa.s; η_{SH} = 0.014 Pa.s). The first experimental results in the isotropic phantom (Figure C) show a robust and constant estimation of both μ and η over the angle θ (μ = 3.109± 0.163 kPa; η = 0.036 ± 0.012 Pa.s).

Conclusions: The use of a gradient-based data assimilation together with AD shows a great potential for MRE reconstructions, with no assumption on the mechanical anisotropy. Although the experiments on anisotropic phantoms and *in vivo* tissue are still ongoing, this AD method shows already substantial benefits for quantitative investigations of complex mechanical properties, such as anisotropic ones.

References: [1] Manduca et al.: Med Image Anal 5(4), 237-254, 2001; [2] Papazoglou et al MRM 56(3), 489-497, 2006; [3] Green M et al.: NMR in Biomed 26, 1387-1394, 2013; [4] Chatelin S et al,: PMB 60, 3639-3654, 2015; [5] Corbin N et al.: MRM 2015; [6] Hasco L & Pascual V, TAPENADE 3.1 user's guide, INRIA report RT-0300, 2004.

053 **NUMERICAL SIMULATION OF WAVE PROPAGATION IN SOFT SOLID FOR ULTRASOUND ELASTOGRAPHY.**

W.Ye [1;3], A.Combescure[1], A.Bel-Brunon[1], S. Catheline[2], M. Rochette[3].*

[1]INSA-Lyon, LaMCoS, France ; [2]INSERM LabTAU, France. [3]ANSYS, FRANCE.

Aims: Transient elastography [1] is a medical characterization technology that estimates the stiffness of biological soft tissues. By imaging the transient propagation of shear wave in soft tissues, one can deduce the shear modulus μ (second Lamé coefficient). Under the assumption of the incompressibility of soft tissues (Poisson's coefficient tends to 0.5), the Young's modulus E can be approximated directly by E=3μ. However, numerous factors, for example, reflection, boundary conditions and pre-stressed could interfere with the accurate measurement of stiffness. Besides the elastic parameter (μ or E), the study of other mechanical properties such as anisotropy, viscoelasticity, and nonlinearity becomes a growing interest in the field of pathology in recent years. Simulations of wave propagation carried by finite element (FE) model help to validate the measurements in elastography. The influential factors can be studied systematically by numerical modelling. In a long term, FE model can be used conversely (like solving an inverse problem) to get more reliable properties of biological tissues as well. However, the property of incompressibility or quasi-incompressibility of tissues leads to two well-known problems in numerical simulations. i) volumetric locking ; ii) no directly explicit scheme exists for mixed formulation.

Methods: In this article, we present a linear triangle element based on a mixed u-p formulation, in which,pressure is interpolated to equal order with displacement. Then, based on the works of [2] and [4], a fractional time-step integration method is implemented in order to give an explicit scheme.

Results: In order to illustrate the performance of above method in elastographic problems, a 2D plane strain model with triangle elements is tested. Fig.3 presents the vertical displacements field of a set of nodes who locate at the left edge of the plate. Fig.1(left) is a typical presentation of elastographic experiments, in which, displacements induced by the shear wave propagation (the slope of deep color band) are usually utilized to deduce the stiffness of soft tissues. Fig.1(right) presents the results more clearly, each line represents the displacements of a tissue slice at one depth. Only a part of nodes (initial height between 20 to 50 mm) is chosen, and the displacements are amplified by a factor of 1000.We mark the extreme values of each displacement with color points. The blue peaks illustrate the propagation of compressional wave which is almost instantaneous, and red peak valleys present the slow shear wave.

Conclusions: In this expression, compressional wave is treated implicitly and shear wave remains explicit. Consequently, stability condition is determined only by the speed of shear wave, which leads to a significant enhancement to the size of time step. However, the matrix inverse procedure will be needed, this work is still under progress.

References:

[1] Catheline, Stefan and Wu, François and Fink, Mathias. A solution to diffraction biases in sonoelasticity : the acoustic impulse technique, The Journal of the Acoustical Society of America, 105, 2941–2950, 1999.

[2] Zienkiewicz, OC and Rojek, J and Taylor, RL and Pastor, M. Triangles and tetrahedra in explicit dynamic codes for solids, International Journal for Numerical Methods in Engineering, 43, 565–583, 1998.

[3] Lahiri, Sudeep K and Bonet, Javier and Peraire, Jaime and Casals, Lluis. A variationally consistent fractional time-step integration method for incompressible and nearly incompressible Lagrangian dynamics, International Journal for Numerical Methods in Engineering, 63, 1371–1395, 2005.

[4] Bonet, J and Marriott, H and Hassan, O. Stability and comparison of different linear tetrahedral formulations for nearly incompressible explicit dynamic applications, International Journal for Numerical Methods in Engineering, 50, 119–133, 2001.

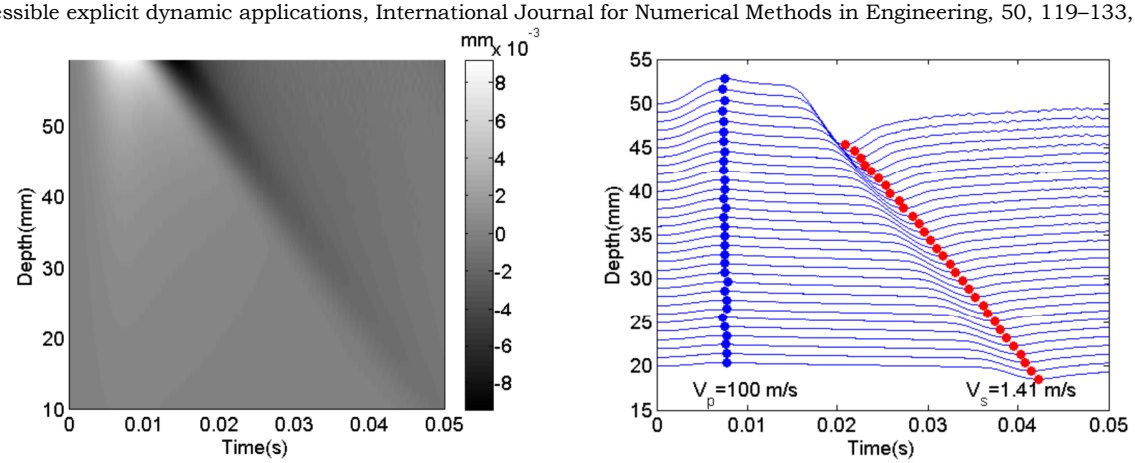

Fig.1 Displacement field results by mixed factional step elements.

* *indicates Presenter*

024 **SIMULATION AND EVALUATION OF ANISOTROPY ON 2D SHEAR WAVE ELASTOGRAPHY (SWE) IN A PHANTOM STUDY.**

Bowen Jin[1], Andrew Evans[1], Xiaowei Zhou[1], Sandy Cochran[1], Katrin Skerl[1].*
[1]University of Dundee, Dundee, Scotland, UNITED KINGDOM.

Background: Anisotropy describes the directional dependence of a property and was obtained on Shear Wave Elastography (SWE) during the assessment of solid breast lesions.

Aims: This project aims to investigate the influence of the lesions dimensions on the anisotropy observed with SWE.

Methods: In this study, twelve agar based phantom lesions were developed in two breast tissue mimicking phantoms. Nine of these lesions were regular shaped lesions (RL) whereas three were irregular shaped lesions (IL) simulating in-vivo breast lesions. Five RL consisted of a solution with 1.5% agar whereas four consisted of a solution with 1.1% agar (size range 10 – 75 mm). The IL were made of a solution with a concentration of 1.5% agar and modelled after the appearance of in-vivo breast lesions. All images were observed along the long and the short axes of the lesions using the ultrasound Aixplorer system, (SuperSonic Imagine, Aix-en-Provence, France). The results of the phantom study were compared to the anisotropy observed in a study-group (1633 patients, 1666 lesions, age range 17-95 years, mean age 58 years).

Results: Anisotropy in phantom and in-vivo increases with lesion size. Our results suggest that this correlation is non-linear. IL have a higher anisotropy than RL with the same concentration of agar and in the same size range. The anisotropy of RL and IL is independent of the concentration of agar. In-vivo lesions are more anisotropic than RL or IL in the same size range.

Conclusion: Anisotropy correlates with lesion size. An irregular shape may cause a higher anisotropy. Hence, anisotropy observed in solid breast lesions is at least partly caused by the dimensions of the lesions. However, as anisotropy in the in-vivo study-group is larger than in our phantom study, further lesion/stromal interactions inside the tissue seem to increase anisotropy. Hence, anisotropy observed in solid breast lesions might give new insights of the pathology of the lesion.

Acknowledgements: This project was performed as part of a PhD project funded by SuperSonic Imagine and the Engineering and Physical Science and Research Council (EPSRC).

037 **PRELIMINARY ANALYSIS OF RSNA-QIBA ULTRASOUND SHEAR WAVE SPEED PHASE II PHANTOM STUDY RESULTS.**

Timothy J Hall[1], Mark Palmeri[2], Shigao Chen[3], Ted Lynch[4], Paul Carson[5], Brian Garra[6,7], Andy Milkowski[8], Kathryn Nightingale[2], Ned Rouze[2], Pengfei Song[3], Matthew Urban[3], Keith Wear[6], Hua Xie[9], Richard Barr[10], Vijay Shamdasani[11], Michael Macdonald[12], Yasuo Miyajima[13].*

[1]University of Wisconsin, Madison, WI, USA; [2]Duke University, Durham, MC, USA; [3]Mayo Clinics, Rochester, MN, USA; [4]Computerized Imaging Reference Systems, Inc. (CIRS), Norfolk, VA, USA; [5]University of Michigan, Ann Arbor, MI, USA; [6]United States Food and Drug Administration, Silver Spring, MD, USA; [7]Veterans Administration Hospital, Washington, DC, USA; [8]Siemens Medical Solutions USA, Inc., Ultrasound Division, Mountainview, CA, USA; [9]Philips Research North America, Briarcliff Manor, NY, USA; [10]Radiology Consultants, Youngstown, PA, Inc., USA; [11]Philips Healthcare-Ultrasound, Bothell, WA, USA; [12]GE Healthcare, USA, [13]Toshiba Medical Research Institute USA, Inc., Tustin, CA, USA.

Background: The Radiological Society of North America (RSNA) Quantitative Imaging Biomarker Alliance (QIBA) ultrasound shear wave speed (SWS) Biomarker Committee has been developing elastic and viscoelastic (VE) phantoms to study system-dependent sources of bias and variance in SWS estimates used to non-invasively characterize liver fibrosis. Previous (Phase I) phantom studies demonstrated intersystem variability ranging from 6-12% in elastic phantoms with nominal SWS of 1.0 and 2.0 m/s, representing values found in healthy and fibrotic human livers. A source of intersystem variability not characterized in the Phase I study was the impact of viscosity, which is known to be present in liver tissue and can lead to group velocity differences between imaging systems because of different shear wave spectral content.

Aims: The objective of our Phase II phantom study is to perform a systematic comparison of ultrasound imaging system-based SWS estimation in phantoms that have VE behavior similar to that observed in normal and fibrotic liver.

Methods: CIRS, Inc. fabricated 3 different phantoms using an oil-emulsion based on their Zerdine material. These phantoms were characterized by their phase velocity at 200 Hz and a linear fit of their phase velocity as a function of temporal frequency ranging from 50 - 1000 Hz to provide an empirical, quantitative metric of their dispersion that is not dependent on an assumed viscoelastic material model. These phantom metrics were compared to human data acquired by Duke and the Mayo Clinic / Philips Research. The 3 phantoms have been circulated to different academic, clinical, and industry imaging sites for measurement on different systems at focal depths of 3, 4.5 and 7 cm.

Results: The 3 VE phantoms match the VE behavior of human data well. As expected, there is greater intrasystem variance in the estimated SWS at the deeper depths. While there are statistically-significant differences across all the systems, the greatest differences were found in the more viscous phantom (C). (Absolute SWS metrics have been withheld due to the ongoing, blinded nature of the study.)

Conclusions: Results to date demonstrate that there is a small, but clinically significant, difference in SWS estimates among systems for clinically relevant scanning conditions. These results, particularly when combined with digital phantom studies, will provide further insight into methods to minimize bias and variance among ultrasound SWS estimates.

Acknowledgements: We gratefully acknowledge the support of CIRS, Inc. who provided the phantoms used in this study with partial support from the US FDA, CDRH. The QIBA effort is funded in part by the RSNA and a contract with the NIBIB (HHSN268201300071C). *Disclaimer: The mention of commercial products, their sources, or their use in connection with material reported herein is not to be construed as either an actual or implied endorsement of such products by the Department of Health and Human Services*

* *indicates Presenter*

046 **A MANUFACTURER INDEPENDENT ULTRASOUND ELASTOGRAPHY ADD-ON MODULE.**

Mohamed Salah[1], Mohamed Tarek[1], Ahmed Sayed[2], and Ahmed M. Mahmoud[1].*

[1]Department of Systems and Biomedical Engineering, Cairo University, Giza, EGYPT; [2]Department of Biomedical Engineering, Misr University for Science & Technology, Giza, EGYPT.

Background: Ultrasound (US) elastography was introduced in the 1990's as a new mode to qualitatively visualize or quantitatively measure the mechanical properties of tissue noninvasively that is important to diagnose liver disease, tumors, atherosclerosis, etc. Common methods for elastography reconstruction compare pre- and post-deformation imaging frames, mostly of radio-frequency (RF) echo signals, to estimate tissue displacements. However, US machines with elastography and/or RF access are expensive and/or not widely used compared to those with only conventional B-mode. Elastography images have been reconstructed from B-mode images [1].

Aims: This work aims to investigate the feasibility to develop a manufacturer independent US elastography add-on module able to extract conventional B-mode images from any US machine via available hardware ports and reconstruct strain maps.

Methods: US images were acquired using, at least, two US machines including 5 MHZ linear array transducer attached to a commercial US machine (DIGISON, IBE, Egypt) and 5 MHZ convex array transducer of another machine (G60S, Siemens, Germany). US data were acquired from a breast elastography phantom (Model 059, CIRS Inc., Norfolk, VA), which includes several solid masses that are at least two times stiffer than the background. Video signals from US scanners were captured by 4 video capture devices (VCDs) of different manufacturers including Forefront Imaging, Hauppauge Computer Works, Diamond Multimedia, and Easycap via the BNC and S-Video ports while manual compressions were being applied via the US transducer. Displacements were estimated using different methods including the commonly used cross-correlation [1], filtered, and then strain was calculated as the derivative of displacement along axial direction using Savitzky-Golay filter.

Results: B-mode videos were captured successfully using the four modules. However, different imaging quality was observed using different VCDs, and consequently strain contrast and SNR were different. Forefront Imaging and Diamond Multimedia VCRs exhibited image quality similar to US machines. We were able to reconstruct strain images and detect the lesions using both systems with the linear and convex arrays. Figure 1 describes the setup and results of the linear array showing the two lesions.

Conclusions: This study showed the feasibility to extract videos of B-mode images similar in quality to those saved by US machines. Strain images were reconstructed successfully from pure B-mode images acquired by VCDs. After further clinical validation, this add-on module shall help healthcare facilities to acquire the elastography mode at lower cost and more standard protocol.

Acknowledgements: This work was supported by the Egyptian Information Technology Industry Development Agency (ITIDA) under ITAC Program CFP #16. Authors would like to thank the Bionics and Rehabilitation Laboratory at Cairo University funded by the STDF, and the Radiology Department at Dar Al Fouad Hospital for providing US machine access.

References:

[1] Y. Han, D.W. Kim and H.J. Kwon," Application of digital image cross-correlation and smoothing function to the diagnosis of breast cancer "J. Mech. Behav. Biomed. Mater, Volume 14, pp.7-18, 2012.

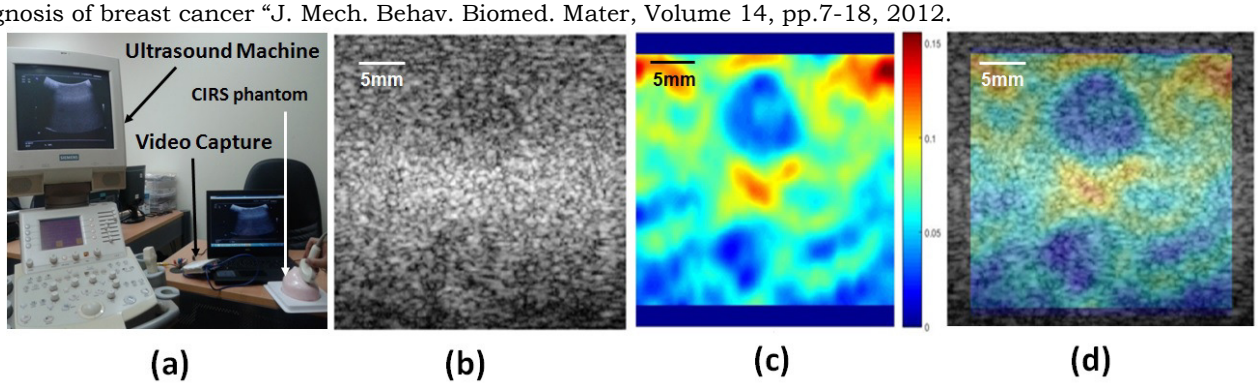

Figure 1: (a) System setup, (b) B-mode image, (c) axial strain image, and (d) strain image superimposed on B-mode.

038 **HARMONIC MOTION IMAGING FOR ELASTICITY MAPPING OF ABDOMINAL ORGANS *IN VIVO.***

Thomas Payen[1], Carmine Palermo[2], Steve Sastra[2], Hong Chen[1], Yang Han[1], Kenneth Olive[2], Elisa E Konofagou[1,3].*

[1]Biomedical Engineering, Columbia University, New York, NY, USA; [2]Herbert Irving Comprehensive Cancer Center, Columbia University, New York, NY, USA; [3]Department of Radiology, Columbia University, New York, NY, USA.

Background: Harmonic Motion Imaging (HMI) assesses tissue viscoelasticity by inducing localized oscillation resulting from a periodic acoustic radiation force [1]. The amplitude of the induced displacement is directly related to the underlying tissue stiffness.

Aims: The objective of this study was to evaluate the capacity of HMI for mapping abdominal organs in vivo based on their differences in stiffness. In the case of the pancreas, feasibility in a pathological case, i.e. chronic pancreatitis, was also studied in vivo in a mouse model.

Methods: A 4.5-MHz focused ultrasound transducer (FUS) generated an amplitude-modulated beam resulting in harmonic tissue oscillations at its focus. Axial tissue displacement was estimated using 1D cross-correlation of RF signals acquired with a 7.5MHz diagnostic transducer (P12-5, ATL) using a plane-wave beam sequence, confocally aligned with the FUS. Phantoms with stiff occlusions were first used to evaluate the performances of this setup in terms of resolution. Ex vivo canine liver, pancreas, spleen and kidney were assessed with HMI, and mechanical indentation was performed as a gold standard. Relative stiffness maps were obtained using HMI in mice in vivo. Ex vivo measurements were then performed in agar gel phantoms for reference. The pancreatitis was induced in mice (N = 15) with daily caerulein injections for 5 days in a transgenic mouse model. In order to allow for pancreatitis to form, the pancreas was scanned using HMI one week later and histology was performed to correlate the HMI values with fibrotic area percentages in the tail and the head of the pancreas.

Results: The results showed that HMI was capable of providing reproducible relative stiffness values of the abdominal region in vivo. The phantom measurements demonstrated the high spatial resolution and sensitivity of HMI. The canine study showed good agreement between mechanical testing and the HMI measurements. The in vivo relative 2D stiffness maps provided values similar to the ones obtained ex vivo with the hardest one first, i.e. kidney, spleen, liver, and pancreas. HMI also enabled pancreatitis detection as shown on relative 2D stiffness maps (Figures A&B). Inflamed pancreases (Figure B) demonstrated HMI displacements on average 2.1 times lower than in the normal pancreas (Figure A) indicating higher overall stiffness. HMI was also capable of identifying the stage of disease as well as the specific location in the pancreas at the earliest stage when the inflammation was not yet systemic.

Conclusions: This work shows that HMI can produce reliable 2D elasticity maps of the abdominal region in vivo. In addition, the technique is sensitive enough to detect and assess elasticity-related pathologies such as pancreatitis that could be used to better differentiate from pancreatic tumors in the clinic.

Acknowledgements: This work was supported by the funding source NIH R01EB014496.

References: [1] Maleke C, Pernot M and Konofagou E E (2006), Single-element focused ultrasound transducer method for harmonic motion imaging. Ultrason. Imaging 28 144–58.

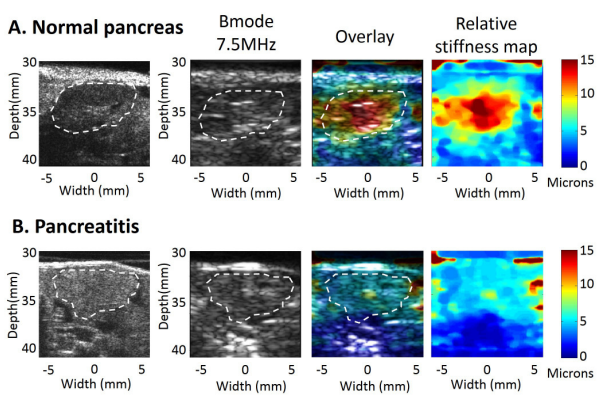

* *indicates Presenter*

049 **EFFECTS OF COHERENT COMPOUNDING ON PULSE WAVE IMAGING (PWI) IN PHANTOMS AND *IN VIVO*.**

IZ Apostolakis[1], RX Li[1], MDJ Mcgarry[1], EA Bunting[1], EE Konofagou[1].*
[1]Columbia University, New York, NY, USA.

Background: Pulse wave imaging (PWI) is a noninvasive technique developed by our group for tracking the propagation of pulse waves along the arterial wall at high spatial and temporal resolution [1], [2]. In order to achieve high frame-rates without relying on stroboscopic techniques (ECG-gating), plane wave acquisitions were implemented. However, single plane-wave transmission results to lower SNR and higher side-lobe levels that further challenge the motion estimation techniques [3]. Coherent compounding is known to significantly improve displacement estimation at the cost of lower frame-rate [3], [4].

Aims: The objective of this study was to use a variety of metrics in order to investigate the PWI performance in tracking the pulse waves with and without compounding.

Methods: A phantom and the right carotid arteries of six healthy subjects (n=6) were scanned using 1-, 3-, 5-, 9- and 12-plane wave acquisitions. The frame-rate of the acquisitions ranged from 8333 Hz (1 plane wave) down to 694 Hz (12 plane waves). Axial wall displacements (AWD) were depicted over time to generate spatiotemporal maps of the pulse propagation. In each case, the regional Pulse Wave Velocity (PWV) and associated coefficient of determination (r^2) were calculated by performing linear regression on the 50%-upstroke markers of the pulse-wave-induced AWDs. The percentage of 50%-upstroke markers that occur at the same time-point (temporal resolution misses) was also estimated. Finally, the SNR of the AWD of the constructed spatiotemporal maps was calculated within 2D windows (0.2 mm × 7 ms) and a stochastic metric of precision (E(SNR|awd)) was computed.

Results: The PWV values were highly reproducible in the same subject over different plane-wave sequences. Furthermore, as shown in Fig. 1, there was excellent agreement between the phantom and *in vivo* findings showing significant increase in both the mean SNR and r^2 with the number of transmitted plane waves, thus indicating higher quality and reliability of the measurements. However, this was at the expense of temporal resolution, preventing further localization of PWV measurements, which is critical for focal arterial disease. Finally, the proposed stochastic metric may aid in optimizing the acquisition sequence for the given wall displacement amplitudes. Analysis will also be performed on atherosclerotic patient datasets.

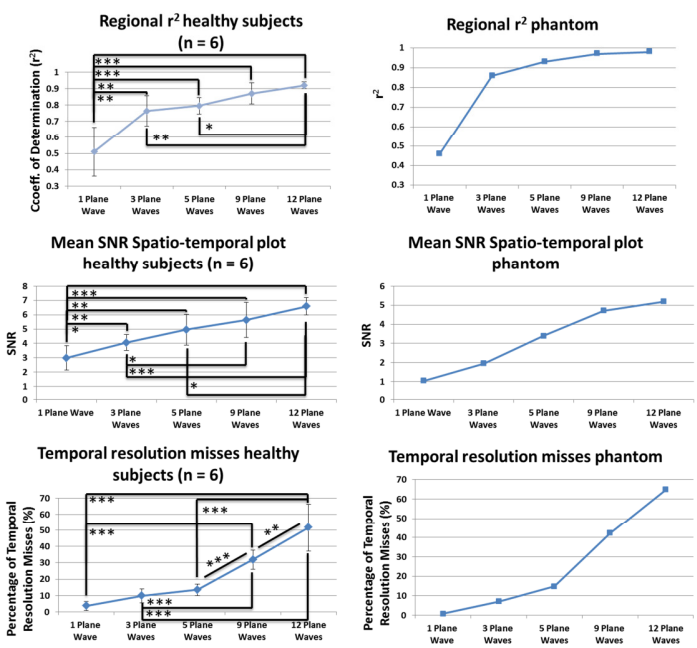

Figure 1: r^2, SNR and temporal resolution misses versus number of plane waves in the case of healthy subjects (left) and phantom (right).

Conclusions: This study showed that the quality of the PWI measurements increases with the number of transmitted plane waves and also demonstrated a trade-off between the SNR and the temporal resolution of our method. The results presented in this study will be used to optimize PWI acquisition sequences.

Acknowledgements: This work was supported in part by R01–HL098830.

References:

[1] K. Fujikura et al.: Ultrason. Imaging, vol. 29, no. 3, pp 137-54, 2007.
[2] J. Luo et al.: IEEE Trans. Med. Imaging, vol. 28, no. 4, pp. 477-86.
[3] G. Montaldo et al.: IEEE Trans. Ultrason. Ferroelectr. Freq. Control, vol. 56, no. 3, pp 489-506, 2009.
[4] M. Tanter et al.: IEEE Trans. Ultrason. Ferroelectr. Freq. Control, vol 49, no. 10, pp. 1363-1374, 2002.

056 **IMPROVING ROTATION ELASTOGRAM QUALITY USING SYNTHETIC APERTURE TECHNIQUE.**

Lokesh B[1], Bhaskara Rao Chintada[1], A K Thittai[*1].*

[1]Indian Institute of Technology Madras, Chennai-600036, INDIA.

Background: It can be inferred from existing literature that benign lesions in breast are loosely bonded, whereas malignant lesions are firmly bonded to the surrounding tissue. It has been shown that when a lesion is asymmetrically oriented w.r.t the axis of compression only the benign ones tend to "slip" at the lesion boundary yielding non-zero axial shear strain values inside the lesion, which has been referred to as "fill-in" [1]. It was argued that the "fill-in" observed in ASSE is a surrogate of the actual rotation undergone by the benign lesion due to slip boundary condition [2]. In order to image this rotation (Eqn. 1) directly it would be necessary to improve the lateral displacement estimation. It has been shown recently in non-invasive vascular elastography context that synthetic aperture approach can be adapted for elastography to improve the lateral displacement estimates [3].

$$W_{x,y}(\text{rotation}) = 0.5(\partial v/\partial x - \partial u/\partial y) \quad (1)$$

$\partial v/\partial x$ – Axial component (ASSE), $\partial u/\partial y$ – Lateral component (LSSE), u- lateral displacement, v-axial displacement and x, y are the lateral and axial directions, respectively.

Aim: To study the use of full Synthetic Transmit Aperture (STA) technique to improve the rotation elastogram quality.

Methods: Finite Element Simulation- We simulated an inhomogeneous phantom model with an overall dimension of 40 mm x 40 mm having an elliptical inclusion (long axis 7 mm and short axis 4 mm) at the center, whose long axis was oriented at 45° w.r.t axis of compression. The inclusion was modeled as 3 times stiffer than the background and an axial compression of 1% was applied to the phantom at the top. The benign lesion was simulated as a loosely-bonded inclusion using contact element pairs with frictional coefficient of 0.01. The simulations were performed in COMSOL(R) (COMSOL AB, Stockholm, Sweden).

Ultrasound Elastography Simulations- The pre- and post- compression RF signals were simulated in FIELD II (centre frequency 5MHz, sampling frequency 40MHz, pitch 0.3mm, Transducer elements 128) using both STA [4] and Conventional Linear Array (CLA) technique. In STA method, one element of the linear transducer array was successively activated during transmission while all elements were active during reception; delay and sum beamforming was applied on the received signal to obtain corresponding high-resolution synthetic aperture RF frame. A multi-level displacement tracking algorithm [1] was used to obtain the axial and lateral displacements. ASSE and LSSE were computed by applying the least-square estimator to the axial and lateral displacements, respectively. The rotation elastogram was obtained through Eqn. 1. In order to compare the two techniques, contrast to noise ratio (CNR) was estimated from the rotation elastograms of the loosely-bonded inclusion obtained by the respective techniques. A region of 4.3mm x 4.8 mm was taken from inside the lesion and the surrounding background at the same depth to calculate the CNR using standard formula available in literature.

Results: Figure 1 clearly demonstrates the improved Point Spread Function (PSF) in the lateral direction when using the STA technique over the CLA (with dynamic receive focus) technique. Rotation elastograms obtained from simulations show that only the loosely-bonded inclusion undergoes a rotation-thereby generating a contrast (Fig. 2b) and not the firmly-bonded inclusion (Fig. 2a). Further, the rotation elastogram obtained from STA technique is of improved quality compared to the one obtained by CLA technique (Fig. 2b&2c). The calculated value of the CNR was ~2 and 1.2 for STA and CLA, respectively.

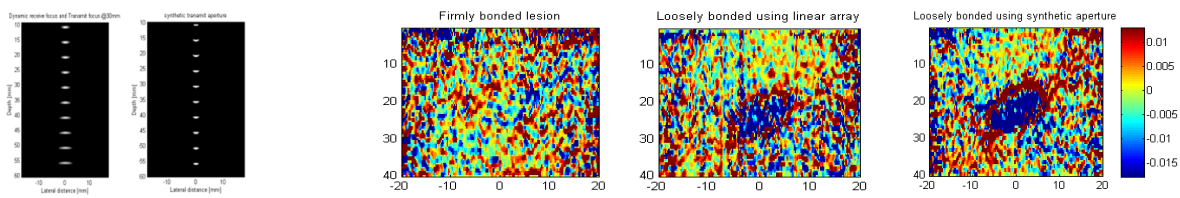

Figure 1: PSF (a) Dynamic receive focus (b) STA. Figure 2: Rotation elastogram obtained from (a) Firmly-bonded lesion and loosely-bonded inclusion using (b) CLA and (c) STA technique.

Conclusions: The results demonstrate that using STA method yields improved rotation elastogram quality. Further work is needed to validated the reported simulation results.

References: [1] Thittai A K, Galaz B and Ophir J. Axial- shear strain distributions in a elliptical inclusion model: experimental validation and in vivo examples with implications to breast tumor classification. Ultras. Med. Biol. 36,814-820, 2010. [2] Thittai A K, Galaz B and Ophir J. On the advantages of imaging the axial-shear strain component of the total shear strain in breast tumors. Ultras. Med. Biol. 38(11), 2031-2037, 2012. [3] Korukonda S and Doyley MM. Estimating axial and lateral strain using a synthetic aperture elastographic imaging system. Ultras. Med. Biol. 37(11), 1893-908, 2011. [4] JA Jensen, SI Nikolov, KL Gammelmark et al. Synthetic aperture in ultrasound imaging. Ultras., 44,5-15, 2006.

054 **MEASUREMENT OF MOTION IN BRAIN TISSUE AFTER EXCITATION BY A DROP EXPERIMENT.**

Anna-Lisa Kofahl[1], Sebastian Theilenberg[1], Jakob Bindl[1], Birgit Schu-Schätter[1], Sylvia Napiletzki[1], Björn Schemmann[1], Jürgen Finsterbusch[2], Carsten Urbach[1], Karl Maier[1].*

[1]HISKP, University of Bonn, Nussallee, Bonn, GERMANY; [2]Department of Systems Neuroscience, University Medical Center Hamburg-Eppendorf, Martinistraße, Hamburg, GERMANY.

Background: The viscoelastic properties of brain tissue are altered by different diseases (e.g. Alzheimer's disease or multiple sclerosis [1, 2]), which makes measuring them an interesting topic, preferable in a high resolution fashion. Such measurements are hindered by the hard cranial bone that cannot be penetrated easily, and have so far only been successful using Magnetic Resonance Elastography (MRE).
In our approach, the brain tissue is globally excited with a high bandwidth by applying a drop experiment over a small distance [3, 4], providing access to the viscoelastic properties of even small structures.
Aims: The aim of the work presented here was the voxel wise reconstruction of the motion of the brain tissue taking place as response to the drop experiment.
Methods: When a falling motion of the head is induced, the equilibrium of forces of all volume elements of the brain tissue is disturbed at once. This leads to a relative motion of individual volume elements relative to the cranial bone (see left side of the figure 1). The exact nature of these trajectories is locally dependent on the viscoelastic properties of the tissue. The falling motion is induced inside the head coil of a magnetic resonance scanner synchronized to a motion sensitive spin-echo echo-planar-imaging sequence, which encodes motion into the phase of the signal via two magnetic field gradients. By varying the time at which the motion is started relative to the MR sequence, the complete time response of the tissue can be sampled (right side of the figure 1).
Results: Phantoms consisting of agar-based hydrogel as well as healthy volunteers were measured using a 1.5 T Siemens Magnetom MR scanner. The motion occurring during and after a drop of about one millimeter was sampled with a temporal spacing of one millisecond. Images reconstructed from the phase data of these measurements show a contrast based on the different trajectories of individual volume elements.
The phase data of the individual measurements was combined to get a steady phase response of the volume elements. By applying the knowledge of the motion sensitizing gradients this phase data was used to reconstruct the trajectories of every voxel individually. By comparing these to the trajectory of the motion creating device, which was measured optically and roughly equals the trajectory of the phantom container respectively the cranial bone, the relative movement of the tissue elements to the surrounding shell was determined. This data represents the mechanical response of the tissue to the excitation.
Conclusions: The presented results show the feasibility of reconstructing the motion during the drop experiment for individual voxels in physical units. Together with the acceleration that took place, this data may be used in the future as input into viscoelastic models of brain tissue, enabling the deduction of physical properties such as shear modulus or viscosity. Such data might add knowledge to the one acquired by MRE.

Figure 1

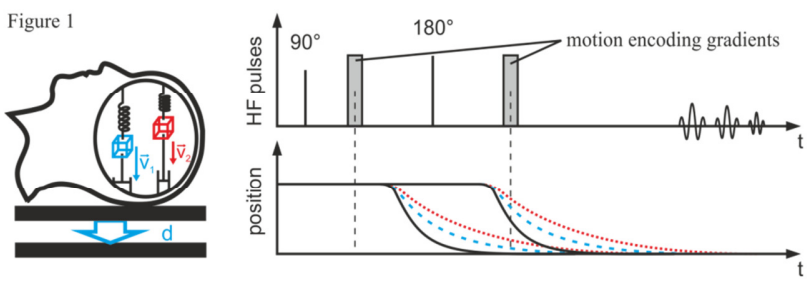

References:
[1] Mariappan,Y. K. et al.: Clin. Anat. 23, pp. 497-511, 2010.
[2] Murphy, M. C. et al.: J. Magn. Reson. Imaging 34, pp. 494-498, 2011.
[3] Theilenberg, S. et al.: Joint Annual Meeting ISMRM-ESMRMB 1690, 2014.
[4] Kofahl, A.-L. et al.: Joint Annual Meeting ISMRM-ESMRMB 1689, 2014.

058 **COMPARABILITY STUDY OF FALL-INDUCED PHASE CONTRAST IMAGES OF PHANTOMS AND THE HUMAN BRAIN.**

Sebastian Theilenberg[1], Jakob Bindl[1], Anna-Lisa Kofahl[1], Sylvia Napiletzki[1], Björn Schemmann[1], Birgit Schu-Schätter[1], Jürgen Finsterbusch[2], Carsten Urbach[1], Karl Maier[1].*

[1]University of Bonn, HISKP, Nussallee, Bonn, GERMANY; [2]University Medical Center Hamburg-Eppendorf, Department of Systems Neuroscience, Martinistraße, Hamburg, GERMANY.

Background: Measuring the viscoelastic properties of the human brain *in vivo* is an active field of research since the knowledge of these properties may aid in the diagnosis of diseases like Alzheimer's disease [1], brain cancer or multiple sclerosis [2].

Aims: The method presented here to image the viscoelastic properties of the brain non-invasively with a good spatial resolution uses an acceleration and creep experiment - a well-known technique from material science – inside an MRI, where a motion encoding EPI sequence is used to measure the relaxation movement of the substance under investigation. Previous results showed the feasibility of this method on the human brain [3] and some promising results imaging differences in stiffness inside a phantom with good spatial resolution [4]. A broader evaluation of the potential of this method for further research applications is presented.

Methods: The principles of measurement are described in figure 1a: For a head at rest at a height h_0 the gravitational force and the restoring forces of the viscoelasticly coupled brain tissue (symbolized by different spring and dash elements inside the hard cranial bone) are in equilibrium. When the head is dropped at a time t_1, the effective gravitational force is reduced by the acceleration of the fall the head performs in its entirety. Thus the equilibrium of forces is disturbed and it comes to an inner excitation of the brain tissue which results in a movement of the brain tissue relatively to the cranial bone. The velocity of this movement occurs with locally different velocities v_1 and v_2 depending of the locally different viscoelastic properties and the geometric boundary conditions. After the head has landed the brain creeps back into its original equilibrium. The rate of the motion (depicted as Δh_1 and Δh_2) is measured using a motion encoding single-shot EPI sequence (fig. 1b) (T_R:3000ms, T_E:120ms, δ:5ms, Δ:40ms, G:25mT/m, motion sensitivity in direction of the fall) and depicted in the phase image. The principle is realized inside a 1.5T Magnetom Avanto scanner equipped with a Head Matrix Tim coil (both Siemens Healthcare) by using a custom made pneumatic lifting device, which lifts the head to a height h_0=1-1.2mm and drops it synchronized to the sequence. By varying the starting point of the drop in relation to the sequence different parts of the brain motion can be depicted in the phase images.

Results: Using homogeneous phantoms consisting of agar-based hydrogel we show how different degrees of stiffness (differences in shear modulus as small as 1 kPa) can be distinguished by comparing the time dependence of the motion induced phase contrast in each phantom. Additionally, measurements of ten healthy volunteers are presented.

Conclusions: The presented results show the feasibility of distinguishing different shear moduli of phantom material using the drop experiment. Considering the group of healthy volunteers a margin for comparability for human subjects can be estimated. In order to achieve quantitative information the stress acting on the system has to be measured with high precision and the strain has to be calculated from the phase data, which are both challenges being addressed in ongoing research work.

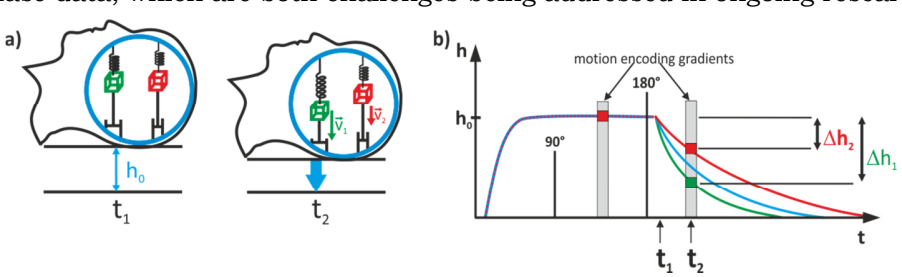

References: [1] M. C. Murphy *et al.* : J. Magn. Reson. Imaging 34:494–498 (2011). [2] Y. K. Mariappan, *et al.*, Clin. Anat. 23:497-511 (2010). [3] Theilenberg, S., *et al.*: Joint Annual Meeting ISMRM-ESMRMB 1690 (2014). [4] Kofahl, A.-L., *et al.*, Joint Annual Meeting ISMRM-ESMRMB 1689 (2014).

033 **HAND-HELD SOUND-SPEED IMAGING FOR THE RECONSTRUCTION OF BULK MODULUS AND POISSON RATIO IN A COMMERCIAL TISSUE-MIMICKING PHANTOM.**

Sergio J Sanabria[1], Corin F Otesteanu[1], Orcun Goksel[1].*
[1]Computer Vision Laboratory, Dept. of Inf Tech and Elec Eng, ETH Zurich, SWITZERLAND.

Background: Most ultrasound (US) elastography research aims at the imaging of Young modulus (E), which is reconstructed from quasi-static/vibrational displacements or from measured shear-wave speed. Bulk modulus K, which determines the longitudinal-wave speed (c), is another elastic parameter of soft tissues, which can be of interest for tissue differentiation, as it is sensitive to breast and hepatic diseases [1]. Additionally, given K and E, the Poisson ratio (υ) can also be imaged. Current c imaging techniques, i.e. US computed tomography, involve complex transducers or scanning setups [1].

Aims: Extension of conventional B-mode US for $c/K/\upsilon$ imaging based on a hand-held setup with a linear-array transducer and a US reflector.

Methods: c-images were generated for the 049 Elasticity QA phantom (CIRS Inc.) made of polyacrylamide hydrogel (Zerdine™), with a background E-modulus of 23 kPa and isoechogenic 10/20 mm spherical inclusions of [8, 18, 48, 80] KPa. A 128x linear US array was operated in multistatic mode (Fig.1a), each element firing (Tx) and the rest receiving (Rx). Adaptive amplitude-tracking measured the delays of echoes reflected at the back-wall of the sample (Fig.1b). Nelder-mead simplex optimization of the 128x128 delay matrix provided mean c_o, reflector distance d_o and inclination θ, together with relative delays Δt due to c heterogeneity. With the known geometric path lengths L, a c contrast image $\Delta c/c_o=-\sigma\cdot c_o$ was reconstructed from time-of-flight data, i.e. $\Delta t=L\sigma$, robustly using total-variation (TV) smoothness regularization. For comparison, axial-strain ε_{ZZ} images were obtained via quasi-static elastography. With c and E, $K = c^2\rho_o + 4KE/(9K - E)$ and $c=\sqrt{[(E/\rho_o)(1-\nu)/(1+\nu)/(1-2\nu)]}$ were computed given $\rho_o=10^3$ kg m^{-3}.

Results: The spherical inclusion can be resolved in c-images (Fig. 1b), with a contrast-to-noise ratio (CNR) of 9.4 dB with respect to 3.2 dB for the ε_{ZZ} elastogram. Due to the limited angular information, the inclusion is axially elongated by $1.5(d_o/w)=360\%$. This causes Δc to be underestimated, thus for quantitative c values the inclusion geometry extracted from ε_{ZZ} was used as prior information. Since $E<<K$, $K\approx c^2\rho_o$ is independent from E to 0.001% accuracy. Nonetheless, $A\approx c_o 2\rho_o/E$ so that Δc does not influence υ. A linear relation ($R^2=0.99$) between c and E is, however, observed for the Zerdine™ hydrogel, which reflects in K(E) (Fig. 1c). This relation seems material-constitutive and needs to be further studied.

Conclusions: Hand-held c-maging complements E-modulus elastography, and allows mapping Bulk modulus and Poisson ratio in tissue. E-modulus is found linearly-related to $c/K/\upsilon$ for Zerdine™ hydrogel.

Acknowledgements: This work is supported by the Swiss National Science Foundation (SNSF).

References:

[1] Glozman T, Azhari H: A method for characterization of tissue elastic properties combining ultrasonic computed tomography with elastography. J Ultrasound Med 29, pp. 387-398, 2010.

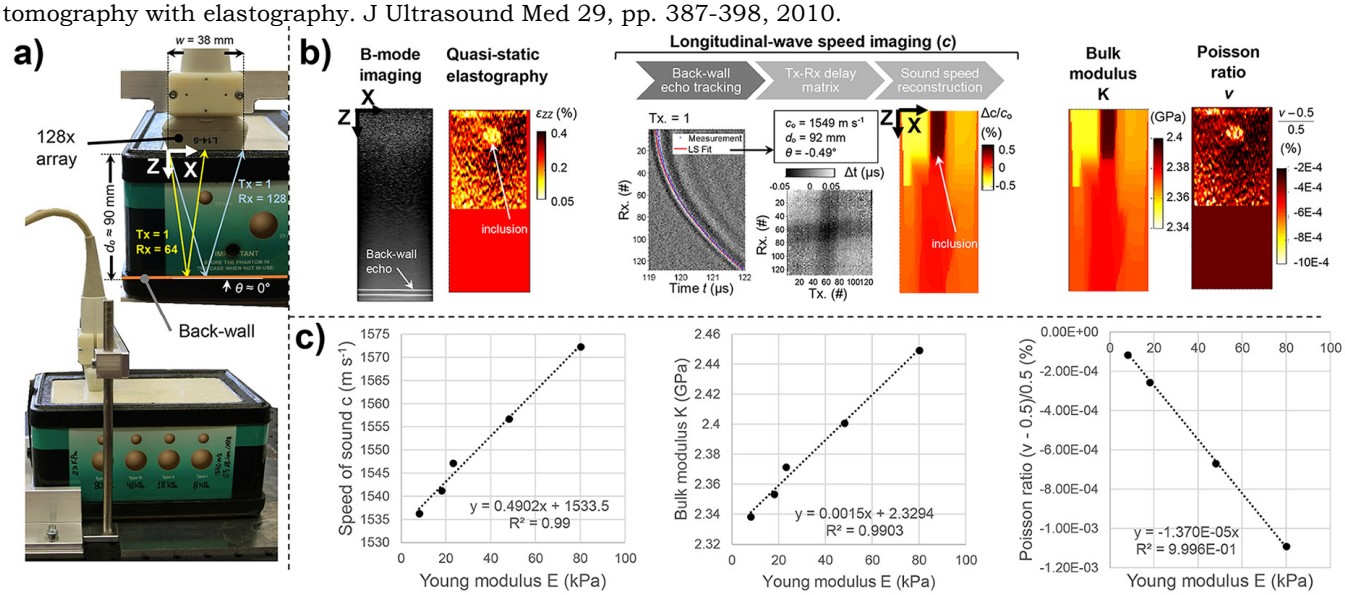

Figure 1: (a) Setup; (b) Imaging of elastic parameters for 48 kPa/10 mm diameter circular inclusion. (c) Speed of sound c, Bulk modulus K and Poisson ratio υ in Zerdine™ hydrogel in function of Young modulus E. Strong correlations ($R^2 > 0.99$) are observed.

064 **INVESTIGATING THE RELEVANCE OF STIFFNESS IMAGES OF AN ULTRASOUND TOMOGRAPHY SCANNER.**

Jérémie Fromageau[1,2], Alessandro Messa[2], Ashley D'Aquino[2], Minty Ledger[2], Anthony Swerdlow[2], Neb Duric[3,4], Maria Schmidt[1,2], Elizabeth O'Flynn[1,2] Jeffrey Bamber[1,2].*

[1]Royal Marsden NHS Foundation Trust, Downs Road, Sutton, London, UK.

[2]Institute of Cancer Research and Royal Marsden NHS Foundation Trust, Downs Road, Sutton, London, UK.

[3]Karmanos Cancer Institute, Wayne State University, 4100 John R Street, Detroit MI 48201

[4]Delphinus Medical Technologies, 46701 Commerce Center Dr, Plymouth, MI, 48170

Background: Although tomography has been investigated since the dawn of medical ultrasound imaging, it was largely supplanted by freehand echography, for practical reasons. With the development of hardware capabilities, a new generation of ultrasound tomography (UST) breast scanners, such as the Delphinus SoftVue® [1], is arising and providing information, such as speed of sound and attenuation coefficient, which is additional to that within the echogram. A UST characterization (USTC) image is derived by combining speed of sound and ultrasound attenuation coefficient to produce a parameter that correlates with the bulk modulus of breast tissue [2]. In this work we investigate the extent to which USTC correlates with Young's modulus, which is obtained from shear wave speed (neglecting shear wave attenuation) using the equation $E = 3\rho c_s^2$. It has been suggested that, as a measure of the viscoelastic bulk modulus, USTC might be biologically correlated with Young's modulus in the breast, because fat has a low Young's modulus and a low sound speed while glandular tissues have higher sound speeds and higher Young's modulus.

Aims: To evaluate (a) the correspondence in phantoms of SoftVue's USTC contrast with Young's modulus contrast determined by shear wave elastography (SWE), and (b) the ability of UST imaging *in vivo* to characterize the proportions of fat and glandular tissue as determined by MRI.

Methods: Two studies were carried out. First, a commercial breast elastography phantom (CIRS, model 059) and a custom built gelatin phantom with inclusions of known speed of sound were imaged using USTC imaging on the SoftVue®, and compared with the Young's modulus images provided by SWE (Aixplorer®, Supersonic Imagine, France). Second, whole breast volume-averaged USTC was estimated with the SoftVue® for both breasts of fifty healthy volunteers, and compared with whole breast volume-averaged water versus fat content determined by a Dixon MRI method.

Results: In the phantoms, a halo signature in the USTC images signifies the presence of the stiff masses (Figure 1a). Volume averaged USTC correlates very well (R=0.937) with breast composition estimated via MRI (Figure 1d).

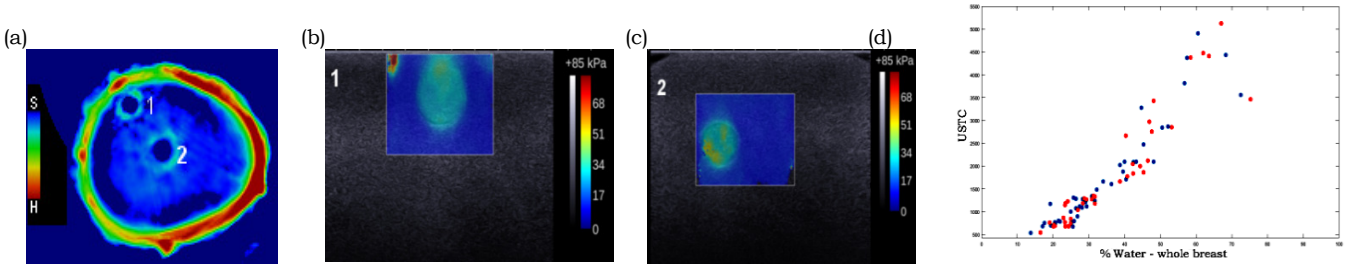

Figure 1: UST characterisation image (a) of a breast phantom, showing two spherical inclusions (1 & 2) identified by strong halo signatures. Shear wave elastograms, of inclusion 1 (b) and inclusion 2 (c), show that both inclusions were identified with a Young's modulus higher than the background. USTC and water content measured with MRI are strongly correlated (d).

Conclusions: Mass stiffness in the breast phantom is visualized differently by UST and SWE, suggesting a need for testing the biological realism of the phantom by gaining clinical experience of the relationship between stiffness in breast masses and their USTC appearances. Clinically, the global properties of breast tissue are well reproduced, with the proportion of fat versus glandular tissue estimated by UST correlating tightly with the MRI estimate.

References: [1] B Ranger, P Littrup, N Duric, et al, "Breast ultrasound tomography versus magnetic resonance imaging for clinical display of anatomy and tumor rendering: preliminary results". AJR. 2012; 198:233–239. [2] Duric, N., Littrup, P., Li, et al. "Whole breast tissue characterization with ultrasound tomography". Proc. SPIE 9419, Medical Imaging 2015: Ultrasonic Imaging and Tomography, 94190G-94190G.

003 **EXTENDED SHEAR WAVEFRONT GENERATION USING CUBIC PHASE WAVEFRONT MODILATING METHOD.**

Chu-Yu Huang[1], Wen-Hun Cheng[1], and Chir-Weei Chang[1].*
[1]Industrial Technology Research Institute, 195, Section 4, Chung Hsing Road, Hsinchu, TAIWAN.

Background: Shear Wave Elasticity Imaging (SWEI) often uses focused ultrasound push beams to induce shear waves in soft tissue. However, conventional spherical focusing has a small Depth of Focus (DOF), that shear wave speed can only be measured within a small range of depths for a single focused push beam. Bercoff, et al., developed a method called Supersonic Shear Imaging (SSI), which constructively produces shear wavefronts over an extended range in depth by combine of several consecutive push beams focused at different depths [1]. However, SSI requires multiple consecutive push beams to construct an extended depth shear wavefront, which means a higher energy output from transducer in a short period of time compared to a single push. In addition, in a complex human organ environment, these push beams may not be able construct a consistent shear wavefront.

Aims: The aims of this work are to (a) Propose a novel cubic phase wavefront modulating (CPWM) beamforming to produce an extended depth of focus (EDOF) push beam for generating a shear wavefront over an extended range in depth with a single push, and (b) Evaluate the performance of the CPWM beamforming method by comparing shear waves generated using the CPWM beamforming with that using only spherical focusing.

Methods: An extended depth of field through wavefront coding technique originally used in optics field [2] was modified and applied here to extend the ultrasound transmit DOF. The standard spherical focusing transmit delay times were altered by applying a cubic phase mask, so that the transmit point-spread function do not change appreciably over an extended range in depth. Using this novel transmit beamforming method, we were able to generate a shear wavefront over an extended range in depth with a single push. A Verasonics ultrasound system (Verasonics, Inc. Redmond, WA) was used in this study to generate shear wave and acquire the ultrafast plane wave images with a linear array transducer (AT5L40B, Broadsound Corp., Hsinchu , TW). The image acquisition rate for each plane wave with depth 60 mm was 10 kHz. The shear wave induced particle axial velocity was calculated from beamformed in-phase/quadrature (IQ) data using autocorrelation method [3]. A elasticity QA phantom (049A, CIRS, Norfolk,VA) was tested in this study to evaluate the performance of the CPWM beamforming method.

Results: The experimental results (Figure 1(b)) showed that the shear wavefront generated by the CPWM push beam were able to extend over a long depth range compared to that generated by the conventional spherical focusing push beam (Figure 1(a)). In the elasticity phantom experiments (Figure 1 (b), (c), (d), (e)), the shear wavefront was distorted when traveling through the hard inclusion due to the shear wave speed difference at different phantom position. The 2-D phantom stiffness map (Figure 1(f)) was obtained by calculating the shear wave propagation speed at each pixel position. The final result showed that the inclusion elasticity is 70.1 kPa which is very close to the CIRS elastic phantom specification: 80 ± 12 kPa.

Conclusions: Here we presented a novel CPWM beamforming method for generating a shear wavefront over an extended depth range. We provided experimental proof that with this method we can significantly extend the shear wavefront over a long depth range with a single push. The phantom elasticity can also be accurately measured by using this extended shear wavefront. This mothed can very effectively reduce the number of push beams required for generate shear wavefront, and therefore increase the shear wave Elastography frame rate and lower the total transmit energy.

Acknowledgements: This research is supported by the Industrial Technology Research Institute.

References: [1] Bercoff et al.: IEEE Trans Ultrason Ferroelectr Freq Control. 2004, 51:396–409. [2]Edward et al.: Appl. Opt. 34, 1859-1866 (1995). [3] Kasai C. IEEE Trans Ultrason Ferroelectr Freq Control. 1986; 33:94.

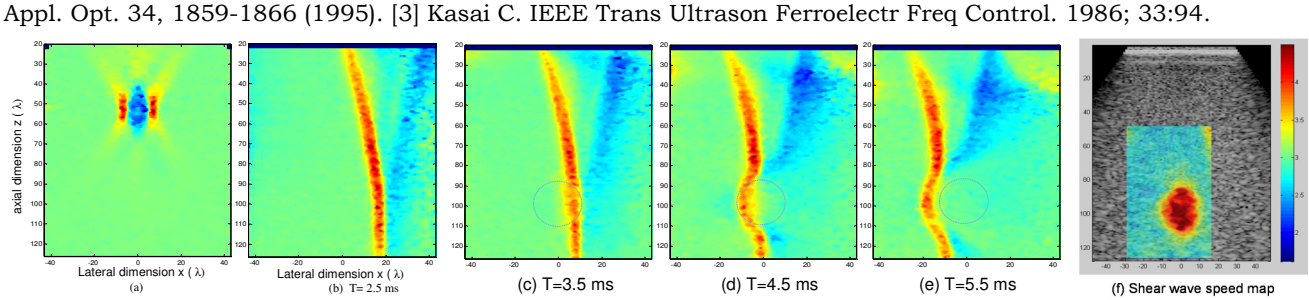

Figure 1: (a) particle axial velocity for spherical push beam, (b) particle axial velocity for CPWM push beam, (c)(d)(e) particle axial velocity for CPWM push beam at time T= 2.5ms, 3.5ms, 4.5ms respectively, (f) 2-D shear wave speed map of the CIRS phantom.

035 **TOTAL-VARIATION REGULARIZATION OF HAND-HELD LIMITED-ANGLE SOUND-SPEED TOMOGRAPHY BASED ON COHERENT REFLECTOR FOR BREAST CANCER DETECTION.**

Sergio J Sanabria[1], Orcun Goksel[1].*
[1]Computer Vision Laboratory, Dept. of Inf Tech and Elec Eng, ETH Zurich, SWITZERLAND.

Background: Sound-speed (SS) imaging is based on Ultrasound Computed Tomography (USCT) and is sensitive to tumorous inclusions (e.g., fibroadenoma, carcinoma, cysts) in the breast tissue, not visible in conventional B-mode images. Complex transducer arrangements and/or mechanical scanning are currently used. Low-cost extensions of B-mode systems for SS-USCT are desirable. Reflector-based methods based on a single transducer suffer from strong limited-angle artifacts (e.g. when using algebraic reconstruction ART [1]) or require prior information about the tumor position.
Aims: We propose total-variation TV (L1-norm smoothness) regularization for prior-less sound-speed imaging and delineation of piecewise homogeneous inclusions.

Methods: A 128-element array was operated in multistatic mode (a), each element individually firing (Tx) and the rest receiving (Rx). Adaptive amplitude-tracking measured the delays of echoes reflected from a plate behind the sample. Nelder-Mead simplex optimization of the 128×128 delay matrix provided average SS, plate distance and inclination, together with relative delays Δt induced by SS inhomogeneities (b). With the known geometric path-lengths L, relative slowness increments σ (low: high SS/hard inclusion; high: low SS/soft inclusion) were solved from an ill-conditioned linear system $\Delta t = L\sigma$. The TV regularization $\text{argmin}_\sigma \{\|\Delta t - L\sigma\|_2 + \lambda\|D\,\sigma\|_1\}$, with D a gradient matrix, was solved with convex optimization (c). The results were compared to conventional ART (5% singular values of L preserved) (d) and B-mode images (e).

Results: The TV reconstruction of synthetic SS-maps, with Δt simulated with ray tracing (a-e.1), achieves sharp edge delineation for adjacent inclusions, which ART fails to resolve. The limited-angle information leads to approx. 150% axial elongation of circular inclusions inside square phantoms. Hard inclusions (circular, 5 mm diameter, <1% SS contrast), invisible in B-mode, were revealed in a gelatin phantom (a-e.2). A soft cystic inclusion was detected in a thick breast-mimicking phantom (a-e.3) based on noisy Δt. In this case, the observed axial resolution was lower than simulated.

Conclusions: Hand-held *c*-maging allows detection of hard and soft inclusions in breast phantoms. The method does not require strong breast compression. On-going work aims at resolution improvement by denoising Δt and by full-wave inversion, together with a real-time implementation for in-vivo testing.

Acknowledgements: This work is supported by the Swiss National Science Foundation (SNSF).

References: [1] Krueger, M, Burow V, Hiltawsky K M, Ermert H (1998). Limited-angle ultrasonic transmission tomography of the compressed female breast. IEEE Ultrasonics Symposium, pp. 1345-1348.

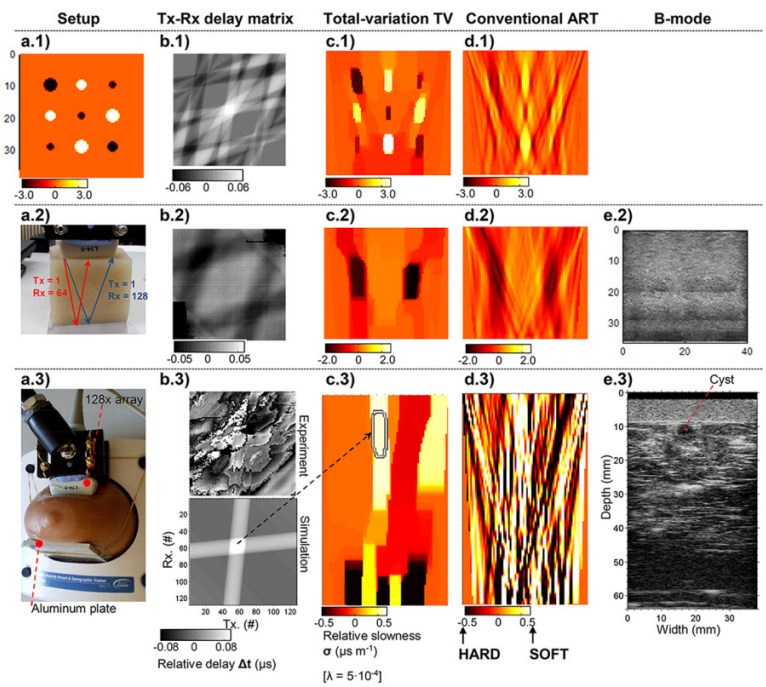

012 **INTRAOPERATIVE STRAIN ELASTOSONOGRAPHY IN BRAIN TUMOR SURGERY.**

Francesco Prada [1], Luca Mattei[1], Alessandro Moiraghi[2], Angela Rampini[2], Massimiliano Del Bene[2], Francesco DiMeco[1].*

[1] Fondazione I.R.C.C.S Istituto Neurologico Carlo Besta, Milan, MI, ITALY; [2] Università Degli Studi Di Milano, Milan, ITALY.

Background: Maximal safe resection represents the gold standard in brain tumor surgery. The evaluation of a lesion's position and boundaries within the healthy brain parenchyma is mandatory. Intraoperative palpation has represented the main tool guiding the surgeon's hands in the past decade in identifying pathological tissues. Intra-operative ultrasound is progressively establishing as an effective intraoperative tool. Strain elastosonography has rarely been used and reported in literature [1-5]. Nevertheless, its potentiality to intra-operatively define in real-time brain lesion and its boundaries is highly desirable.

Aims: In this study we try to assess the safety of strain elastosonography, along with its capabilities to define different cerebral lesions and possibly correlate them to histopathology.

Methods: From December 2011 to February 2015, we recorded data regarding patients operated on for the removal of a brain tumor. Every patient enrolled was in good clinical conditions (American Society of Anesthesiologists ASA score I-III; Karnofsky Performance Scale KPS> 70). Every patient was thoroughly informed about the surgical procedure, and an informed consent was obtained. For every patients, elastograms were obtained intraoperatively, (Esaote MyLab Twice, LA332 multifrequency probe, 3-11 Mhz) and a postoperative off-line qualitative analysis was performed, in order to try to describe different types of lesions by means of elastography.

Results: 71 patients were analyzed in this study. F 27, M 44, mean age 54. Histologically there were 30 Globlastoma, 2 Anaplastic Astrocytomas, 3 low grade Astrocytomas, 2 Oligodendrogliomas, 4 Anaplastic Oligodendrogliomas, 2 Oligoastrocytomas, 4 Anaplastic Oligoastrocytomas, 8 Meningiomas, 4 Metastases, the remaining comprising a variety of different histological types. It was possible to obtain B-mode scans and elastograms for every patient. No damage to brain cortex was caused by the technique. In every case, the intraoperative impression of the operator about the lesion's consistency matched the off-line analysis. 100% of agreement was observed between the 2 authors conducting independently the off-line analysis. The appearance of the different histological types at elastography was reported.

Conclusions: Elastosonography is a safe, feasible, and low cost technique, that seems to be a promising tool in assisting the surgeon in tumor identification and removal. In every case, elastosonography was able to highlight and define the lesion and its borders. Even if further studies are needed, in our paper we tried to define patterns of appearance of different brain tumors by means of elastosonography, especially glial tumors.

Acknowledgements: none

References:

1: Bamber J, Cosgrove D, Dietrich CF, Fromageau J, Bojunga J, Calliada F, Cantisani V, Correas JM, D'Onofrio M, Drakonaki EE, Fink M, Friedrich-Rust M, Gilja OH, Havre RF, Jenssen C, Klauser AS, Ohlinger R, Saftoiu A, Schaefer F,Sporea I, Piscaglia F. EFSUMB guidelines and recommendations on the clinical use of ultrasound elastography. Part 1: Basic principles and technology. Ultraschall Med. 2013 Apr;34(2):169-84. doi: 10.1055/s-0033-1335205. Epub 2013 Apr 4. PubMed PMID: 23558397.

2: Selbekk T, Bang J, Unsgaard G. Strain processing of intraoperative ultrasound images of brain tumours: initial results. Ultrasound Med Biol. 2005 Jan;31(1):45-51. PubMed PMID: 15653230.

3: Scholz M, Noack V, Pechlivanis I, Engelhardt M, Fricke B, Linstedt U, Brendel B, Ing D, Schmieder K, Ermert H, Harders A. Vibrography during tumor neurosurgery. J Ultrasound Med. 2005 Jul;24(7):985-92. PubMed PMID: 15972713.

4: Scholz M, Lorenz A, Pesavento A, Brendel B, Khaled W, Engelhardt M, Pechlivanis I, Noack V, Harders A, Schmieder K. Current status of intraoperative real-time vibrography in neurosurgery. Ultraschall Med. 2007 Oct;28(5):493-7. PubMed PMID: 17918047.

5: Selbekk T, Brekken R, Indergaard M, Solheim O, Unsgård G. Comparison of contrast in brightness mode and strain ultrasonography of glial brain tumours. BMC Med Imaging. 2012 May 23;12:11. doi: 10.1186/1471-2342-12-11. PubMed PMID:
22621614; PubMed Central PMCID: PMC3468395.

075 **CLINICAL POINT OF VIEW:**

Carlo Filice [1]*.

[1] Ultrasound Unit, Infectious Diseases Dept., Fondazione IRCCS Policlinico San Matteo, University of Pavia, 27100, ITALY.

In chronic liver diseases the prognosis and management largely depend on the extent and progression of liver fibrosis. In patients with chronic hepatitis C fibrosis is the most important predictor of outcome and influences the indication for antiviral treatment. Recent works suggest that liver fibrosis may be modified by treatment.

Liver biopsy is the reference standard, however it has several limitations: it is an invasive procedure with poor patient compliance and risk of complications; the diagnostic accuracy of scoring systems is affected by intra- and interobserver variability; it is not an ideal procedure for repeated assessment of disease progression; the costs should be taken into account.

Chronic liver disease affects millions of people worldwide and patients need to be followed-up.

Liver elastography is useful for the evaluation of diffuse liver diseases with a high level of evidence. It is capable of distinguishing significant fibrosis (F2 or more) from not significant fibrosis (F0 - F1). Elastography has been accepted by clinicians for the management of patients.

In the clinical practice liver elastography can be used before treatment for fibrosis assessment, to follow-up patients under treatment, and to assess the prognosis. The use of elastography in chronic viral hepatitis C has been suggested by clinical guidelines. The recommendations of the European Association for the Study of the Liver (EASL) for the treatment of patients with chronic HCV hepatitis with the new antiviral drugs have endorsed the use of non-invasive methods to diagnose liver fibrosis, reserving the liver biopsy to cases with uncertain or complex etiology. The document also states that elastography is useful in the follow-up of patients not treated or who have not responded to antiviral therapy.

The use of elastography allows the reduction of the number of liver biopsy, decreasing costs and risks.

074 **DIFFUSE LIVER DISEASE.**

Giovanna Ferraioli [1].*
[1]Ultrasound Unit, Infectious Diseases Dept., Fondazione IRCCS Policlinico San Matteo, University of Pavia, 27100, ITALY.

In the last decade ultrasound-based techniques for estimating the stage of liver fibrosis have become commercially available.

Transient elastography (TE) has been the pioneer technique for liver stiffness assessment. Several studies and meta-analyses have shown that TE is a reliable method for staging liver fibrosis. TE cannot technically be performed in patients with ascites and has a high rate of failure in subjects with body mass index greater than 30. The recent availability of the XL probe has overcome this latter limitation.

Ultrasound (US) shear wave elastography methods have the advantage of being integrated into US systems thus, also conventional US could be performed and the operator can choose the most appropriate acoustic window for stiffness assessment.

Several studies have shown that the shear wave elastographic methods are reproducible and accurate for staging liver fibrosis. Elastography plays an important role in the management of patients with chronic liver disease because it allows also to monitor progression or regression of liver fibrosis over time.

When using elastography methods some confounding factors should be taken into account. In fact, independently from fibrosis, the stiffness of the liver increases in acute viral hepatitis, in case of transaminases flares, in congestive heart failure, after food intake, in extrahepatic cholestasis and with Valsalva maneuver.

Because the majority of the studies have been conducted in patients with chronic hepatitis C, the cut-offs need to be further validated for other etiologies of diffuse liver disease.

The European Federation of Societies for Ultrasound in Medicine and Biology (EFSUMB) and the World Federation for Ultrasound in Medicine and Biology (WFUMB) have produced guidelines and recommendations for the clinical use of elastography [1,2].

The Society of Radiologists in Ultrasound (SRU) also convened a panel of specialists to arrive at a consensus regarding the use of elastography in the assessment of liver fibrosis in chronic liver disease. The recommendations were based on analysis of current literature and common practice strategies, and could represent a reasonable approach to noninvasive assessment of diffuse liver fibrosis [3].

References

1. Cosgrove D, Piscaglia F, Bamber J, Bojunga J, Correas JM, Gilja OH, Klauser AS, Sporea I, Calliada F, Cantisani V, D'Onofrio M, Drakonaki EE, Fink M, Friedrich-Rust M, Fromageau J, Havre RF, Jenssen C, Ohlinger R, Săftoiu A,Schaefer F, Dietrich CF; EFSUMB. EFSUMB guidelines and recommendations on the clinical use of ultrasound elastography. Part 2: Clinical applications. Ultraschall Med, pp. 34:238-53, 2013.
2. Ferraioli G, Filice C, Castera L, Choi BI, Sporea I, Wilson S, Cosgrove D, Dietrich CF, Amy D, Bamber JC, Barr R, Chou YH, Ding H, Farrokh A, Friedrich-Rust M, Hall TJ, Nakashima K, Nightingale KR, Palmeri ML, Schafer F, Shiina T, Suzuki S, Kudo M. WFUMB guidelines and recommendations on the clinical use of ultrasound elastography PART 3: Liver. Ultrasound in Medicine and Biology, 41, pp. 1161-79, 2015.
3. Barr RG, Ferraioli G, Palmeri ML, Ehmans RL, Goodman ZD, Myers R, Rubin J, Garra B, Garcia-Tsao G, Wilson SR, Rubens D, Levine D. Elastography assessment of liver fibrosis: Society of Radiologists in Ultrasound consensus conference statement. Radiology, PMID 26079489, 2015.

078 **LIVER STEATOSIS.**

Raffaella Lissandrin
Ultrasound Unit, Infectious Diseases Dept., Fondazione IRCCS Policlinico San Matteo, University of Pavia, 27100, ITALY

Hepatic steatosis is a common finding in the general population, with a prevalence of 16-30%. It is a benign and reversible condition in most of the cases, but it may sometimes progress to nonalcoholic steatohepatitis and liver cirrhosis. The current gold standard for the evaluation and quantification of liver steatosis is the liver biopsy, which is an invasive, costly and prone to sampling error procedure. Liver steatosis can be detected and estimated also with imaging techniques such as ultrasound (US), computed tomography and magnetic resonance imaging (MRI). US is the most widely used imaging technique for the assessment of liver steatosis, however it is an operator and machine dependent technique that can't provide a quantitative estimation of liver steatosis.

Recently, a new parameter called Controlled Attenuation Parameter (CAP) has been introduced on the Fibroscan device. Using the postulate that fat affects ultrasound propagation, CAP is able to measure the liver ultrasonic attenuation due to the presence of steatosis using the same signal acquired by the Fibroscan for the assessment of liver stiffness. The results are expressed in dB/m. CAP provides an immediate and quantitative evaluation of hepatic steatosis. It is operator and machine independent, and can explore 100 times more liver volume than liver biopsy. Unlike liver biopsy, it can be easily repeated and it is well accepted by the patients.

Several studies have shown that CAP is a reproducible and accurate method to evaluate and quantify liver steatosis. CAP has been evaluated in the general population and in patients with liver disease due to different aetiologies using liver biopsy as the reference standard. These studies have shown that CAP values are directly related to the percentage of hepatocytes with lipid droplets and they are significantly correlated with steatosis grade and body mass index at multivariate analysis. The performance of CAP is excellent for the differentiation between two or three steatosis grades but it is lower for one grade difference. The performance is not influenced by different aetiologies of liver disease and it is higher than that of other non-invasive tests.

In obese and overweight patients CAP has shown a good correlation with US or other more costly and less available imaging diagnostic methods, such as dual-energy X-ray absorptiometry and MRI.

077 **FOCAL LIVER MASSES: DIFFERENTIATION OF BENIGH FROM MALIGNANT WITH SONOELASTOGRAPHY.**

Stephanie R Wilson[1*], *Hojun Yu*[2].
University of Calgary, Foothills Medical centre, 1403 29 Street NW, Calgary AB CANADA; Queen Elizabeth II Hospital, Grande Prairie AB CANADA

Background: Historically, liver masses were diagnosed by either their surgical excision or biopsy. The last 4 decades, however, have shown a progressive trend away from such invasive procedures and we now live in an era of noninvasive liver mass diagnosis. This noninvasive evaluation of liver masses is important as benign and insignificant masses are frequently encountered. Elastography, or elasticity imaging, is a relatively new noninvasive technology which measures the natural tendency of tissue to resume its original size and shape after being subjected to a deforming force or stress. It is highly successful for the determination of the stiffness of the liver and for superficial tumors such as those in the breast.

Aims: Here, we address the application of elastography to the diagnosis of focal liver masses in any liver and the differentiation of those that are malignant from those that are benign.

Methods: Numerous approaches to elastography have been described in the literature but three in particular are considered best for this application. They are: point shear wave elastography (Acuson S2000, Siemens Medical Solutions, Mountain View, CA); 2D shear wave elastography (SWE), (Aixplorer, Supersonic Imagine, Aix-en-Provence, France); and strain elastography. Our experience is largely based on point shear wave technology, ARFI

Results: In our own published study of ARFI evaluation of 105 masses in 89 patients [10] there were28 hepatocellular carcinoma (HCC), 13 metastases, 35 hemangiomata, 15 focal nodular hyperplasia (FNH), 8 focal fat sparing, 4 focal fat deposits , and 2 adenoma. Successful measurements of mass stiffness were possible in the overwhelming majority of tumours. Receiver operating characeristic (ROC) analysis was determined to pick the optimal cutoff value to show the accuracy of ARFI to separate benign from malignant liver tumors, Although we did show a statistically significant different ARFI value for benign (1.73 [SD 0.78] m/sec)and malignant liver tumors (2.57 [SD 1.01] m/sec), the area under the ROC curve was 0.744, suggesting only fair accuracy (54). For differentiation of malignant from benign masses, the sensitivity, specificity, positive predictive value, and negative predictive value were 68% (28/41), 69% (44/64), 58% (28/48), and 77% (44/57), respectively, when 1.9 m/sec was chosen as a cutoff value, reflective of a wide variation of ARFI values in each diagnosis. Further, in our own experience, not only is there variation of stiffness measurements within masses with the same diagnosis, there may also be variation of stiffness measurements from within the margins of a single focal mass, as well.

Conclusions: There is wide variation and overlap in the stiffness of benign and malignant liver masses, making their differentiation on this basis unreliable.

Acknowledgements: Equipment support from Siemens.

References:

[1] 1. Yu H, Wilson SR Differentiation of Benign From Malignant Liver Masses With Acoustic Radiation Force Impulse Technique. Ultrasound Quarterly, 27, 217Y223, 2011.
[2] Cho SH, Lee JY, Han JK, Choi BI. Acoustic Radiation Force Impulse Elastography for the Evaluation of Focal Solid Hepatic Lesions: Preliminary Findings. Ultrasound Med Biol, 36, pp. 202-208, 2010
[3] Heide R, Strobel D, Bernatik T, Goertz DE. Characterization of Focal Liver Lesions (FLL) with Acoustic Radiation Force Impulse (ARFI) Elastometry. Ultraschall Med, 31, pp. 405-409, 2010

068 **BREAST ELASTOGRAPHY: AN OVERVIEW.**

Richard G Barr[1,2].*
[1]Northeastern Ohio Medical University, 4209 OH-44, Rootstown, Ohio 44272, USA; [2]Southwoods Imaging 7623 Market Street, Youngstown, Ohio 44512, USA.

Background: Conventional ultrasound, mammography and MRI have poor specificities in characterizing breast masses as benign or malignant. Elastography, both strain and shear wave, have been shown to have high specificity and sensitivity of characterizing breast masses as benign or malignant.

Aims: To review the state of the art strain (SE) and shear wave (SWE) imaging of the breast.

Methods: A review of the literature as well as expert opinion will be discussed on how to use elastography in breast imaging.

Results: Both SE and SWE have high sensitivity and specificity in characterizing breast masses as benign or malignant. Certain disease states such as mastitis or fat necrosis are often false positive while lymphoma is false negative. Sensitivities and specificity of studies using both SE and SWE have sensitivities of 85%-99% and specificities of 80-90%. A review of artifacts is provided. A review of recommended use of SE and SWE is presented.

Conclusions: SE and SWE are an important modality in characterizing breast masses as benign or malignant and should be a routine part of breast ultrasound.

References:

[1]Barr RG, Nakashima K, Amy D, et. al.: "WFUMB GUIDELINES AND RECOMMENDATIONS FOR CLINICAL USE OF ULTRASOUND ELASTOGRAPHY: PART 2; BREAST" UMB 2015.
[2] Barr RG and Zhang Z. "Shear-Wave Elastography of the Breast: Value of a Quality Measure and Comparison with Strain Elastography". Radiology, pp. 275:45-53, 2015.
[3] Barr RG, Destounis, Lackey LB, et al.: "Evaluation of Breast Lesions Using Sonographic Elasticity Imaging A Multicenter Trial" JUM, 31, pp. 281-287, 2012.
[4] Berg WA, Cosgrove DO, Doré CJ, et al.: Shear-wave elastography improves the specificity of breast US: the BE1 multinational study of 939 masses. Radiology,262 (2), pp. 435–449, 2012.

070 **BREAST CANCER SONOELASTOGRAPHY: CONSIDERATIONS COMING FROM DAILY PRACTISE OF A RADIOLOGIST.**

Antonio Pio Masciotra[1]*

[1]Casa di Cura Villa Maria, Campobasso, ITALY.

Clinical cases of breast cancer will be presented with analysis of the new answers to old questions and of the new questions and insights that sono-elastography brings to the diagnostic workup compared to the other imaging techniques used in the daily practice of a radiologist.

069 **THYROID ELASTOGRAPHY: AN OVERVIEW.**

Richard G Barr [1,2]*

[1]Northeastern Ohio Medical University, 4209 OH-44, Rootstown, Ohio 44272, US; [2]Southwoods Imaging 7623 Market Street, Youngstown, Ohio 44512, USA.

Background: Thyroid nodules are a common finding. Which lesions merit biopsy is a subject of much research. Many benign lesions are biopsied. Elastography, both strain (SE) and shear wave (SWE) have been evaluated as a method to improve thyroid lesion characterization and improve selections of lesions for biopsy.

Aims: To review the state-of-the-art elastography imaging of the thyroid

Methods: A review of the literature as well as expert opinion are reviewed and discussed.

Results: The results of thyroid lesion characterization with both SE and SWE have varying results. This is partly due to pre-selection bias, varying techniques, and different methodologies. Results are reviewed and reasons for variability are discussed. A review of added elastography to conventional ultrasound of the thyroid is discussed.

Conclusions: Thyroid elastography has varying results in the literature. A more defined protocol is needed. Results need to be integrated with conventional ultrasound findings.

Acknowledgements:

References:

[1] Azizi G, Keller J, Lewis M, et al.: "Performamce of Elastography for the Evaluation of Thyroid Nodules: A Prospective Study". Thyroid, 23, pp. 734-740, 2013.

[2] Bojunga J, Herman E, Meyer G, et al.: "Real-Time Elastography for the Differntiation of Benign and Malignant Tyroid Nodules: A meta Analysis" Thyroid, 20, pp. 1145-1150, 2010.

[3] Samir AE, Dhyani M, Anvari A, et al.: "Shear-Wave Elastography for the Preoperative Risk Stratification of Follicular-patterned Lesions of the Thyroid: Diagnostic Accuracy and Optimal Measurement Plane" Radiology 2015 published ahead of print.

[4] Cantisani V, Consorti F, Guerrisi A et al.: Prospective comparative evaluation of quantitative-elastosonography (Q-elastography) and contrast-enhanced ultrasound for the evaluation of thyroid nodules: preliminary experience. *Eur J Radiol*, Nov; 82(11), pp. 1892-8, 2013.

072 **SHEAR WAVE AND STRAIN ELSTOGRAPHY IN SUPERFICIAL ORGANS.**

Vito Cantisani[1]*.

[1]Department of Radiological, Oncologic, Pathology Sciences, Policlinico Umberto I, Univ. Sapienza, Rome, VialeReginaElena324, 00197, Rome, ITALY.

Background and Methods: Thyroid gland examination by palpation is a basic method in the assessment of thyroid nodules as firm and anelastic lesions should be suspected being of malignant nature. On the other hand, US, despite its high sensitivity for the detection of thyroid lesion, has limited accuracy to differentiate benign and malignant lesions. Hypervascularity, irregularity of margins, microcalcifications and hypoechogenicity are the most prominent features of malignancies however also CDUS has variable accuracy. [1,2] To date, FNAC is still considered the gold standard for optimal characterization of thyroid lesions, but still in 15% to 25% of cases FNAC findings can be suspicious and in 5% to 15% of cases inconclusive.

Elastography is a new imaging modality where elastic tissue parameters related to the structural organization of normal and pathological tissues are imaged. Clearly, not all nodules found at physical examination or at any imaging method should undergo fine needle biopsy. New tools allowing non-invasive real-time evaluation of these lesions thus needed. Any technique used to determine which nodules can be safely monitored without biopsy should have a sensitivity close to 100%, and this is not the case of CDUS. Techniques of elastography applied to thyroid use principally two different approaches according to the type of compression force (excitation) and elasticity evaluation: the free-hand ultrasound strain elastography (SE) with its qualitative and semi-quantitative variants, and the quantitative approach with the transducer induced high acoustic pulse and measuring the speed of the shear wave generated , shear-wave elastography (SWE). Shear wave elastography can be performed using the Acoustic Radiation Force Impulse technology (ARFI) either in a small ROI (point- shear wave elastography, p-SWE) or over a larger field of view using color-coding to visually display the stiffness values, 2D-shear wave elastography (2D-SWE). The guidelines of EFSUMB [3] and those recently published of WFUMB [4] provided a deep analysis of the various elastography techniques and their classification, which offers clarity in the almost confusing panoply of techniques and denominations offered by the manufacturers. However, to date, still some issues may be answered. How accurate it is? How reproducible is it? Which role may have in thy 3 nodule characterization? We will discuss the different techniques, suggesting how we can improve accuracy, and reduce interobserver variability. We will present our personal experience and review the literature. In addition an overview on other superficial organs such as Testicle [5] and salivary glands will be also provided

Conclusions

Elastography both with shear wave and strain elastographic techniques is feasible and an additional tool which may improves Baseline ultrasound efficacy in superficial organs evaluation. A much larger systematic clinical study is required for the characterization of testicular and salivary gland lesions with this newly developed technique.

References

[1] Itoh A, Ueno E, Tohno E et al.: Breast disease: Clinical Application of US Elastography for Diagnosis. Radiology 239, May (2) pp.341-50, 2006.

[2] Aigner F, De Zordo T, Pallwein-Prettner L, et al.: Real-Time Sonoelastography for the Evaluation of Testicular Lesions. Radiology, 263 May (2) pp. 584-9, 2012.

[3] JC Bamber, D Cosgrove, CF Dietrich, J Fromageau, J Bojunga, F Calliada, V Cantisani et al.: EFSUMB Guidelines and Recommendations on the Clinical Use of Ultrasound Elastography. Part 1: Basic Principles and Technology. Ultraschall Med., Apr 34(2) pp. 169-84, 2013.

[4] Shiina T, Nightingale KR, Palmeri ML, Hall TJ, Bamber JC, Barr RG, et al.: WFUMB Guidelines and Recommendations for Clinical Use of Ultrasound Elastography: Part 1: Basic Principles and Terminology. Ultrasound Med Biol., May 41(5)pp. 1126-47, 2015.

[5] Correas JM, Drakonakris E, Isidori AM, Hélénon O, Pozza C, Cantisani V, Di Leo N, Maghella F, Rubini A, Drudi FM, D'ambrosio F: Update on Ultrasound Elastography: Miscellanea. Prostate, testicle, musculo-skeletal. EUR J Radiol., Nov, 82 (11), pp. 1904-12, 2013.

073 **US-ELASTOGRAPHY IN THE ASSESSMENT OF PATHOLOGICAL BOWEL WALLS: TECHNICAL FEASIBILITY, INTEROBSERVER VARIABILITY AND DISEASE ACTIVITY CORRELATION.**

Laura Romanini[1], Alessandro Colleoni[2].*
[1]Dept. of Radiology, University of Pavia, Viale Camillo Golgi 19, 27100, Pavia, ITALY; [2]Dept. of Radiology, University of Brescia, Piazzale Spedali Civili 1, 25123, Brescia, ITALY.

Background: Ultrasounds are widely employed in the evaluation of inflammatory bowel diseases [1,2]. Increased thickness and loss of echo-stratification are considered pathological findings. US elastography (USE) is a non-invasive method, which allows to evaluate tissues' stiffness [3, 4].

Aims: Investigate the feasibility of elastosonography in the assessment of the abnormal bowel wall; the correlation between the bowel wall layering on color maps and B-mode images and between layering and color pattern of the pathological bowel wall and activity disease; the inter-observer variability.

Methods: 60 consecutive patients with at least one bowel segment with thickened walls (>3 mm) were enrolled from September 2012 to June 2014. Disease activity was evaluated by B-mode, color-Doppler and power-Doppler. E9-GE equipment (GE Healthcare, Wauwatosa, USA) with multi-frequency convex and linear probes was employed. All the affected segments were studied by USE using linear probe at two different frequencies: 5 MHz and 7.5 MHz. The color-box was placed about 1 cm below the skin surface.

Results: Overall 63 pathological segments were evaluated. A statistically significant difference was identified concerning the depth from the skin of the pathological bowel tract for applying USE. A correlation between the stiffness of the bowel wall and the disease activity was identified. An almost perfect to substantial agreement was determined between evaluations given by two different radiologists.

Conclusions: USE may feasible to evaluate thickened pathological bowel walls. The depth of bowel loop seems to be the feature that more influence the elastographic evaluation. The color map acquired at 7.5 MHz overlapped more precisely the B-mode layering of the pathological walls. A substantial-to-almost perfect agreement was determined between two different radiologists.

References:

1. Rodgers P.M. et al.: Transabdominal Ultrasound for Bowel Evaluation. Radiol Clin North Am. 2013 Jan; 51(1): pp. 133-48.
2. Ødegaard S. et al.: High-frequency ultrasonographic imaging of the gastrointestinal wall. Expert Rev Med Devices. 2012 May; 9(3): pp. 263-73.
3. Ophir J. et al.: Elastography: a quantitative method for imaging the elasticity of biological tissues" Ultrason. Imaging 13(2), pp. 111–134, 1991.
4. Bamber J., Cosgrove D., Dietrich C. F, et al. EFSUMB Guidelines and Recommendations on the. Clinical Use of Ultrasound Elastography. Part 1: Basic Principles and Technology. 2013 Ultraschall in Med, 34, pp. 169– 184, 2013.

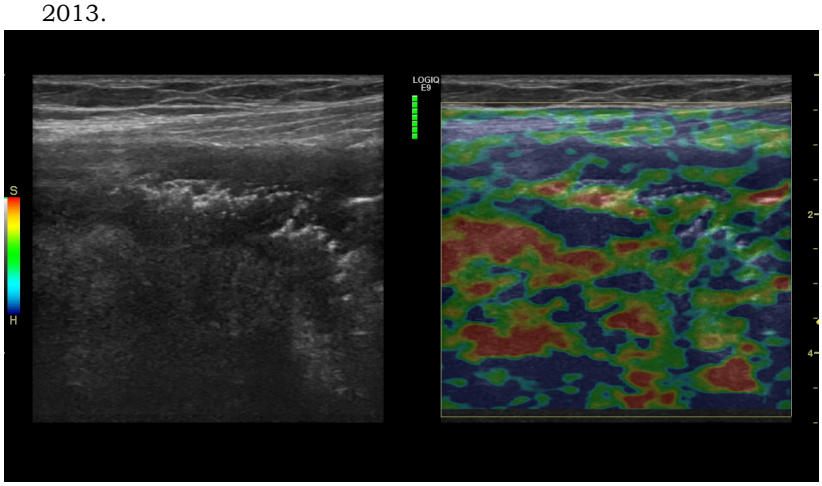

Figure 1: USE evaluation of last ileal loop. B-mode evaluation shows not-layered, thicked wall with. On elastogram, acquired at 5 MHz, the bowel wall is predominantly blue, that means increased stiffness.

067 **ELASTOGRAPHY OF THE PANCREAS.**

L Romanini[1].*
[1]Pavia, ITALY.

Background: Elastography has recently been presented in clinical studies as a new technique applied to US imaging.

Aims: The challenge of this new technique is to distinguish different tissues on the basis of their specific consistency. Since malignant tumors tend to be harder than benign lesions and parenchyma, this new approach could result clinically relevant. Initial clinical experiences in US elastography have been promising in differentiating breast, thyroid and prostate nodules.

Methods: Pancreatic applications of US elastography are relatively recent and under validation with several studies so far published in literature. The pancreatic elastography can be performed by means of two different approaches: the percutaneous and the endoscopic.

Results: .Basically, pancreatic ductal adenocarcinoma is a stiffer mass than the adjacent parenchyma owing to the presence of fibrosis and marked desmoplasia, thus characterized by a higher wave velocity value. Possible application of elastography in course of a ultrasound study is for mass characterization or identification or more suspicious areas useful for targeting further diagnostic procedures.

Conclusions: Elastography is a complementary techniques useful in clinical ultrasound studies.

References:

Cosgrove D, Piscaglia F, Bamber J, Bojunga J, Correas JM, Gilja OH, Klauser AS, Sporea I, Calliada F, Cantisani V, D'Onofrio M, Drakonaki EE, Fink M, Friedrich-Rust M, Fromageau J, Havre RF, Jenssen C, Ohlinger R, Săftoiu A, Schaefer F, Dietrich CF; EFSUMB. EFSUMB Guidelines and Recommendations on the Clinical use of Ultrasound Elastography. Part 2: Clinical Applications. Ultraschall Med., Jun; 34(3): pp. 238-53, 2013. doi: 10.1055/s-0033-1335375. Epub 2013 Apr 19. PubMed PMID: 23605169.

071 **COMPARISON OF STRAIN AND REAL-TIME SHEAR WAVE ULTRASOUND ELASTOGRAPHY IN THE DETECTION AND CHARACTERIZATION OF PROSTATE CANCER.**

Alfredo Goddi[1]*, Giovanni Magistretti[1], Andrea Sacchi[1], Alberto Roggia[2], Raffaele Novario[3]
[1]SME-Diagnostica per Immagini Medical Center, 31 Via L.Pirandello, Varese, 21100, ITALY; [2]Urology Unit, CAMPUS Medical Center, 31 Via L.Pirandello, Varese, 21100, ITALY; [3]Department of Biotechnology and Life Sciences - Medical Physics, University Hospital of Varese, 57 Viale L. Borri, Varese, 21100, ITALY.

Background: There is increasing evidence that strain (SE) and real-time shear-wave elastography (2D-SWE) facilitates detection of prostate cancer (PCa) [1-11]. SE evaluates the relative elasticity and provides only qualitative information [12]. SWE measures shear wave velocity in m/s and quantifies the tissue stiffness in kilopascals [13]. A comparison of results obtained on the same patients is not reported; also because it is not available on the market a system that allows the use of both techniques on the prostate.

Aims: To compare performances of SE and SWE in the detection of PCa in patients with PSA>4 ng/ml and to analyze the possible diagnostic benefit provided by the combination of these two techniques.

Methods: Transrectal B-mode ultrasound (TRUS), SE and SWE were performed in 97 patients with PSA>4 ng/ml and/or abnormal digital rectal examination. Two US machines were used equipped with different elastography technology (SE: MyLab Twice HD, 3-9 MHz end-fire transducer, Esaote, Genoa, Italy; SWE: Aixplorer, SuperSonic Imagine, 3-12 MHz end-fire transducer, Aix-en-Provence, France). Sensitivity, specificity, positive predictive value (PPV) and negative predictive value (NPV) were calculated for each modality. Receiver operating characteristic (ROC) curves and the areas below the ROC curves (AUCs) of strain ratio (SR), elasticity ratio (ER) and Mean kPa were compared with histological findings to identify the respective cutoff. Different combinations of SE and SWE parameters were evaluated.

Results: PCa was detected in 24.7% of 97 patients. Patient-level TRUS, qualitative SE and quantitative SWE (cutoff >35 kPa) yielded sensitivity 50.0%, 83.3%, 87.5%, specificity 75.3%, 72.6%, 67.1%; PPV 40.0%, 50.0%, 46.7%; and NPV 82.1%, 93%, 94.5%, respectively. Comparison of SR (cutoff >1.5) with ER ER (cutoff >2.3) and Mean kPa (cutoff >39 kPa) in detecting cancer showed sensitivity, specificity and AUC of 87.5%, 76.7%, 0.79; 83.2%, 79.4%, 0.88 and 87.5%, 68.4%, 0.83, respectively. The difference between ER and Mean kPa was statistically significant (p = 0.0392), whereas the difference between ER and SR was not (p = 0.1389). Performance assessment of the various combinations of Strain, SR, Mean kPa and ER did not show an improvement in the differentiation between benign and malignant when inclusion criteria was the positive outcome of all parameters. Instead, evaluating the positive outcome of at least one parameter or the combination of two parameters of the same technology did increase the performances: sensitivity, specificity and AUC rose to 95.8%, 73.9% and 0.85 (95% CI), respectively.

Conclusions: A comparison of SE and SWE carried out in the same patients showed that both methods are accurate, although SWE AUC is higher than SE AUC. The combination of SE and SWE, acting as independent features, increases diagnostic accuracy. This is probably linked to the different viscoelastic responses to the two types of mechanical stress, a factor that in some cases benefits one method rather than the other in detecting tissue anomalies. If this improvement, showed by our preliminary results, is confirmed by further studies, it might be worth joining the two technology solutions in the same equipment to eliminate the current limitations.

References: available on request at goddi.alfredo@libero.it

076 **MUSCULOSKELETAL ELASTOSONOGRAPHY**

P Minafra[1]*, C Bortolotto[2],
[1]*Euromedic International – Modena, [2]Institute of Radiology – Policlinico S. Matteo - Pavia University. ITALY.

Background

Several studies have already shown elastosonography is a reliable method applied to magnetic resonance for the study of the muscular response in relation to the type of contraction. Nevertheless MRI is still a static examination which does not allow a real time visualization of the musculoskeletal components examined

Aims: By our study we aim at demonstrating ultrasound elastosonography is a reliable method in the functional study of the musculoskeletal system, by comparing the elastosonography values detected at rest and under dynamic stress in subjects with a different level of athletic training to the results obtained from specific muscular work functional tests and by evaluating the possible increase in muscular elasticity in a 5-weeks-training focused on the development of the physical force.

Methods: 40 healthy volunteers, aged between 18 and 45, practicing sports, both amateurs and professionals, have been assessed by ultrasound equipment provided with specific elastosonography software. Upper and lower limb muscles have been examined bilaterally, both in release and active contraction and in clino and orthostatism as regards the lower limb.

All the subjects have performed specific tests for muscular contractility assessment, which are universally acknowledged strength-power parameters as predictors of sprinting performance, counter movement jump-test (CMJ), mono and bipodalic isokinetic test, comparing the parameters relative to the musculo-tendinous contracting response to the data obtained by the elastosonography study.

Results: At the end of training, each group showed a statistically significant improvement in muscle performance, demonstrated both in the CMJ test ($p > 0.001$) and the isokinetic test ($p > 0.01$). In the CMJ test, muscle explosive force increased by 11.7% after the 5 weeks training sessions. The isokinetic test showed a considerable increase of 11.6% in extensor muscles and an increase of 28% in flexor muscles. In all subjects it has been possible to confirm, the exact correspondence found between the values obtained by the specific functional tests and the elastosonography response.

Conclusion: Ultrasound examination is universally acknowledged as a primary examination in the study of the musculoskeletal system, thanks above all to the dynamic evaluation of muscular components. The possibility of appreciating also the elasticity grade further complements the ultrasound study, also in terms of preventive evaluation at the start of any professional training planning, allowing targeted trainings for each single athlete, in the attempt to avoid the risk of traumas often occurring when starting to do sport again, both after a trauma and seasonal breaks.

References:

1) Basford JR, Jenkyn TR, An KN, et al.: Evaluation of healthy and diseased muscle with magnetic resonance elastography. Arch Phys Med Rehabi. 2) Callaghan MJ, McCarthy CJ, Al-Omar A, Oldham JA The reproducibility of multi-joint isokinetic and isometric assessments in a healthy and patient population. "Clin Biomech (Bristol, Avon)" 2000 Nov;15(9)pp. 678-83. 3)Dresner MA, Rose GH, Rossman PJ, et al.: Magnetic resonance elastography of skeletalmuscle. J Magn Reson Imaging. 2001;13, pp. 269–276.4) Fukashiro S, Itoh M, Ichinose Y, et al.: Ultrasonography gives directly but noninvasively elastic characteristic of human tendon *in vivo*. Eur J Appl Physiol Occup Physiol.1995; 71, pp. 555–557. 5) Garfinkel S, Cafarelli E. Relative changes in maximal force, EMG, and muscle crosssectionalarea after isometric training. Med Sci Sports Exerc. 1992;24, pp. 1220–1227.6) Heers G, Jenkyn T, Dresner MA, et al.: Measurement of muscle activity with magnetic resonance elastography. Clin Biomech (Bristol, Avon). 2003;18, pp. 537–542. 7) Jenkyn TR, Ehman RL, An KN. Noninvasive muscle tension measurement using the novel technique of magnetic resonance elastography (MRE). J Biomech. 2003;36, pp. 1917–1921. 8) Martin BJ, Park H-S. Analysis of tonic vibration reflex: influence of vibration variables on motor unit synchronization and fatigue. Eur J Physiol 1997;75, pp. 504-11. 9) Manduca A, Oliphant TE, Dresner MA, et al.: Magnetic resonance elastography: non-invasive mapping of tissue elasticity. Med Image Anal. 2001;5, pp. 237–254.10) Martin BJ, Park H-S. Analysis of tonic vibration reflex: influence of vibration variables on motor unit synchronization and fatigue. Eur J Physiol 1997;75, pp. 504-11. 11)Monetti G., Minafra P. - Ultrasound Elastosonography. Musculo-Scheletal Ultrasound Vol I: Anatomy, Tecnique and Integrated Imaging. 2010, pp. 190-230 - (Timeo Ed.) 12) Moritani, T., and DeVries, H. (1979) Neural factors versus hypertrophy in the time course of muscle strength gain. American Journal of Physical Medicine 58, pp. 115-130. 13)Muthupillai R, Lomas DJ, Rossman PJ, et al.: Magnetic resonance elastography by direct visualization of propagating acousticstrain waves. Science. 1995;269, pp. 1854–1857.14) Ophir J, et al:. A Quantitative method for imaging the elasticity of biological tissues. Ultrasonic Imaging, 1991; 13, pp. 111-134. 15) Parker KJ, et al.: Tissue response to mechanical vibrations for "Sonoelasticity imaging". Ultrason Med Biol, 1990; 16, pp. 241-246. 16) Pesavento A, et al.: New real-time strain imaging concept using diagnostic ultrasound. Phys Med Biol, 2000 Jun 45 (6), pp. 1423-1435.17) Prior BM, Foley JM, Jayaraman RC, Meyer RA. Pixel T2 distribution in functional magnetic resonance images of muscle. J Appl Physiol. 1999;87, pp. 2107–2114. 18) Segal RL, Using imaging to assess normal and adaptive muscle function.Phys Ther.2007; 87, pp. 704–718. 19) Shina T, et al.: Real Time tissue Elasticity Imaging using Combined Autocorrelation Method: J. Med Ultrasound 1999; 26, pp. 57-66. 20)Smirniotou A, Katsikas C, Paradisis G, Argeitaki P, Zacharogiannis E, Tziortzis S. Strength-power parameters as predictors of sprinting performance. Journal of sports med and phys fitness. 2008 Dec;48(4), pp. 447-54 21) Torvinen, S., Kannus, P., Sievanen, H., Jarvinen, T.A.H., Pasanen, M., Kontulainen, S., Jarvinen, T.L.N., Jarvinen, M., Oja, P. and Vuori, I. (2002a) Effect of a vibration exposure muscular performance and body balance. Randomized cross-over study. Clinical Physiology and Functional Imaging 22, pp. 145-152.

Please Fill Out Both Sides

Conference Evaluation and Questionnaire

OVERALL CONFERENCE

	Poor		Mid		Excellent
Overall Conference Evaluation	1	2	3	4	5
ITEC & Sono Elastography Meeting over-lap Day	1	2	3	4	5
General comments/suggestions:					

SCIENTIFIC PROGRAM

	Poor		Mid		Excellent
Quality of the Presentations	1	2	3	4	5
Relevance of Presentations to the Conference's Theme	1	2	3	4	5
Time Allotted for Presentations	1	2	3	4	5
Time Allotted for Discussion	1	2	3	4	5
Poster Session	1	2	3	4	5
Tutorials	1	2	3	4	5
Short Presentation Category	1	2	3	4	5
Student Participation	1	2	3	4	5
Equipment Exhibit	1	2	3	4	5
Additional comments/suggestions:					

CONFERENCE MATERIALS

	Poor		Mid		Excellent
Printed Proceedings Book	1	2	3	4	5
CD Proceedings	1	2	3	4	5
Other Registration Materials	1	2	3	4	5
CD only or Printed Proceedings Book and CD	CD Only		Proceedings Book and CD		
Additional comments/suggestions:					

CONFERENCE FACILITIES AND SOCIAL PROGRAMME

	Poor		Mid		Excellent
Lecture Hall	1	2	3	4	5
Registration Desk	1	2	3	4	5
Meals: Dining facilities	1	2	3	4	5
Conference Lunches	1	2	3	4	5
Conference Dinner and Entertainment	1	2	3	4	5
Coffee Breaks	1	2	3	4	5
Opening Dinner Reception	1	2	3	4	5
Closing Cocktail Party	1	2	3	4	5
Audio–Visual: Screen Visibility	1	2	3	4	5
Sound Level	1	2	3	4	5
Presentation Transition	1	2	3	4	5
Internet Connectivity:	1	2	3	4	5
Additional comments/suggestions:					

Please Fill Out Both Sides

Conference Evaluation and Questionnaire

VENUE AND HOTEL

	Poor		Mid		Excellent
Venue: Lake Garda, Verona, Italy and Environs	1	2	3	4	5
Would you return to this area?	Yes		Perhaps		No
Area Attractions	1	2	3	4	5
Hotel: Overall	1	2	3	4	5
Reservations	1	2	3	4	5
Transportation and Accessibility	1	2	3	4	5
Reception and Check–In	1	2	3	4	5
Accommodations	1	2	3	4	5
Facilities	1	2	3	4	5
Parking	1	2	3	4	5
Would you return to this hotel?	Yes		Perhaps		No
Would you like to co-host ITEC in the future?	Yes		Perhaps		No
If yes, please state your organization name and city:					
Where would you like to see ITEC hosted?					
Additional comments/suggestions:					

CONFERENCE ADMINISTRATION

	Poor		Mid		Excellent
Website	1	2	3	4	5
Registration off–site	1	2	3	4	5
Registration on–site	1	2	3	4	5
Administrative staff	1	2	3	4	5
Correspondence	1	2	3	4	5
Additional comments/suggestions:					

GENERAL INFORMATION

I am a Returning Delegate	Yes		No
I plan to attend the next conference in 2016	Yes	Perhaps	No
and present a paper(s) / poster(s)	Yes	Perhaps	No
Other(s) from my lab would attend the next conference	Yes	Perhaps	No
and he/she / they would present a paper(s) / poster(s)	Yes	Perhaps	No
How did you learn of this conference? (Check all that apply)	☐ Email Announcement		
☐ Internet	☐ Website		
☐ Other	☐ Colleague		
Tutorial Topic Suggestions for next year:			
Additional Comments/suggestions:			

If you would be willing to host the Conference in your city, please give your name to the Conference Staff. Questions, comments or suggestions are welcome at any time at <secretariat@elasticityconference.org> Thank You!

CÆSIUS CONGRESS CENTER